Politecnico di Torino

POLITECNICO DI TORINO

Master Degree in Physics of Complex Systems

Final Dissertation

Vortex crystals with empty and filled cores

Supervisors:

Prof. Vittorio Penna
Dr. Andrea Richaud

Author:

Riccardo Ferrini

Academic Year 2023/2024

Abstract

A generic quasi two-dimensional superfluid confined in a rotating circular trap could present quantum vortices. According to the Point Vortex model, each vortex is effectively described as a point-like particle around which the superfluid flows with quantized circulation. It has been proven that at equilibrium the vortex-array is a composition of concentric regular polygonal structures. Non-trivial excitations of these stable configurations are the so called Tkachenko modes, microscopically associated to elliptical precessions of each vortex around its equilibrium position, representing a macroscopic deformation of the vortex-crystal. Recently it has been also proposed a model for point-like vortices hosting in their cores massive particles. The goal of this thesis is the characterization of the main effects ensuing from the "vortex mass" on the formation of the vortex crystal depending on the rotation rate of the trap and on the creation of their non-trivial excitations. Principal consequences of such a massive description are the centrifugal forces acting on each massive vortex core and the typical cyclotronic-like orbits characterizing their dynamics. The study was carried out in an analytical way, and was based on the minimization of system free energy, as well as on the study of the equations of motions of many-vortex systems.

Acknowledgements

This thesis project marks the the end of fundamental part of my life, during the which I have been accompanied by some important people who I would like to thanks.

It has been almost 6 years since when I moved to Turin for my studies Physics.
Despite all my initial doubts and uncertainties, I am very proud and satisfied of my own academic path.
Firstly, I would like to thank Prof. Vittorio Penna for having made me realized with his lectures my true interest in the *theoretical condensed matter physics*, especially in Bose-Einstein condensation and quantum vortices and for having given me the possibility to collaborate for this thesis with Dr. Andrea Richaud. I am particularly grateful to Andrea for his guidance and support during these last six months, in which thanks to him I have spent three months of an outgoing mobility project (under his supervision) at the Department of Physics of the Universitat Politècnica de Catalunya (Barcelona). A special thanks goes to all the research team which hosted me and to Prof. Pietro Massignan, who also supervised me and helped me figuring out some important passages of my research work.

Looking back to this entire path of studies, I can't help thinking that I would not be here without my family. Thank you mum for all your trust on my skills and for all the strength given to me whenever I have doubted of myself. Thank you dad for the huge patient and love you show me every day. Thanks to my sister, Beatrice, for the true joy of our moments together.
A further thank you to my grandmother, Tina, and to my aunt, Pupa, who have always motivated me on my academic path and supported me whenever I needed.

Furthermore, during these years thanks to Gifra Torino I have met special brothers and sisters with whom I grew living concretely my own faith. Especially thank you Alessia, Roberta, Chiara, Agnese F., Alberto, Marco, Pietro and Davide. Last, but not least, I really would like to thanks Fra Vittorio and Fra Mauro for having accompanied me during these years.

Contents

Introduction

The liquefaction of helium, realized by Heike Kamerlingh Onnes in 1908, has been a crucial step in the study of the fundamental physical properties of materials at very low temperatures. Exploiting the liquid helium refrigerant power to cool mercury (Hg), below 4 K (Kelvin), Onnes was the first to observed the *Superconductivity*, a physical state characterized by electrical currents flowing without resistance. Further studies on liquid helium showed the presence in the heat capacity curve of a discontinuous phase transition, the so called *"lambda" transition* [1], around a temperature of 2.2 K. Such a behaviour highlights the existence of two different liquid phases for the helium according to a critical temperature value T_λ: a ^{3}He phase for $T > T_\lambda$ and a ^{4}He phase for $T < T_\lambda$. In particular the latter low temperature phase, corresponding to bosonic isotopes, shows some peculiar non classical physical properties of liquid helium, such as remaining liquid even at temperatures very close to 0 K (the absolute zero), reluctance to boil and an extremely high internal mobility, that makes it flow with no viscosity.
Due to the analogy with *Superconductivity*, in 1938 Kaptiza defined this ^{4}He liquid phase as "superfluid", introducing for the first time the technical term *Superfluidity*. In the same year the 1925 Einstein's model for ideal gases of bosons was taken into account by London, in order to explain this non classical physical state. Such a model predicted the *Bose-Einstein condensation* effect (we will discuss about it in section 1.1), meaning that a significant number of the particles should condense in a unique quantum state and the remaining particles should act conventionally, and showing the presence of a discontinuity in the heat capacity, very similar to the one observed in the liquid helium (further information in Ref. [2]). This led to the so called *two-fluid* model [3], where Tizsa and Landau described the ^{4}He as it is composed by a nonviscous superfluid and a viscous "normal fluid" (obeying the classical physics). However since the Bose-Einstein condensation restricted the explanations of the *Superfluidity* only bosonic systems (such as ^{4}He atoms), at first it was not so clear if and how such a phenomenon could be responsible for the *Superconductivity*, where electrons flow with no internal resistance. Indeed electrons are fermionic particles obeying to the Pauli exclusion principle, which prevents two identical fermions to occupy the same quantum state. It was thanks to the *BCS theory*, by Bardeen, Cooper and Schreiffer, that it was proposed the concept of the *Cooper pairs*, consisting in the coupling of two electrons mediated by positive ions in the lattice, which correspond to composite bosons (bosonic quasi-particles). Such a paring mechanism was later confirmed in 1972 with observation the superfluid behaviour in fermionic helium isotope ^{3}He, at temperatures around 2 mK.
So *superfluid helium* and *superconductors* are both manifestations of *Bose-Einstein condensation*, since they arise from the *condensate*, the macroscopic quantum state occupied by a large fraction of particles, and they represent examples of *quantum fluids*, fluids of particles governed by quantum mechanics laws. However, these kind of systems are much more complicated than an ideal gas described by the Einstein's model, because of the presence of strong interactions between particles, typical of fluids and solids.
The most important hallmarks characterizing a superfluid include its capacity to flow without viscosity (nonviscous fluid), the existence of a break down of the superflow occurring above a certain critical velocity, a persistent flow, Josephson currents associated to

macroscopic tunnelling, and the presence of vortices around which the flow shows quantized circulation. Further information on Superconductivity, Superfluidity and Bose-Einstein condensates can be found in Ref. [4].
It was only in the 1995 that the first gaseous Bose-Einstein condensate was realized by cooling a gas of rubidium atoms (^{87}Rb) down to 200 nK (nano Kelvin) [5]: above the critical temperature T_c the atomic particles presented a wide/broaden momentum distribution, corresponding to an *energetic* and *thermal gas*; while approaching T_c a narrow peak appears in the momentum distribution, indicating the condensation of a large portion of atoms into a almost zero energy and momentum quantum state. Nowadays the most common atomic species used in the formation of Bose-Einstein condensates (with typically 99% of condensed atoms) are the rubidium (^{87}Rb) and the sodium (^{23}Na) [6]. It is also possible to obtain multi-component condensates, i.e. two-component Bose-Einstein condensates [7], and fermionic Bose-Einstein condensates, i.e. using a ultracold gas of potassium atoms (^{40}K) [8].

Ever since Feynman's seminal article [9] about the quantum properties of liquid helium has been published, the scientific community has been vividly interested in the appearance of quantum vortices in superfluids. They are topological defects consisting in a depletion effect of the quantum fluid density, strictly associated to a phase shift: in fact one can imagine them as whirlpools around which the fluid flows with quantized vorticity (this will be discussed in section 2.2). At the beginning they were observed only in superfluid helium [10], but after the realization of the first ultracold atomic Bose-Einstein condensate [5], quantum vortices were also observed in such a new class of superfluids, [7, 11, 12]. The dynamics of quantum vortices (with empty cores) in a superfluid confined in quasi two-dimensional domains is defined by the Helmholtz-Kirchhoff equations, containing no inertial term and corresponding to first order differential dynamical equations (see Ref. [13] and section 4.1).
Recently it has been proposed that whenever the core of a vortex, that is usually empty, may behave as a potential well, massive particles could be trapped by a quantum vortex [12]. Such a non-zero core mass introduces a second order time derivative derivative in the motion equation, which makes their description significantly different from that of their massless counterpart. In particular a generalized point-like dynamical model has been developed within a time-dependent variational approach [14, 15], which has predicted as effect of the core mass the presence of small amplitude transverse radial oscillations affecting the well-known vortex trajectories [13] (this will be discussed in subsection 4.1). The reason for such a "massive" modeling lays on the fact that in the past few years it has been (accidentally and/or deliberately) realized how, in real world experiments, quantum vortices almost always host some massive particles. These particles, localized in the vortex cores, are generally related to the (realistic) presence of atomic impurities, thermal, tracer atoms, or atoms from a different bosonic component: i.e. a concrete experimental example can be find in Ref. [12]. Since the presence of quantized vortices is a distinctive signature of a superfluid system, such as the *liquid helium*, the *Bose-Einstein condensates*, the *fermionic superfluids* and the so called *quantum fluids of light*, the study about the properties of *massive vortices* is of fundamental importance nowadays. The goal of this thesis is to characterize the effects of the core mass both on the formation of

vortex crystals at equilibrium, and on the creation of their non-trivial excitations. More precisely, the considered analysis focuses on the simple case of a quasi two-dimensional uniform condensate bounded in a rotating circular domain, presenting point-like vortices of vanishingly small core size compared to the typical system size. The study has been based on the semi-analytical global minimization of the system free energy, as well as on the study of the equations of motions for many-vortex systems.

In the following we will present some generic information about the organization of the main topics discussed in this thesis work.

Chapter 1 represents a general review of systems of bosonic particles. Through the analysis of the non interacting regime, we will introduce the *Bose-Einstein condensation* effect, and consequently we will describe a Bose gas in the regime of weak interactions, within the main assumption of a dilute gas at very low temperatures. In the end, by considering a mean field approach, we will present and properly discuss the *Gross-Pitaevskii* model of the Bose-Einstein condensate.

Chapter 2 is devoted to show the deep link between the fluid dynamics and the Gross-Pitaevskii model describing a condensate. We will firstly analyze the Hydrodynamic picture of this model, discussing the *superfluid dynamics equations*. Then, within this interpretation, we will mainly focus on the nature of quantum vortices characterizing a superfluid, analyzing their point-like description in both cases of infinitely large and confined quasi two-dimensional condensates. The end of the chapter is dedicated to the introduction of the concept of *"massive" quantum vortices* and of their effective point-like modeling.

In **Chapter 3**, we will face the problem of the global minimization of the system's free energy in order to reproduce at first the well-known absolute stable equilibrium patterns of quantum vortices with empty cores, formed in a quasi two-dimensional condensate confined in a circular rotating trap. After this initial verification, we will investigate the main effects ensuing from the presence of a non-zero small core mass on the formation of such equilibrium many-vortex configurations.

Chapter 4 focuses on the analysis of the dynamics of quantum vortices within the *Point-Vortex model*, highlighting the main characteristics and properties of the dynamical equations, which define the motion of quantum vortices, both in the "massless" and in "massive" vortex descriptions. The second part of this chapter will be centered on the non-trivial excitations of vortices around their equilibrium positions in a stable vortex crystal, analyzing in particular the effect of the core mass on the well-known *Tkachenko modes*, which define the excitations of massless vortex crystals.

Chapter 1

Bose-Einstein condensates and their modeling

This first chapter consists in a general and introductory review of systems of bosonic particles. Starting from the analysis of the ideal Bose gas, a system of non interacting bosons, we will introduce the effect of the Bose-Einstein condensation. Consequently, we will describe a Bose gas in the weak interactions regime, within the main assumption of a dilute gas at very low temperatures. Finally by considering the mean field approach, we well present and properly discuss the Gross-Pitaevskii model of the Bose-Einstein condensate.

1.1 Ideal Bose gas

A system of bosonic particles, which do not interact, obeys the *Bose-Einstein* statistics. In such a gas, particles (of identical mass m) are distributed according to the *Bose distribution function* and can be treated in a *Grand Canonical ensemble* (we have considered as references Ref. [16, 17, 18]): we can consider a set of possible values for the particle momentum $\vec{p}$, which essentially labels the occupied states with energy (per mode $\vec{p}$) $\epsilon_{\vec{p}}$

$$\epsilon_{\vec{p}} = \frac{(\vec{p})^2}{2m}, \quad \text{with} \quad \vec{p} = \hbar\vec{k} \quad (\vec{k} \text{ the wave vector}). \tag{1.1}$$

Then the *Grand Canonical partition function* $\mathcal{Z}_{\mathcal{B}}$ associated to a system of indistinguishable bosonic quantum particles assumes the form of

$$\mathcal{Z}_{\mathcal{B}} = \prod_{\vec{p}} \frac{1}{1 - e^{\beta(\mu - \epsilon_{\vec{p}})}} = \prod_{\vec{p}} \frac{1}{1 - ze^{-\beta\epsilon_{\vec{p}}}}, \qquad z = e^{\beta\mu} \text{ (fugacity)}, \tag{1.2}$$

where $\beta = 1/k_bT$ (being k_b the Boltzmann constant) and μ the chemical potential. If the number of particles at a certain mode $\vec{p}$ is $n_{\vec{p}}$ and the total number of bosons is just $\sum_{\vec{p}} n_{\vec{p}}$, then exploiting $\mathcal{Z}_{\mathcal{B}}$ it is possible to compute the average values of these quantities as

$$N = \langle N \rangle = -\partial_\mu \left[k_B T \ln \mathcal{Z}_{\mathcal{B}} \right] = \sum_{\vec{p}} \frac{ze^{-\beta\epsilon_{\vec{p}}}}{1 - ze^{-\beta\epsilon_{\vec{p}}}} = \sum_{\vec{p}} \langle n_{\vec{p}} \rangle \,. \tag{1.3}$$

Furthermore, assumed that the gas occupies a volume V at a pressure P and temperature T, the **state equation** results to be:

$$PV = k_B T \ln \mathcal{Z}_{\mathcal{B}} = -k_B T \sum_{\vec{p}} \ln \left[1 - z e^{-\beta \epsilon_{\vec{p}}}\right]. \tag{1.4}$$

In the **thermodynamic limit** (where $N, V \to \infty$, but $V/N = constant$), the summation over a non zero discrete momentum vector ($\vec{p} \neq 0$) could be transformed into an integral in the reciprocal space over a continuous momentum vector, $\sum_{\vec{p}\neq 0} \to \frac{4\pi V}{h^3} \int_0^\infty d\vec{p}\, p^2$, allowing us to write equations (1.3) and (1.4) in the following form:

$$N = \frac{z}{1-z} + \frac{4\pi V}{h^3} \int_0^\infty d\vec{p}\, p^2 \frac{z e^{-\beta \epsilon_{\vec{p}}}}{1 - z e^{-\beta \epsilon_{\vec{p}}}} \tag{1.5}$$

$$\frac{PV}{k_B T} = -\ln(1-z) - \frac{4\pi V}{h^3} \int_0^\infty d\vec{p}\, p^2 \ln \left[1 - z e^{-\beta \epsilon_{\vec{p}}}\right] \tag{1.6}$$

These two formulas are obtained by first isolating the zero mode $\vec{p} = 0$ from the rest of the sum, and then going on with the integrations we finally write:

$$N = \frac{z}{1-z} + \frac{V}{\lambda^3}\, g_{3/2}(z), \qquad g_{3/2}(z) = \sum_i^\infty \frac{z^i}{i^{3/2}}; \tag{1.7}$$

$$\frac{PV}{k_B T} = -\ln(1-z) + \frac{V}{\lambda^3}\, g_{5/2}(z), \qquad g_{5/2}(z) = \sum_i^\infty \frac{z^i}{i^{5/2}}, \tag{1.8}$$

with $\lambda = \sqrt{2\pi\hbar^2/(m k_B T)}$ and $v = V/N$ the volume per particle.

These two last equations are of fundamental importance, because they intrinsically contain a relation between the thermodynamical quantities V, P and T defining a *special purely quantum regime* apart from the high temperature (low density) and low temperature (high density) regimes. Let us focus our attention to equation (1.7) expressed in terms of the system volume per particle v as

$$\frac{1}{v} = \frac{z}{V(1-z)} + \frac{1}{\lambda^3}\, g_{3/2}(z), \tag{1.9}$$

and considering the ratio $\frac{\lambda^3}{v}$ to be a function $F(z)$ of the fugacity (or better of the chemical potential), so that using the equation (1.9) one finds

$$\frac{\lambda^3}{v} := F(z) = \; g_{3/2}(z)\; \frac{\frac{N}{N+1}(1-z)}{\frac{N}{N+1} - z}. \tag{1.10}$$

Observe that, in order to be N and P meaningful physical quantities, the range of fugacity must be $0 \leq z < 1$, with divergent behaviour of λ^3/v for $z \to N/N+1$ implied by equation

(1.10). Thus, by directly comparing the functions $g_{3/2}(z)$ and $\frac{\lambda^3}{v} := F(z)$, we are capable of defining the two following regimes (still the in thermodynamic limit):

$$\textbf{1)}\ \ z \to \frac{N}{N+1} \simeq 1 \ \ \text{with} \ \ \frac{\lambda^3}{v} := F(z) \to \infty, \ \ g_{3/2}(\frac{N}{N+1}) \simeq \ g_{3/2}(1) = 2.612 \tag{1.11}$$

$$\textbf{2)}\ \ 0 \leq z < \frac{N}{N+1} \ \ \text{with} \ \ \frac{\lambda^3}{v} := F(z) \simeq \ g_{3/2}(z) \leq g_{3/2}(1) \tag{1.12}$$

Since the average population of the zero mode $\langle n_0 \rangle = z/(1-z)$, using formula (1.7) it can be written as

$$\frac{\langle n_0 \rangle}{N} = 1 - \frac{V}{\lambda^3}\ g_{3/2}(z), \tag{1.13}$$

consequently we find in the case $\left(\frac{\lambda^3}{v} > g_{3/2}(1)\right)$ a non zero fraction of particles populating the zero mode (corresponding to the lowest energy state $\epsilon_0 = 0$). In this way at the *Ground state* a significant amount of condensed particles form a macroscopic many-body, known as the **condensate**.

$$\textbf{1)}\ \frac{\langle n_0 \rangle}{N} \simeq 1 - \frac{v}{\lambda^3}\ g_{3/2}(1), \ \ \left(\frac{\lambda^3}{v} > g_{3/2}(1)\right); \ \ \textbf{2)}\ \frac{\langle n_0 \rangle}{N} = 0, \ \ \left(\frac{\lambda^3}{v} \leq g_{3/2}(1)\right) \tag{1.14}$$

Notice that the zero mode average population $\langle n_0 \rangle / N$, known as the *condensate fraction* for the case **1)**, strictly depends on the temperature and volume and in fact and therefore it is possible to obtain the following equation

$$\frac{\langle n_0 \rangle}{N} \simeq 1 - \frac{v}{\lambda^3}\ g_{3/2}(1) = 1 - \left(\frac{T}{T_c(v)}\right)^{\frac{3}{2}} \ \ \text{with} \ \ T_c(v) = \frac{2\pi\hbar^2}{m k_B}\left(v g_{3/2}(1)\right)^{-\frac{2}{3}}, \tag{1.15}$$

where $\boldsymbol{T_c(v)}$ is the **critical temperature** (depending on the volume per particle v), which actually represents the driving parameter of this phenomenon, known as the **Bose-Einstein condensation**.

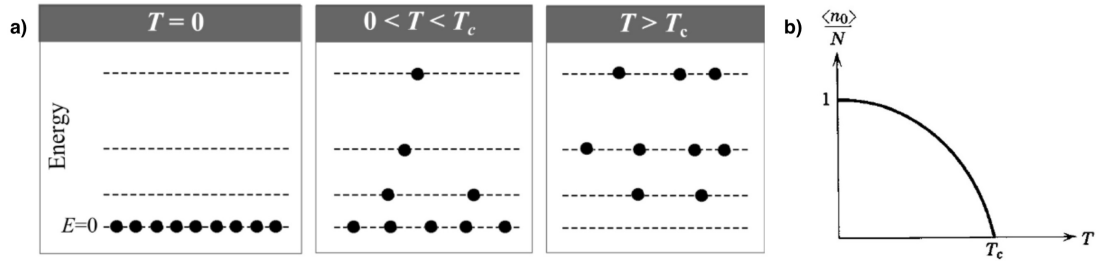

Figure 1.1: a) Occupation of the energy levels in the Ideal Bose gas at temperature T. The Figure has been taken from Ref. [2]. **b)** Curve of condensate fraction $\langle n_0 \rangle / N$ at the Ground state as function of temperature fraction T/T_c according to equation (1.15) (picture taken from Ref. [16]).

In fact, at $T = 0$ all the N particles in the gas are in the lowest energy level $E = \epsilon_{\vec{p}} = 0$, corresponding to the Ground state (the zero mode $\vec{p} = 0$ state). As the temperature increases the number of exited particles increases, so for $0 < T < T_c(v)$ the Ground state is still macroscopically occupied, but its fraction of the condensed bosons decreases, up to $T = T_c(v)$ where all the particles are excited and the Ground state is completely depleted. In Figure 1.1, the left panel **a)** shows the bosonic occupation of the energy levels according to the temperature T of the gas, while the right panel **b)** shows the profile of the condensate fraction of bosons $\langle n_0 \rangle / N$ at the Ground state according to (1.15).
In the end, it is also possible to identify a *critical volume per particle* v_c, describing the phase transition from a thermal gas to a Bose-Einstein condensate (BEC) in the (T, v) plane:

$$v_c = \frac{1}{g_{3/2}(1)} \left(\frac{2\pi\hbar^2}{m k_B} \right)^{\frac{3}{2}} \frac{1}{T^{3/2}}. \tag{1.16}$$

As already anticipated above for this discussion we took as references Ref. [2, 16, 17, 18, 19], where it is possible to achieve furter information about the Bose-Einstein statistics and the mathematical relations involving other important physical quantities, characterizing the ideal Bose gas.

1.2 Weakly interacting Bose gas

In general when dealing with many-body systems composed of bosonic interacting particles subjected to the action of an external field, a proper description lays on the **Bosonic Quantum Field Theory** based on the *Second Quantization formalism* [18, 20, 21].
Within this representation, each boson at a certain position $\vec{r}$ and time instant t is identified by the **bosonic field operators** of *creation* and *annihilation* $\hat{\Psi}^+(\vec{r}, t)$, $\hat{\Psi}(\vec{r}, t)$, which obey the *canonical commutation relation*

$$\left[\hat{\Psi}(\vec{r}, t), \hat{\Psi}^+(\vec{s}, t) \right] = \delta^3(\vec{r} - \vec{s}). \tag{1.17}$$

The total average number of bosons N in the system (occupying a volume V) is given by the associated total number operator $\hat{N}$, which is defined as

$$\hat{N} = \int_V d\vec{r}\ \hat{\Psi}^+(\vec{r}, t) \hat{\Psi}(\vec{r}, t); \tag{1.18}$$

then the volumetric average density is just $n = N/V$, while the average interparticle distance is $d = n^{-1/3}$.

Considering the system generally confined by an external (time-independent) potential $V(\vec{r})$, the **field Hamiltonian $\hat{\boldsymbol{H}}$** is defined as the sum of two different functional integrals: $\hat{H}_0$ the functional associated to the non-interacting regime and $\hat{U}$ the one associated to

the many-body bosonic interactions [18]. Thus being

$$\hat{H} = \hat{H}_0 + \hat{U}, \quad \hat{H}_0 = \int d\vec{r}\, \hat{\Psi}^+(\vec{r},t) H_0(\vec{r}) \hat{\Psi}(\vec{r},t) = \int d\vec{r}\, \hat{\Psi}^+(\vec{r},t) \left[-\frac{\hbar^2}{2m}\nabla^2 + V(\vec{r}) \right] \hat{\Psi}(\vec{r},t), \tag{1.19}$$

in principle it is possible to write the bosonic fields as a linear combination of the energy eigenstates $\phi_\alpha(\vec{r})$ of the non interacting Hamiltonian function $H_0(\vec{r})$ (corresponding to take a complete set of orthonormal wavefunctions

$$\hat{\Psi}(\vec{s},t) = \sum_\alpha a_\alpha(t)\phi_\alpha(\vec{r}), \qquad \hat{\Psi}^+(\vec{s},t) = \sum_\alpha a_\alpha^+(t)\phi_\alpha^*(\vec{r}). \tag{1.20}$$

with $a_\alpha,\ a_\alpha^+$ the bosonic ladder operators. In the particular case of a gas confined into a cubic box of volume $V = L^3$ with periodic boundary conditions, the eigenstate is nothing but the plane-wave $\phi_k(\vec{r})$ $\{\phi_\alpha(\vec{r})\}$) [21]:

$$V(\vec{r}) = \begin{cases} 0 & \vec{r} \in V \\ \infty & else \end{cases}; \quad \phi_k(\vec{r}) = \frac{e^{i\vec{k}\cdot\vec{r}}}{\sqrt{V}}, \quad \vec{k} = \frac{2\pi}{L}(n_x, n_y, n_z) \quad n_x, n_y, n_z = 0, \pm 1, \pm 2, \dots \tag{1.21}$$

The interaction functional $\hat{U}$, contributing to the field total field Hamiltonian $\hat{H}$ as in equation (1.19), is defined by the energy potential function associated to the many-body interactions between the bosons in the system. When the interparticle forces, governing the overall interacting regime of the bosonic gas, are characterised by a spatial range r_0 much smaller then the average interparticle distance d, meaning $\boldsymbol{r_0 \ll d}$, the gas is said to be very **dilute** (or *rarefied*). In such a regime **only two-body interactions** are significant [18, 21], all the others many-body interactions are negligible, and then the interaction potential function $U(|\vec{r} - \vec{s}|)$ associated to two bosons (at two generic positions $\vec{r},\ \vec{s}$) enables us to write the interaction functional $\hat{U}$ as:

$$\hat{U} = \frac{1}{2} \int d\vec{r} \int d\vec{s}\ \hat{\Psi}^+(\vec{r},t) \hat{\Psi}^+(\vec{s},t)\ U\left(|\vec{r} - \vec{s}|\right) \hat{\Psi}(\vec{r},t) \hat{\Psi}(\vec{s},t). \tag{1.22}$$

A further consequence is the possibility to describe the relative motion of two bosons (e.g. at $\vec{r}, \vec{s}$) through a wavefunction in an asymptotic expression $\Phi(\vec{r} - \vec{s})$ depending on the scattering amplitude $f(\theta)$:

$$\Phi(\vec{R}) = \Phi(\vec{r} - \vec{s}) = e^{i\vec{k}\cdot(\vec{r}-\vec{s}))} + \frac{f(\theta)}{|\vec{r} - \vec{s}|} e^{ik|\vec{r}-\vec{s}|}, \quad \vec{R} = \vec{r} - \vec{s}. \tag{1.23}$$

If in addition we also consider the gas to be at **very low temperature $\boldsymbol{T}$** (close to 0 K), then we are for sure in the low energy regime *far below the critical temperature* value T_c ($\boldsymbol{T \ll T_c}$) for the Bose-Einstein condensation and the particle momentum typical value p undergoes the following:

$$\begin{cases} E = p^2/(2m) \approx 3/2\ k_B T \\ d^2 \approx (\pi\hbar^2)/(m k_B T_c) \end{cases} \implies \frac{p r_0}{\hbar} \ll \frac{pd}{\hbar} = \sqrt{\frac{3\pi T}{T_c}} \ll 1 \implies \frac{p r_0}{\hbar} \ll 1. \tag{1.24}$$

For such p values, indicating slow particles, the *Standard Scattering Theory* ensures that the scattering amplitude $f(\theta)$ only depends on the *s-wave scattering length* a_s and by means of the *first order Born approximation* we have:

$$\begin{cases} f(\theta) \simeq -a_s \\ f(\theta) \simeq -\frac{m}{4\pi\hbar^2}\int d\vec{R}\; U(\vec{R}) \end{cases} \implies U(|\vec{r}-\vec{s}|) = g\;\delta^3(\vec{r}-\vec{s}), \quad g = \frac{4\pi\hbar^2}{m}a_s. \tag{1.25}$$

In the end the approximation scheme used allows us to consider two-body potential U as nothing but a **contact potential** [21] of amplitude g depending on the s-scattering wave length a_s.

The total field Hamiltonian for such a ***weakly-interacting*** **Bose gas** finally becomes

$$\hat{H} = \int d\vec{r}\;\hat{\Psi}^+(\vec{r},t)\left[-\frac{\hbar^2}{2m}\nabla^2 + V(\vec{r})\right]\hat{\Psi}(\vec{r},t) + \frac{g}{2}\int d\vec{r}\;\left(\hat{\Psi}^+(\vec{r},t)\right)^2\left(\hat{\Psi}(\vec{r},t)\right)^2, \tag{1.26}$$

leading to the following **field dynamical equation** (with $H_0(\vec{r})$ as in (1.19)):

$$i\hbar\partial_t\hat{\Psi} = \left[\hat{\Psi},\hat{H}\right] \implies i\hbar\partial_t\hat{\Psi}(\vec{r},t) = H_0(\vec{r})\hat{\Psi}(\vec{r},t) + g\hat{\Psi}^+(\vec{r},t)\hat{\Psi}^2(\vec{r},t), \tag{1.27}$$

where the right hand side term of the equation on the left, is nothing but the commutator of the field operator $\hat{\Psi}$ with the field Hamiltonian $\hat{H}$, which leads to the final equation on the right by considering the canonical commutation relation (1.17) and the form of $\hat{H}$ given by (1.26).

Note that the very low temperature condition, $T \ll T_c$, should imply that the **zero mode $\vec{k}=\mathbf{0}$** state (at energy $\epsilon_k = \hbar^2k^2/(2m) = 0$), corresponding to the *Ground state* of the system, is **macroscopically occupied**. Such an observation agrees with the Bose Einstein condensation effect, previously introduced within the ideal non interacting model in subsection 1.1, and in fact, by considering $n_{\vec{k}}$ the average number of bosons per mode $\vec{k}$, the total average number of particles N results the sum of two different contributions (see Ref. [21, 22]):

$$N = \sum_{\vec{k}} n_{\vec{k}} = n_0 + \sum_{\vec{k}\neq 0} n_{\vec{k}}\;, \quad N \simeq n_0 \gg 1 \quad \text{for} \;\; n_0 \gg n_{\vec{k}} \quad \forall\vec{k}\neq 0 \tag{1.28}$$

where n_0 is the average number of particles condensed at the Ground state.
The latter assumption taken in the formula above sets the bases of the ***Bogoliubov Approximation***, where the zero mode bosonic ladder operators a_0 and a_0^+ are seen as commuting operators and can be written as $a_0 = \sqrt{N}e^{i\eta}, a_0^+ = \sqrt{N}e^{-i\eta}$. In this way equation (1.20) for the case $V = 0$ becomes

$$\hat{\Psi}(\vec{r},t) = a_0(t)\phi_0(\vec{r}) + \sum_{\vec{k}\neq 0} a_{\vec{k}}\phi_{\vec{k}}(\vec{r}) \simeq \sqrt{N}e^{i\eta}\phi_0(\vec{r}) + \Delta\psi, \quad \Delta\psi = \sum_{\vec{k}\neq 0} a_{\vec{k}}\phi_{\vec{k}}(\vec{r}) \tag{1.29}$$

which applied to the field dynamical equation (1.27) gives $\eta = \frac{gN}{V\hbar}t$ showing how this approximation is a quite reasonable solution for this case.

However when the system generically couples to an external potential $V(\vec{r})$, then the expansion (1.20) done with respect to the set of the Hamiltonian H_0 eigenstates does not match with the Bogoliubov approximation. Indeed, in these cases it is required the ***Generalized Bogoliubov approach*** [21, 22], where basically the previous approximation scheme is extended by considering the following new form of the field operator:

$$\hat{\Psi}(\vec{r},t) = \sum_{\ell} A_\ell(t)\phi_\ell(\vec{r}) = \psi(\vec{r},t) + \Delta\psi(\vec{r},t), \tag{1.30}$$

$$\psi(\vec{r},t) = A_0(t)\phi_0(\vec{r}) = \sqrt{N}\phi_0(\vec{r}), \quad \Delta\psi(\vec{r},t) = \sum_{\ell\neq 0} a_\ell\phi_\ell(\vec{r}). \tag{1.31}$$

This expansion for the bosonic field operator $\hat{\Psi}$ is done with respect to both **unknown** basis $\{\phi_\ell(\vec{r})\}$ and mode operators $\{A_\ell(t)\}$ satisfying the Bogoliubov approximation property $[A_0, A_0^+] \simeq 0$.

This picture enables us to reduce the bosonic field operator into a single-particle wavefunction $\psi(\vec{r},t)$, known as the **condensate wavefunction** (or **order parameter**), with an operator $\Delta\psi(\vec{r},t)$ associated to the **vanishing number of excited bosons** out of the Ground state. In particular the *statistical average* $\langle\Delta\psi\rangle$ of this last operator (done with respect $|E_0\rangle$ the energy ground eigenstate) regards both the *quantum fluctuations* and *thermal fluctuations* which are negligible since the gas is ultracold and very diluted. At $T = 0$ and at thermodynamic limit ($N, V \to \infty, n = const$) it follows

$$\langle\Delta\psi\rangle \to \langle E_0|\,\Delta\psi(\vec{r},t)\,|E_0\rangle \simeq 0 \implies \left\langle\hat{\Psi}\right\rangle \to \langle E_0|\,\hat{\Psi}(\vec{r},t)\,|E_0\rangle \simeq \psi(\vec{r},t). \tag{1.32}$$

In the light of all of this (see Ref. [21, 22]), taking the expectation value of both side of the dynamical equation (1.27), we firstly can consider

$$i\hbar\partial_t\left\langle\hat{\Psi}(\vec{r},t)\right\rangle = H_0(\vec{r})\left\langle\hat{\Psi}(\vec{r},t)\right\rangle + g\left\langle\hat{\Psi}^+(\vec{r},t)\hat{\Psi}^2(\vec{r},t)\right\rangle, \tag{1.33}$$

and after some mathematical manipulations exploiting formulas (1.31) and (1.32) we derive the **Gross-Pitaevskii equation (GPE)**

$$i\hbar\partial_t\psi(\vec{r},t) = H_0(\vec{r})\psi(\vec{r},t) + g|\psi(\vec{r},t)|^2\psi(\vec{r},t). \tag{1.34}$$

It is important to notice how, thanks to this *Mean field* procedure, the model in **Second Quantization formalism for a weakly-interacting Bose gas in the purely quantum regime of Bose-Einstein condensation can be reduced to a model in First Quantization scheme** with a single-particle wavefunction $\psi(\vec{r},t)$ describing the condensate as a unique macroscopic body. In particular we can also see that the dynamical equation (1.34) is nothing but a Schrodinger equation (which well describes the non interacting regime) with an *additional cubic non linear term*, which indeed describes the **quantum regime** of the fully and macroscopically occupied lowest-energy quantum state.

1.3 The Gross-Pitaevskii model of the condensate

The Gross-Pitaevskii model of a condensate, based on the GPE (1.34), avoids to describe it as a many-body system, composed by N weakly-interacting bosonic particles of mass m at ultracold temperatures and governed by a many-body Schrödinger equation associated to a many-body wavefunction $\psi(\vec{r}_1, \ldots, \vec{r}_N, t)$ [2]. In fact, the whole system is instead considered a *"unique macroscopic body"*, described by a single-particle wavefunction $\psi(\vec{r}, t)$, with the following normalization rule:

$$N = \int d\vec{r}\, |\psi(\vec{r}, t)|^2, \quad M = mN \ \text{ (the total condensate mass).} \tag{1.35}$$

Such a condensate wavefunction $\psi(\vec{r}, t)$, as seen before in subsection (1.2), is the solution of the the Gross-Pitaevskii equation (GPE), defined in equation (1.34), which can be written in its following extended form by considering the non interacting Hamiltonian H_0 according to (1.19):

$$i\hbar\partial_t\psi(\vec{r}, t) = -\frac{\hbar^2}{2m}\nabla^2\psi(\vec{r}, t) + V(\vec{r}, t)\psi(\vec{r}, t) + g|\psi(\vec{r}, t)|^2\psi(\vec{r}, t); \tag{1.36}$$

with on the right hand side receptively the kinetic, (time-dependent) external potential and interaction energetic terms. Remind that the cubic non-linear term, defined by the interaction amplitude g, derives from the two-body mean field interactions between extremely close atoms (in presence of the contact potential U (1.25) due to the weakly-interacting regime we are considering, see section 1.2).
Considering its definition (1.25), g depends on the atomic species of the condensate with its own s-wave scattering length value a_s (e.g. ^{23}Na $a_s = 2.8$ nm), and the interactions are ***repulsive*** for $g > 0$, ***attractive*** for $g < 0$ and absent when $g = 0$.

This model implies also that the field Hamiltonian $\hat{H}$, defined within the Second Quantization scheme in equation (1.19), here corresponds to the following functional integral $\mathcal{H}$ [2, 10, 21] associated to the condensate wavefunction $\psi(\vec{r}, t)$ (instead of the field operators $\hat{\psi}$, $\hat{\psi}^+$):

$$\mathcal{H} = \int d\vec{r}\, \left[\frac{\hbar^2}{2m}|\nabla\psi(\vec{r}, t)|^2 + V|\psi(\vec{r}, t)|^2 + \frac{g}{2}|\psi(\vec{r}, t)|^4\right] = E_{kin} + E_{pot} + E_{int}. \tag{1.37}$$

where E_{kin}, E_{pot}, E_{int} are respectively the kinetic, the potential and the interaction energies of the whole system.

Note that the condensate wavefunction $\psi(\vec{r}, t)$ is a complex function and it is possible to express it in terms of the condensate *real valued* (numerical) **density** and **phase distributions functions** $\boldsymbol{n}(\vec{\boldsymbol{r}}, \boldsymbol{t})$, $\boldsymbol{S}(\vec{\boldsymbol{r}}, \boldsymbol{t})$, equivalently also called fields:

$$\psi(\vec{r}, t) \ = \ \sqrt{n(\vec{r}, t)}\, e^{iS(\vec{r}, t)}, \quad \text{with} \ \ |\psi(\vec{r}, t)|^2 = n(\vec{r}, t) \tag{1.38}$$

Such a formula, called *Madelung Transform*, is crucial whenever the condensate is described as a fluid, within a *fluid dynamics interpretation* of the Gross-Pitaevskii equation, as we will see in chapter 2 and on Ref. [2].

1.3.1 The time-independent Gross-Pitaevskii equation

The entire following discussion is based on Ref. [2].

In the particular case of a **time-independent external potential** $V(\vec{r},t) = V(\vec{r})$, the solution of the GPE $\psi(\vec{r},t)$ can be assumed to satisfied the following condition

$$\psi(\vec{r},t) = \psi(\vec{r})\ e^{-i\mu t/\hbar}, \quad n(\vec{r},t) = |\psi(\vec{r})|^2 \ \text{ (constant in time)} \tag{1.39}$$

where $\psi(\vec{r})$ is the time-independent solution of the GPE and $\mu = const$ is the *chemical potential* (the phase freely evolves with time and uniformly in the system).
Applying this ansatz to the GPE (1.36), we recover the **Time-independent Gross-Pitaevskii equation**

$$\mu\psi(\vec{r}) = -\frac{\hbar^2}{2m}\nabla^2\psi(\vec{r}) + V(\vec{r})\psi(\vec{r}) + g|\psi(\vec{r})|^2\psi(\vec{r}), \tag{1.40}$$

from which by first multiplying both sides by $\psi^*(\vec{r})$ and then integrating and looking to (1.37) we obtain that energy eigenvalue of the time-independent GPE μ [2] is:

$$\mu = \frac{1}{N}(E_{kin} + E_{pot} + 2E_{int}) \quad \text{with } N = \int d\vec{r}\, n(\vec{r},t) \tag{1.41}$$

Nowadays, several experimental studies on atomic condensates have been based on bowl-like confining potential $V(\vec{r})$. Here the following of this subsection would like to analyse some trivial but important cases of time-independent (*stationary*) external potentials.

If there is **no external trapping potential**, $V = 0$, the system is considered to be of infinite extension and governed by the time-independent GPE (1.40) which is now

$$\mu\psi(\vec{r}) = +g|\psi(\vec{r})|^2\psi(\vec{r}) \implies n(\vec{r}) = |\psi(\vec{r})|^2 = \mu/g = const. \tag{1.42}$$

This way, since the parameters $\mu,\ g$ are defined as constants, then also the square norm of the stationary solution needs to be a constant implying that this last $\psi(\vec{r})$ is a **real valued** function representing an *infinitely large uniform condensate* with

$$\psi(\vec{r}) = \psi_0 = \sqrt{\mu/g}, \quad n = n_0 = |\psi_0|^2 = \mu/g, \tag{1.43}$$

and mass density $\rho = \rho_0 = m\mu/g$ (Ref. [2]).

The insertion of a *hard domain wall* in a such configuration would correspond to the case of a **semi-infinite** confined condensate. Considering for the sake of simplicity a *one-dimensional* trapping potential $V(x)$

$$V(x) = \begin{cases} \infty & x < 0 \\ 0 & x \geq 0 \end{cases}, \tag{1.44}$$

we can note how the (one-dimensional) GPE in equation (1.42) is still valid, but only for $x \geq 0$ and presents two important conditions: at $x = 0$ no particle exists, $\psi(0) = 0$,

while far away from the wall ($x \to \infty$) $\psi \to \psi_0$. So such a system is governed by following one-dimensional time-independent GPE

$$\mu\psi(x) = -\frac{\hbar^2}{2m}\frac{\partial^2\psi(x)}{\partial x^2} + g|\psi(x)|^2\psi(x) \quad \text{for } x \geq 0 \tag{1.45}$$

correctly solved by

$$\psi(x) = \psi_0 \tanh\left(\frac{x}{\xi}\right), \quad \psi_0 = \sqrt{\frac{\mu}{g}}. \tag{1.46}$$

The complex wavefunction is said to *heal* at the boundary according to the parameter ξ, called **healing length**, which represents the characteristic scaling of the spatial changes of the wavefunction ψ, and then also of the density n [2]. Thus by balancing the scaling of each term on the right-side of equation (1.45) ξ is defined as:

$$\xi = \frac{\hbar}{\sqrt{gmn_0}}, \tag{1.47}$$

highlighting the fact that the condensate presents repulsive ($g > 0$) interparticle interactions.

Such a confinement could be extended to the case of an infinite one-dimensional square potential well, composed by two infinite domain walls. For sake of simplicity, let us consider the potential well centered in $x = 0$, with the two walls respectively at a distance $\pm L$ (width of $2L$) much larger than the healing length ξ. Then here, the equations (1.45) and (1.46) describes the local behaviour of the wavefunction $\psi(x)$ near each wall ($x = \pm L$) allowing us to write:

$$\psi(x) = \begin{cases} \psi_0 & -L < x < L, \\ \psi_0 \tanh\left[(L-x)/\xi\right] & x \simeq +L, \\ \psi_0 \tanh\left[(L+x)/\xi\right] & x \simeq -L. \end{cases} \tag{1.48}$$

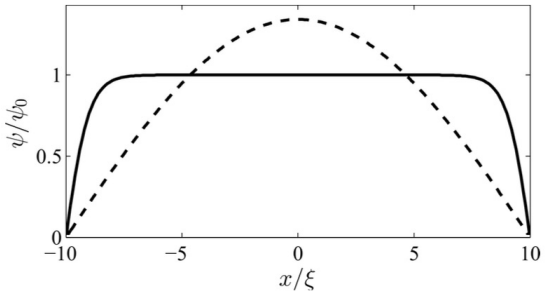

Figure 1.2: Profile of the condensate wavefunction ψ (in terms of ψ_0) as function of the position x (in terms of ξ) in the case of a one-dimensional infinite square potential well (here of width 20ξ centered in $x = 0$). Dashed curve for $g = 0$ and solid curve for $g > 0$. Figure taken from Ref. [2].

These conditions underline that, far from the two domain walls the profile of ψ would be flat (for $-L < x < L$) recovering its *bulk value* ψ_0, while as approaching to the boundaries (for $x \simeq \pm L$) it would quickly tend to zero, as an hyperbolic tangent $\tanh\left[(L \pm x)/\xi\right]$, according on healing length ξ (much smaller than L). Such a profile for the wavefunction ψ is quite different from the one describing a non-interacting condensate, corresponding to $g = 0$, analogously confined between two hard walls: the ground state would be $\psi \sim \sin(\pi x/L)$ (given by the Schrödinger equation). Then as one can see in Figure 1.2, the presence of interparticle interactions broaden and flatten the condensate wavefunction profile and consequently also the density one.

1.3.2 Stationary solutions in different harmonic potentials

The entire following discussion is based on Ref. [2].

So far we have considered just a trivial stationary potential ($V = 0$), but in general one of the most common ways of confining a condensate lays on the use of a (time-independent) **harmonic trap**.

Considering in particular the *spherically symmetric* case, the trapping potential $V(\vec{r})$ at a frequency ω_r is of the form

$$V(\vec{r}) = \frac{1}{2} m \omega_r^2 r^2 \quad \text{with} \quad r = \sqrt{|\vec{r}|^2} = \sqrt{x^2 + y^2 + z^2} \tag{1.49}$$

characterized by the *harmonic oscillator length* ℓ_r (its characteristic length scale)

$$\ell_r = \sqrt{\frac{\hbar}{m\omega_r}}. \tag{1.50}$$

It also possible to take into account the so called *interaction parameter* $\frac{Na_s}{\ell_r}$ which allows us to better identify the three physical interactions regimes: no interactions ($g = 0$), *strong repulsive* interactions ($\frac{Na_s}{\ell_r} \gg 1$) and *weak* interactions ($\left|\frac{Na_s}{\ell_r}\right| \ll 1$).

The **strong repulsive interactions** have the main effect (similarly to the one-dimensional infinite square well case, visible in Figure 1.2) of broadening and flattening the condensate wavefunction profile. For such a case a good analytic solution is given by the *Thomas-Fermi approximation* which neglects the spatial variations represented by the $\nabla^2\psi(\vec{r})$ term of the GPE giving:

$$\mu\psi(\vec{r}) = \frac{1}{2} m \omega_r^2 r^2 \psi(\vec{r}) + g|\psi(\vec{r})|^2 \psi(\vec{r}). \tag{1.51}$$

The definition of the density field $n(\vec{r})$ (1.38), entailing that it is positive valued, allows us to write

$$n(\vec{r}) = |\psi(\vec{r})|^2 = \frac{\mu}{g}\left(1 - \frac{m\omega_r^2 r^2}{2\mu}\right) \quad \text{for} \quad \mu \geq \frac{1}{2} m \omega_r^2 r^2; \quad \text{otherwise} \quad n(\vec{r}) = 0, \tag{1.52}$$

or equivalently in terms of the *Thomas-Fermi radius* $R_r = (\frac{2\mu}{m\omega_r^2})^{\frac{1}{2}}$ [2] as

$$n(r) = \begin{cases} m\omega_r^2(R_r^2 - r^2)/(2g) & r \leq R_r \\ 0 & r > R_r \end{cases}. \tag{1.53}$$

Note that this density profile corresponds to an inverted parabola and approximates very well the true numerical solution, which differs only at the boundaries where the neglected term here is significant reaching zero values through an inversion of the slope.

When the harmonic potential V is *anisotropic* in the three-dimensional space, with a frequency $\bar{\omega} = (\omega_x\omega_y\omega_z)^{\frac{1}{3}}$, and can be written as

$$V(x,y,z) = \frac{m}{2}(\omega_x^2x^2 + \omega_y^2y^2 + \omega_z^2z^2), \quad \bar{\ell} = \sqrt{\frac{\hbar}{m\bar{\omega}}}, \tag{1.54}$$

with $\bar{\ell}$ the characteristic length, then we could generalize the Thomas-Fermi approximation for $Na_s/\bar{\ell} \gg 1$ considering an ellipsoidal surface of the three Thomas-Fermi Radii R_x, R_y, R_z such that:

$$\mu = \frac{1}{2}m\omega_x^2R_x^2 = \frac{1}{2}m\omega_y^2R_y^2 = \frac{1}{2}m\omega_z^2R_z^2 \tag{1.55}$$

$$n(x,y,z) = \begin{cases} (\mu/g)\left[1 - (x/R_x)^2 - (y/R_y)^2 - (z/R_z)^2\right] & \text{only within the ellipsoid} \\ 0 & \text{otherwise} \end{cases}. \tag{1.56}$$

Meanwhile the **weak interactions** (either positive or negative) case can be studied through a ***variational approach*** [2]. In the **limit of no interactions** $g = 0$ the GPE is just the (stationary) Schrödinger equation presenting a Gaussian ground state harmonic oscillator solution

$$\psi(\vec{r}) = \psi(r) = \left(\frac{N}{\pi^{3/2}\ell_r^3}\right)^{1/2} \exp\left(-\frac{r^2}{2\ell_r^2}\right). \tag{1.57}$$

So for the weakly interacting confined condensate we can consider the following Gaussian *trial wavefunction* of width $\sigma\ell_r$, with σ the *variational parameter* and ℓ_r the harmonic oscillator length (1.50):

$$\psi(\vec{r}) = \psi(r) = \left(\frac{N}{\pi^{3/2}\sigma^3\ell_r^3}\right)^{1/2} \exp\left(-\frac{r^2}{2\sigma^2\ell_r^2}\right). \tag{1.58}$$

Note that this method, coherently to equation (1.57), requires $g = 0$ for $\sigma = 1$ and calculating the energetic functional integral (1.37) we obtain the following energy spectrum

$$E(\sigma) = \hbar\omega_r N\left[\frac{3}{4\sigma^2} + \frac{3\sigma^2}{4} + \frac{\sigma^{-3}}{\sqrt{2\pi}}\left(\frac{Na_s}{\ell_r}\right)\right]. \tag{1.59}$$

The variational solution is nothing but the lowest energetic variational state, corresponding to the minimum of $E(\sigma)$ and associated to the variational parameter σ_{min}. It is possible to plot the energetic spectrum function $E(\sigma)$ (1.59) for some values of the interaction parameter Na_s/ℓ_r, as in Figure 1.3, in order to show the different behaviours according to where the interactions are repulsive or attractive [2]:

- ***repulsive interactions*** have a spectrum $E(\sigma)$ diverging to infinity for $\sigma \to 0$ due to the first kinetic energy term and the third interaction energy term, and also for $\sigma \to \infty$ due to the second potential energy term. Being $E(1) = 3/2\ N\hbar\omega_r$ the non interacting ground state energy, the condensate size enlarges increasing g and σ_{min}.
- ***attractive interactions*** presents a divergence to minus infinite of the $E(\sigma)$ as $\sigma \to 0$ due to the third negative term. Despite this limit corresponds to unstable ground state (a wavepacket of zero width), for weak attractions $\left|\frac{Na_s}{\ell_r}\right| \ll 1$ at non zero width there exists a stable condensate of finite size, corresponding to a energy spectrum *local minimum*. Instead stronger attractions makes the condensate narrower and more peaked up to some *critical value attraction value*, after which there are no more stable solutions and all the states collapse to zero width.

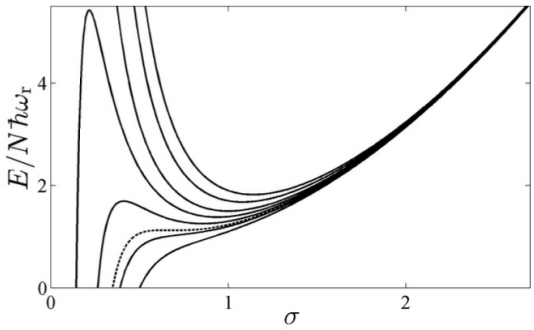

Figure 1.3: Profiles of the energy $E/(N\hbar\omega_r)$ as function of the variational parameter σ according to formula (1.59), for different fixed interaction parameter Na_s/l_r, here $\{-1,\ -0.75,\ -0.67,\ -0.5,\ -0.25,\ 0,\ 0.5,\ 1\}$ from top to bottom. Dashed curve for $Na_s/l_r = -0.67$, representing the critical point. Figure taken from Real Ref. [2].

Condensates of reduced dimensionality.
At this point we could conclude this section by recalling that **the form of the trapping potential gives the shape to the condensate**: we have analyzed the case of a spherical bounded condensate and the more generalized one of an ellipsoidal condensate.
In particular it is worth to mention that by exploiting the different possible anisotropies of a harmonic potential V defined as equation (1.54) we could obtain a description of a condensate in a reduced dimensionality. Indeed when in a highly elongated harmonic trap (i.e. $\omega_x, \omega_y \gg \omega_z$) the transverse potential energy scale is $\hbar(\omega_x\omega_y)^{1/2} \gg \mu$ the chemical potential, the only dominating dynamics is along the z direction, with effective reduction to a *one-dimensional condensate*. Similarly in a highly flatten harmonic trap

(i.e. $\omega_x, \omega_y \ll \omega_z$) when $\hbar\omega_z \gg \mu$ the condensate is *two-dimensional*.
In the following, we briefly show how to obtain a GPE in both reduced dimensions.
Let us first consider a generic representation of the wavefunction confining the condensate along a direction where essentially it is locked: a suitable form is the already used the Gaussian ground harmonic oscillator state here written as:

$$G_{x_i}(x_i) = \frac{1}{(\pi\ell_{x_i}^2)^{1/4}} e^{-x_i^2/(2\ell_{x_i})^2}, \quad \ell_{x_i} = \sqrt{\frac{\hbar}{m\omega_{x_i}}}, \quad \text{for } (x,y,z) = (x_1, x_2, x_3). \tag{1.60}$$

At this point we can assume

$$\begin{cases} \psi(x,y,z,t) = \psi_z(z,t)G_x(x)G_y(y) \;\; \text{with} \;\; N = \int dz|\psi_z|^2 & \text{if} \;\; \omega_x, \omega_y \gg \omega_z \\ \psi(x,y,z,t) = \psi_\perp(x,y,t)G_z(z) \;\; \text{with} \;\; N = \int dxdy|\psi_\perp|^2 & \text{if} \;\; \omega_x, \omega_y \ll \omega_z \end{cases} \tag{1.61}$$

and by applying them to the GPE and manipulating a little bit the results we can write down the **one-dimensional time-independent GPE**,

$$\mu_{1D}\psi_z(z) = -\frac{\hbar^2}{2m}\frac{d^2\psi_z(z)}{dz^2} + g_{1D}|\psi_z(z)|^2\psi_z(z) + \frac{1}{2}m\omega_z^2 z^2\psi_z(z), \tag{1.62}$$

$$\text{with} \quad g_{1D} = \frac{g}{2\pi\ell_x\ell_y}, \quad \mu_{1D} = \mu - \frac{\hbar\omega_x}{2} - \frac{\hbar\omega_y}{2}, \tag{1.63}$$

and the **two-dimensional time-independent GPE**

$$\mu_{2D}\psi_\perp = -\frac{\hbar^2}{2m}\left(\frac{d^2\psi_\perp}{dx^2} + \frac{d^2\psi_\perp}{dy^2}\right) + g_{2D}|\psi_\perp|^2\psi_\perp + \frac{1}{2}m(\omega_x^2x^2 + \omega_y^2y^2)\psi_\perp, \tag{1.64}$$

$$\text{with} \quad g_{2D} = \frac{g}{\sqrt{2\pi}\ell_z}, \quad \mu_{2D} = \mu - \frac{\hbar\omega_z}{2}. \tag{1.65}$$

Notice that the physical quantities μ and g, respectively the chemical potential and the amplitude of the contact potential associated to the two-body interactions, are now in such model of a reduced dimensionality identified by the subscript 1D or 2D according to which model we are going to consider, a one-dimensional model or a two-dimensional one.

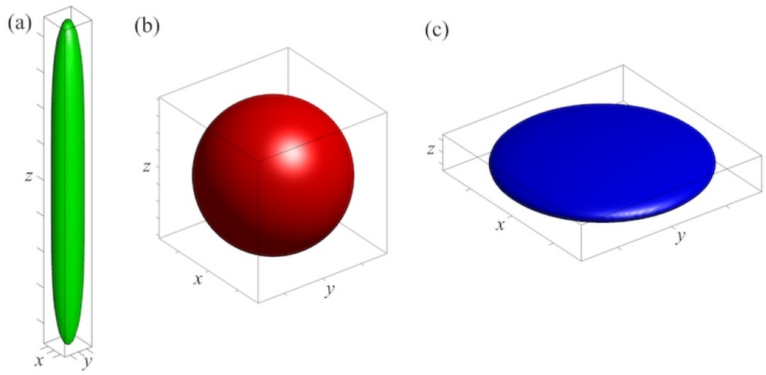

Figure 1.4: Representation of the most common shapes for a BCE, realizable by meas of an asymmetric harmonic trapping potential: (a) cigar (quasi one-dimensional) condensate for $\omega_x, \omega_y > \omega_z$, (b) spherical condensate for $\omega_x = \omega_y = \omega_z$, and (c) pancake (quasi two-dimensional) condensate for $\omega_x, \omega_y < \omega_z$. Picture taken from Ref. [2].

Chapter 2

Superfluid vortices and Point-Vortex Model

This chapter focuses on showing the deep connection existing between the Gross-Pitaevskii model for a condensate and the fluid dynamics. We will firstly analyze the Hydrodynamic picture of this model discussing the *superfluid dynamics equations*. Then, within this interpretation, we will mainly focus on the nature of quantum vortices characterizing a superfluid, analyzing their point-like description in both cases of infinitely large and confined quasi two-dimensional condensates. The end of the chapter is dedicated to the introduction of the concept of *"massive" quantum vortices* and of its effective point-like modeling.

2.1 Fluid dynamics interpretation of the GPE

The modeling of the condensate through the *Gross-Pitaevskii* equation (discussed in section 1.3) exhibits a deep connection with a fluid dynamical representation, such that we can talk about the **Hydrodynamic picture** of the condensate.

The starting point of this interpretation lays on the equation (1.38), regarding the complex valued condensate wavefunction $\psi(\vec{r},t)$: such a formula is better known as the ***Madelung transform*** and implies a physical description of the system in terms of the numerical density $n(\vec{r},t)$ and the phase $S(\vec{r},t)$ functions (both real valued),

$$\psi(\vec{r},t) = \sqrt{n(\vec{r},t)}\; e^{iS(\vec{r},t)}. \tag{2.1}$$

Taking into account the definition of the velocity field $\vec{v}(\vec{r},t)$ associated to the flow of the condensate we obtain

$$\vec{v}(\vec{r},t) = \frac{\hbar}{2\pi m|\psi|^2}\left(\psi^*\nabla\psi - \psi\nabla\psi^*\right) = \frac{\hbar}{m}\vec{\nabla}S(\vec{r},t), \tag{2.2}$$

while the functional Hamiltonian, defined in (1.37) and associated to the condensate wavefunction ψ, within this notation reduces to the following energy integral H [2]:

$$H = \int d\vec{r} \left[\frac{\hbar^2}{2m} (\nabla\sqrt{n})^2 + \frac{mnv^2}{2} + Vn + \frac{gn^2}{2} \right] \tag{2.3}$$

Note that the first kinetic energy term E_{kin} of equation (1.37) here corresponds to the sum of first two contributions: the first is the quantum kinetic energy, vanishing for uniform condensate and coming from the zero-point motion of the system, instead the second term is the kinetic energy due to the flow of the fluid.

At this point the dynamics of the system within this picture could be derived, by applying the definition (2.1) to the Gross-Pitaevskii equation (1.36) and splitting the real part from the imaginary one. Thus, the so called **superfluid hydrodynamic equations** (Ref. [2, 21]) are of following form:

$$\frac{\partial n}{\partial t} + \vec{\nabla} \cdot (n\vec{v}) = 0, \qquad m\frac{\partial \vec{v}}{\partial t} = -\vec{\nabla} \left(\frac{mv^2}{2} + V + gn - \frac{\hbar^2}{2m} \frac{\nabla^2\sqrt{n}}{\sqrt{n}} \right) \tag{2.4}$$

The first equation is the well known classical ***continuity equation***, expressing the conservation of the total number of bosons $N = \int d\vec{r}\, |\psi(\vec{r}, t)|^2$ in the system.
Instead, in the second equation the term $\nabla^2\sqrt{n}/\sqrt{n}$ is strictly related to the ***quantum pressure P′***, which differs from the (classical) pressure P according to the following definitions:

$$P' = -\frac{\hbar^2}{4m} n\nabla^2(\ln n), \qquad P = \frac{gn^2}{2}. \tag{2.5}$$

Notice that the *pressure* P depends only on the density n, meaning that the condensate is a **barotropic fluid** [2]: constant pressure surfaces are also surfaces of constant density.
Considering such equations for the two different pressures, the second superfluid dynamic equation can be written in the equivalent following form:

$$mn \left(\frac{\partial \vec{v}}{\partial t} + (\vec{v} \cdot \vec{\nabla})\vec{v} \right) = -\vec{\nabla}(P + P') - n\vec{\nabla}V \tag{2.6}$$

The quantum pressure P', created by the zero-point motion of the fluid, contrasts any effect of condensate squashing or bending and it goes as:

$$P' \sim \frac{\hbar^2 n}{m\xi^2}, \tag{2.7}$$

with ξ the *healing length* (1.47), which is the characteristic length scale governing the spatial variations of the density n. From the latter formula it is evident how the **quantum pressure is negligible** ($P' \ll P$) **whenever the healing length ξ is much smaller then the typical length scale of the system**, meaning that the condensate is *approximately uniform* (coherently to equation (2.5)). In particular, the typical ξ value in an atomic BEC is $\xi \sim 10^{-6}$ m, and in superfluid helium (^{4}He) $\xi \sim 10^{-10}$ m.

If in addition to the latter approximation we also consider an external potential $V = 0$, it follows that the superfluid hydrodynamic equation (2.6), of the form,

$$mn\left(\frac{\partial \vec{v}}{\partial t} + (\vec{v}\cdot\vec{\nabla})\vec{v}\right) = -\vec{\nabla}P \tag{2.8}$$

reduces to the ***classical Euler equation***, with describes a nonviscous fluid.

2.2 Quantized vortices and their point-like description

In this section we will focus on the studying, within the previous discussed *Hydrodynamic picture*, one of the most important distinctive features of a superfluid, i.e. the presence of quantized vortices.

First of all, the fact that the condensate wavefunction ψ is a single valued complex function implies that the integrated variations of the phase ΔS along an arbitrary closed path γ (being $d\vec{l}$ the integration line element) results to be

$$\Delta S = \oint_\gamma \vec{\nabla}S \cdot d\vec{l} = 2\pi q, \qquad q = 0, \pm 1, \pm 2, \dots \tag{2.9}$$

This formula shows the existence, for $q \neq 0$, of a singular behaviour of the phase S: there must be a *phase defect* [2] in the region encircled by the path γ. Furthermore, its main consequence is the **quantization** of the **circulation** (see Ref. [10, 23]) defined as the following integral:

$$\oint_\gamma \vec{v}\cdot d\vec{l} = \frac{\hbar}{m}\Delta S = q\frac{h}{m}, \qquad k = q\frac{h}{m}, \quad q = 0, \pm 1, \pm 2, \dots \tag{2.10}$$

where the h/m is the *quantum of circulation*. Coherently to the Semiclassical Bohr-Sommerfeld *quantization rule*, this purely quantum effect provides the circulation of a **topological meaning**: classes of topologically-inequivalent closed paths γ, characterized by an index n (*homotopy index*), could be defined. The nature of this singularity (or topological excitations) is strictly related to the concept of the formation of a **quantized vortex line** in the condensate, as a *response to the rotation of the system*. A valid descriptive picture for the vortex is the one of an empty tube (a hole in the condensate) around which the fluid particles flow rotating in a direction defined by the sign of the discrete valued **vortex charge q**, or equivalently **vortex strength k** ($k = qh/m$). In particular the radius of the depleted region in the condensate is called **vortex core radius**, here indicated as $\boldsymbol{a_0}$ [2]. Generally speaking the vortex line could be *bent* or more specifically could be *straight*, allowing in this last case to treat the vortex as a point in a 2 *dimensional* plane perpendicular to the vortex line, since the vortex appears to be the same in all its perpendicular planes (see Figure 2.1).

From now on we will consider the case of **straight vortex line** parallel to the z axis,

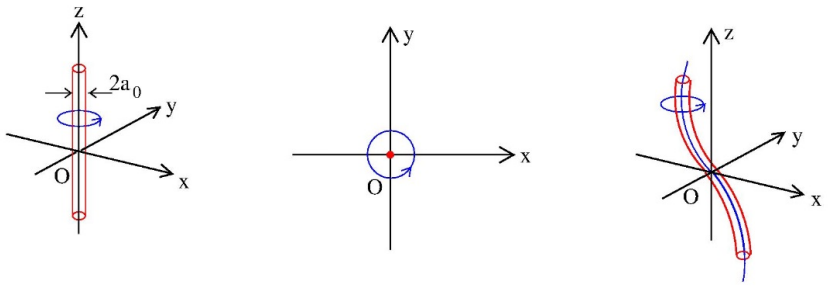

Figure 2.1: Left: Representation of a three-dimensional straight vortex line lying on the z axis as a tube of radius a_0, representing the vortex core. Middle: Point-like representation on the xy plane of the previous straight line vortex. Right: Scheme of a generic three-dimensional bent vortex line. This figure has been taken from Ref. [2].

modeling the vortex as point in a two-dimensional xy plane.

Let us consider in an **infinitely large planar condensate** (no trapping potential, $V = 0$) a circular closed path γ of radius r, *centered at the vortex position* $\vec{r}_0 = (0,\ 0)$, which corresponds to the center of the xy plane (simplified case). Expressing the position vector $\vec{r} = (x,\ y)$ in polar coordinates (r, θ) and considering equation (2.10) for the circulation, we obtain

$$\int_0^{2\pi} d\theta\ r\ \vec{v}\cdot\hat{e}_\theta \implies v_\theta(r) = \vec{v}\cdot\hat{e}_\theta = \frac{qh}{2\pi m}\frac{1}{r}; \tag{2.11}$$

showing how the azimuthal component v_θ of velocity field $\vec{v}$ decreases as moving towards regions far from the singularity (i.e. $v_\theta \to 0$ for $r \to \infty$) and increases as approaching it [2, 10, 23].

Please note that such an hyperbolic divergence of the velocity as $r \to 0$, would never be reached because of the depletion effect (for $r < a_0$) of the condensate around the vortex axis: then there is no fluid particle flowing at infinite velocity.

Going back to Cartesian coordinates and considering $\hat{e}_z$ (or equivalently $\hat{z}$) the unit vector of z axis perpendicular to the xy plane, we can write the velocity field $\vec{v}$ from equation (2.11) as:

$$\vec{v}(\vec{r}) = \frac{k}{2\pi}\hat{e}_z \times \frac{\vec{r}}{|\vec{r}|^2}, \quad k = q\frac{h}{m}, \quad q = 0, \pm1, \pm2, \ldots. \tag{2.12}$$

But being $\vec{v}$ defined with respect to the phase field S (2.2), the vortex velocity filed presents another equivalent definition in terms of the **potential flow function** $\boldsymbol{A}(\vec{\boldsymbol{r}})$:

$$\begin{aligned} \vec{v}(\vec{r}) &= \frac{k}{2\pi}\hat{e}_z \times \frac{\vec{r}}{|\vec{r}|^2} = \frac{\hbar}{m}\ \hat{e}_z \times \vec{\nabla}A(\vec{r}), \\ \vec{\nabla}S &= \hat{e}_z \times \vec{\nabla}A, \quad A(\vec{r}) = \frac{q}{2}\ln\left(\frac{x^2+y^2}{a_0^2}\right). \end{aligned} \tag{2.13}$$

However, by comparing its two definitions (2.2) and (2.13), the velocity field leads to an **apparent contraction** affecting the local rotation of the fluid, that is defined by the *vorticity field* $\vec{\omega} = \nabla \times \vec{v}$:

$$\vec{\omega} \propto \nabla \times (\vec{\nabla}S) = 0 \quad vs \quad \vec{\omega} \propto \nabla \times (\hat{e}_z \times \vec{\nabla}A(\vec{r})) = -\nabla \times [\nabla \times (A(\vec{r})\ \hat{e}_z)] \neq 0. \tag{2.14}$$

The first condition, coming form equation (2.2), contains a the gradient of the phase function S, which is singular for $\vec{r} = 0$. Then $\vec{\nabla}S$ is not an actual gradient but a **pseudo-gradient**, meaning that the vorticity $\vec{\omega}$ is zero almost everywhere, expect for the singular point ($\vec{r} \to 0$) of the phase

$$\vec{\omega} = k\delta^2(\vec{r})\ \hat{e}_z, \qquad \text{with the Dirac's delta function } \delta^2(\vec{r}) \tag{2.15}$$

Therefore the considered condensate is an **irrotazional fluid but with isolated vortex line singularities**. Additionally, since we are talking about a pseudo-gradient, the *incompressibility condition* for the fluid $\vec{\nabla} \cdot \vec{v} = 0$ strictly relates to the scaling of the spatial variations of the density function n (governed by healing length ξ) [2].
More precisely, in such a case the depletion effect associated to the presence of the quantized vortex corresponds to a condensate density field going to zero, as approaching the vortex (here at the center $(0,\ 0)$), with a characteristic profile given by the vortex core radius a_0. Typically the vortex core size is of the order of the healing length, meaning that a_0 is a tiny multiple of ξ. But, since we are in an unconfined static condensate ($V = 0$), the vortex density profile *n heals back to the background density $n_0 = const$* (density of the uniform condensate without vortices) according to ξ: here the characteristic healing profile is wider than the one given by equation (1.46) seen in section 1.3.1 (Figure 2.2). Such a slower density relaxation is due to the presence of an outwards centrifugal force generated by the flow circulating around the vortex.

However, considering a single charged point-like vortex in an unconfined homogeneous two-dimensional condensate and the healing length ξ, the whole density field profile can be approximated [2] as:

$$n(\vec{r}) = n_0\left(1 - \frac{1}{1+(\vec{r}/\xi)^2}\right), \quad n_0 = const \ \text{ background density.} \tag{2.16}$$

We remark the fact that this formula well approximates the condensate density profile, whenever the vortex core radius a_0 is of the order of the healing length ξ, which governs the spatial variations of n.

Especially, being the condensate infinitely large and ξ vanishingly small (of the order

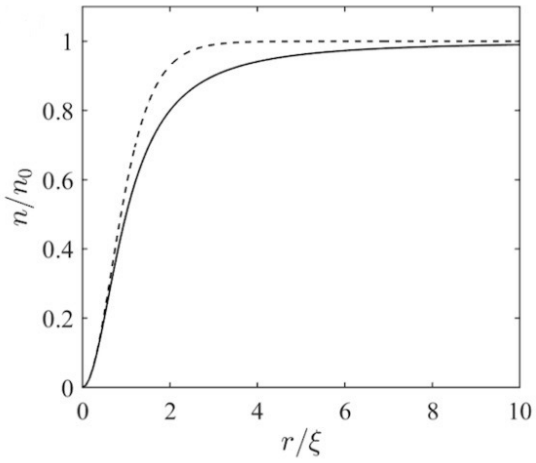

Figure 2.2: Profile of the radial density $n(r)$ in terms of the constant background density n_0 of an homogeneous condensate for a $q = 1$ vortex (solid line), compared to the healing profile for a static condensate for $V = 0$ with a density pinned to zero (dashed line). Picture taken from Ref. [2].

of micrometers), equation (2.16) gives $n \sim n_0 = const$, corresponding to a **uniform condensate**, and at the same time the fluid is **nonviscous** (according to the end of section 2.1).
It follows that in general it is realistic to **consider the condensate to be incompressible whenever the healing length ξ is much smaller than the size of the system**.

Let us now, focus on the more generic **many-vortex configuration for a two-dimensional unconfined** ($V = 0$) and **uniform** ($n \sim const$ since ξ vanishingly small) **condensate**. Recall form what we have seen above that such a system is a nonviscous, irrotational and incompressible fluid, and assuming the presence of N_v vortices, each placed at $\vec{r}_j = (x_j, y_j)$ with charge q_j (or strength $k_j = q_j h/m$), the associated velocity field $\vec{r}$ can be written as:

$$\vec{v}(\vec{r}) = \sum_{i=1}^{N_v} \frac{k_i}{2\pi} \hat{e}_z \times \frac{\vec{r} - \vec{r}_i}{|\vec{r} - \vec{r}_i|^2} = \frac{\hbar}{m} \hat{e}_z \times \sum_{i=1}^{N_v} q_i \vec{\nabla} A_i(\vec{r}) = \frac{\hbar}{m} \hat{e}_z \times \vec{\nabla} A(\vec{r}) = \frac{\hbar}{m} \vec{\nabla} S \tag{2.17}$$

$$A(\vec{r}) = \sum_{i=1}^{N_v} q_i A_i(\vec{r}) = \sum_{i=1}^{N_v} \frac{q_i}{2} \ln \left[\frac{(x - x_i)^2 + (y - y_i)^2}{a_0^2} \right], \tag{2.18}$$

$$\vec{\nabla} S = \hat{e}_z \times \vec{\nabla} A(\vec{r}) \iff S = \sum_{i=1}^{N_v} q_i \arctan\left(\frac{y - y_i}{x - x_i} \right), \quad \Delta S = \sum_{i=1}^{N_v} 2\pi q_i. \tag{2.19}$$

From these formulas which are respectively relative to the velocity field $\vec{v}$, the potential flow function $A(\vec{r})$ and the phase S, it is clear that for a many-vortex configuration the previous description (just for a vortex) formally is not changed but just generalized. Notice

also that the last expression for the ΔS (many-vortex generalization of (2.9)) implies that the circulation integral (2.10) is here generalized as [23]:

$$\oint_\gamma \vec{v} \cdot d\vec{l} = \frac{\hbar}{m}\Delta S = \sum_{i=1}^{N_v} q_i \frac{h}{m} = \sum_{i=1}^{N_v} k_i, \quad q_i = 0, \pm 1, \pm 2, \dots \quad \forall i. \tag{2.20}$$

Consequently, also the vorticity field $\vec{\omega} = \nabla \times \vec{v}$ is here the many-vortex generalization of equation (2.15), written as:

$$\vec{\omega} = \sum_{i=1}^{N_v} k_i \delta^2(\vec{r} - \vec{r}_i)\ \hat{e}_z. \tag{2.21}$$

Furthermore this system is energetically defined by the ***effective Hamiltonian***, obtained by considering the energy integral H (2.3), which apart from a constant (ensuing from the interaction term) reduces to the *kinetic energy* related to the fluid flow (see Ref. [23]):

$$H_\infty(\vec{r}_1, \dots, \vec{r}_{N_v}) = -\frac{mn_0}{4\pi} \sum_i \sum_{j \neq i} k_i k_j \ln\left[\frac{|\vec{r}_i - \vec{r}_j|}{a_0}\right]. \tag{2.22}$$

Note that this H_∞ contains all the kinetic contributions coming from two-body interactions only, since the original assumption for the system is to be a diluted condensate (i.e. negligible higher many-body interactions).

Whenever an external (time-independent) potential $V(\vec{r})$ acts on the condensates, confining it into a finite-sized spatial region, the previous vortex analysis should be slightly modified. In fact, the presence of a boundary implies **zero velocity field at the border**.
Among all the common types of confining potential (typically bucket-like or harmonic ones), let us focus on the simple case of **a circular circular trap of radius $\boldsymbol{R}$**, (much bigger the ξ), defined by a *bucket-like* trapping potential $V(\vec{r})$ of the form:

$$V(\vec{r}) = \begin{cases} 0 & |\vec{r}|^2 < R^2, \\ \infty & else. \end{cases} \tag{2.23}$$

In such a case, the presence of the domain wall can be treated as if, for each vortex in the system, there is an *opposite-charged virtual vortex symmetrically located* (with respect to the boundary) outside the bucket, ensuring that overall a purely the existence of boundary-tangent velocity field $\vec{v}$: these are known as the **"image vortices"** (see Ref. [2, 13]).
Therefore considering a configuration of N_v vortices, each at $\vec{r}_j = (x_j,\ y_j)$, each image vortex would be at a position $\vec{r}\,'_j = (x'_j,\ y'_j)$ defined as:

$$\vec{r}\,'_j = (x'_j,\ y'_j) = \frac{R^2}{x_j^2 + y_j^2}(x_j,\ y_j), \quad \rightarrow \quad x_j = \frac{R^2}{x_j^2 + y_j^2} x_i, \quad y_j = \frac{R^2}{x_j^2 + y_j^2} y_j. \tag{2.24}$$

It follows that the point-like vortex modeling including the presence of the image vortices,

representing the boundary effects, is still formally equivalent to the one for an unbounded system, but with the following potential flow function $A(\vec{r})$ and phase distribution $S(\vec{r})$:

$$A(\vec{r}) = \sum_{j=1}^{N_v} q_j \ \ln\left|\frac{\vec{r}-\vec{r}_j}{\vec{r}-\vec{r}\,'_j}\right|, \tag{2.25}$$

$$\vec{\nabla}S = \hat{e}_z \times \vec{\nabla}A(\vec{r}) \iff S = \sum_{i=1}^{N_v} q_i \left[\arctan\left(\frac{y-y_i}{x-x_i}\right) - \arctan\left(\frac{y-y_i'}{x-x_i'}\right)\right]. \tag{2.26}$$

By applying the two latter formula to the two possible and equivalent definitions for the velocity field $\vec{v}$ of the system, both contained in (2.17), one can directly write the the *effective Hamiltonian* H (2.3), still corresponding to the kinetic energy related to the flow of the fluid [14]:

$$\begin{aligned} H(\vec{r}_1,\ldots,\vec{r}_{N_v}) = &+ \sum_{i=1}^{N_v} \frac{mn_0k_i^2}{4\pi} \ln\left(1-\frac{r_i^2}{R^2}\right) \\ &- \frac{mn_0}{4\pi}\sum_i\sum_{j\neq i} k_ik_j \ln\left[\frac{R^2-2\vec{r}_i\cdot\vec{r}_j+r_i^2r_j^2/R^2}{r_i^2-2\vec{r}_i\cdot\vec{r}_j+r_j^2}\right]. \end{aligned} \tag{2.27}$$

The first energy contribution represents the interaction of all the vortices with only their own images, while the second one contains the two-body interactions between each vortex and all the others presents, included their own images.

Please remember that the two kinetic energy functions H_∞ (2.22) and H (2.27) coincide with the total effective Hamiltonians of the two different systems only apart from a constant, because in both of the two cases, the two-dimensional condensate is assumed to be uniform $n \sim n_0 = const.$ Especially in the latter case of a circular trap, the presence of the domain wall implies that the condensate density field n rapidly heals back to its background value n_0 according to equation (1.46), since the healing length ξ is vanishingly small (as assumed before to guarantee the incompressability of the fluid).

Lagrangian formalism and massive vortices.
An equivalent description of such a system could be achieved by using the *Lagrangian formalism* [13, 15] and considering first of all the following *functional Lagrangian* $\mathcal{L}$ associated to the Gross-Pitaevskii equation

$$\begin{aligned} \mathcal{L} = &\frac{i\hbar}{2}\int\left(\psi^*(\vec{r},t)\frac{\partial\psi(\vec{r},t)}{\partial t} - \frac{\partial\psi^*(\vec{r},t)}{\partial t}\psi(\vec{r},t)\right)d^2r \\ &- \int\left(\frac{\hbar^2}{2m}|\nabla\psi(\vec{r},t)|^2 + V|\psi(\vec{r},t)|^2 + \frac{g}{2}|\psi(\vec{r},t)|^4\right)d^2r. \end{aligned} \tag{2.28}$$

Indeed the *Euler-Lagrangian* equation for $\mathcal{L}$ corresponds to the GPE, defined in equation (1.37), and furthermore the second term in the formula (2.28) is the function Hamiltonian (of opposite sign) $\mathcal{H}$ (1.37).

Recall that the considered case is the one of a 2D condensate trapped into a circular domain of radius R, defined by a bucket-like potential $V(\vec{r})$ as formula (2.23). In particular we take into account $\psi(\vec{r},t)$ according to the Madelung Transform (2.1), making the following *time-dependent variational ansatz*

$$n(\vec{r}) = \begin{cases} n = const & |\vec{r}| < R, \\ 0 & |\vec{r} - \vec{r}_j| < \xi \ \wedge |\vec{r}| > R, \end{cases}$$
$$S(\vec{r}) = \sum_{i=1}^{N_v} q_i \left[\arctan\left(\frac{y - y_i}{x - x_i}\right) - \arctan\left(\frac{y - y_i'}{x - x_i'}\right) \right] \tag{2.29}$$

corresponding to the assumptions previously taken when dealing with the Hamiltonian formalism. Notice that, being N the total number of fluid particles in the circle of radius R, we can consider the constant planar numerical density n in (2.29) as $N/(\pi R^2)$. It is also important to note that the vortex solution for the phase field S explicitly depends just on positions $\vec{r} = \vec{r}(t)$ and $\vec{r}_j = \vec{r}_j(t)$'s: the time dependence implicitly enters only through these variables since the flow actually acts on the vortices leading to a vortex dynamics, which is related to the vortex velocities $\dot{\vec{r}}_j$'s as we wiil see in section 4.1.

Then the *Effective Lagrangian* L deriving from the functional (2.28) (for such a wavefunction ψ) results to be

$$\begin{aligned} L = &\sum_{j=1}^{N_v} \left[\frac{k_j mn}{2} (\dot{\vec{r}}_j \times \vec{r}_j \cdot \hat{z}) \frac{r_j^2 - R^2}{r_j^2} - \frac{k_j^2 nm}{4\pi} \ln\left(1 - \frac{r_j^2}{R^2}\right) \right] \\ &- \sum_{j>i=1}^{N_v} \frac{k_i k_j nm}{4\pi} \ln\left[\frac{R^2 - 2\vec{r}_i \cdot \vec{r}_j + r_i^2 r_j^2 / R^2}{r_i^2 - 2\vec{r}_i \cdot \vec{r}_j + r_j^2} \right]. \end{aligned} \tag{2.30}$$

that is

$$L = \sum_{j=1}^{N_v} \frac{k_j mn}{2} (\dot{\vec{r}}_j \times \vec{r}_j \cdot \hat{z}) \frac{r_j^2 - R^2}{r_j^2} - H \tag{2.31}$$

As expected this description is completely equivalent to the one above since the effective Lagrangian L correctly corresponds to the Effective Hamiltonian H (2.27). In particular the *Euler-Lagrange equations* associated to such a Lagrangian L, would correspond to the *Helmholtz-Kirchhoff equations* [13], governing the dynamics of these quantum vortices (see section 4.1, dedicated to the dynamics of vortices).

The reason why this equivalent approach was introduced lays on the fact that it is a useful tool in modeling the particular case of quantum vortices with cores filled by massive particles.

The point-like vortex description, known also as the *Point-Vortex* model, has been based on

the assumption of empty vortex cores, coherently also with the depletion effect. However, recent studies suggest that the vortex core could constitute a potential well hosting massive particles, e.g. when in a condensate there are some impurities [12]. The presence of massive particles filling the vortex core allow us to describe the vortex as a massive point (we will use the term ***massive vortex***) [13, 14, 15, 24]. This massive description leads to some intriguing effects due to the *non-zero small core mass*: i.e. the dynamics of a massive vortex is characterized by the usual trajectories of a massless vortex with superimposed small-amplitude transverse radial oscillations [13]. This effect would be later discussed in details in section 4.1, where we will properly analyze the dynamics of a vortex in both the pictures.
Instead in the following we will focus on deriving a suitable description for a system presenting massive vortices.

Therefore the massive particles confined into the vortex cores could be thought to form a new condensate: the entire system could treated as a **two-component diluted BEC condensate** [14, 15]. Let think consider its *a-component* corresponding to the condensate having N_a particles, each of atomic mass m_a, and N_v quantum point-like vortices with empty cores, which is described by the wavefunction ψ_a, according to equation (2.1) and to the time-dependent variational ansatz taken in (2.29). Instead the whole of non-rotating particles of mass m_b confined in the N_v vortex cores (each with $N_{b,j}$ particles) constitutes the *b-component* described by the wavefunction ψ_b. The vortices are spatially defined by the position vectors $\vec{r}_1, \dots, \vec{r}_{N_v}$, which here we assume to also represent the positions of all the impurity particles inside each core.

Then, the *a-component* is nothing but corresponding to the superfluid condensate confined in the circular trap of radius R, which is irrational, nonviscous and incomprissible (this is exactly the massless case analyzed before). Therefore the effective Lagrangian L_a, associated to the a-component of the whole condensate, is equivalent to the one defined in (2.30) and it is written as:

$$\begin{aligned} L_a = &\sum_{j=1}^{N_v} \left[\frac{k_j m_a n_a}{2} (\dot{\vec{r}}_j \times \vec{r}_j \cdot \hat{z}) \frac{r_j^2 - R^2}{r_j^2} - \frac{k_j^2 n_a m_a}{4\pi} \ln\left(1 - \frac{r_j^2}{R^2}\right) \right] \\ &- \sum_{j>i=1}^{N_v} \frac{k_i k_j n_a m_a}{4\pi} \ln\left[\frac{R^2 - 2\vec{r}_i \cdot \vec{r}_j + r_i^2 r_j^2 / R^2}{r_i^2 - 2\vec{r}_i \cdot \vec{r}_j + r_j^2} \right], \end{aligned} \tag{2.32}$$

where $n_a = N_a/(\pi R^2)$ is the constant numerical density of the superfluid a-component, accordingly to the ansatz (2.29).
Considering the assumptions taken for the wavefunction *b-component*, the ψ_b could be written a linear combination of Gaussian wave packets [13, 15]

$$\psi_b(\vec{r}, t) = \sum_{j=1}^{N_v} \sqrt{\frac{N_{b,j}}{\pi\sigma^2}}\, e^{\frac{-|\vec{r}-\vec{r}_j(t)|^2}{2\sigma^2}}\, e^{i\vec{r}\cdot\vec{\alpha}_j(t)}, \tag{2.33}$$

which its time dependence derives from the positions of the vortices and the time-dependent variational parameters α_j. This last ones provide the vortices of local flow velocities

$\dot{\vec{r}}_j = \hbar\vec{\alpha}_j/m_b$ $j = 1, \ldots, N_v$. The parameter σ corresponds to the width of the Gaussian and is much smaller than the distance separating two vortices (well separated vortices and very small cores $\sigma << |\vec{r}_i - \vec{r}_j|$). For further information about such a wavefunction for the massive component see Ref. [15].
By taking into account the field Lagrangian $\mathcal{L}$ associated to the massive particles wavefunction ψ_b, the effective Lagrangian of the *b-component* results to be

$$L_b = \frac{1}{2}\sum_{j=1}^{N_v} N_{b,j} m_b (\dot{\vec{r}}_j)^2, \qquad M_{b,j} = N_{b,j} m_b \tag{2.34}$$

implying that *the total effective Lagrangian* $L = L_a + L_b$ is

$$\begin{aligned} L = &\sum_{j=1}^{N_v}\left[\frac{M_{b,j}}{2}(\dot{\vec{r}}_j)^2 + \frac{k_j m_a n_a}{2}(\dot{\vec{r}}_j \times \vec{r}_j \cdot \hat{z})\frac{r_j^2 - R^2}{r_j^2} - \frac{k_j^2 n_a m_a}{4\pi}\ln\left(1 - \frac{r_j^2}{R^2}\right)\right] \\ &- \sum_{j>i}^{N_v}\frac{k_i k_j n_a m_a}{4\pi}\ln\left(\frac{R^2 - 2\vec{r}_i\cdot\vec{r}_j + r_i^2 r_j^2/R^2}{r_i^2 - 2\vec{r}_i\cdot\vec{r}_j + r_j^2}\right). \end{aligned} \tag{2.35}$$

Notice how, within such a massive vortex modeling, the presence of the non zero core mass leads to an effective "massive" Lagrangian L (2.35), differing from the massless one (2.30) only for an additional term depending on the vortex velocity and on the core mass as $M_{b,j}(\dot{\vec{r}}_j)^2$. More precisely, such a core mass term is responsible for the appearance in the associated *Euler-Lagrange equations* of a second time derivative of the vortex position, an inertial term, distinguishing the dynamics of a massive vortex form a massless one (later discussed in section 4.1).

Chapter 3

Equilibrium Vortex Patterns in a rotating superfluid

After having discussed which physical quantity drives the equilibrium description of vortices in a confined two-dimensional condensate, this chapter focuses on the analysis about the variation of the number of the formed vortices and the stability of their equilibrium configurations according to the external trap rotation. The first part is dedicated to the analysis about the global minimization of the system free energy in order to obtain the equilibrium configurations of massless vortices, corresponding to the well known vortex crystals (or lattices). While in the second part we will extend such a semi-analytical study to the generalized case of massive vortices, particularly focusing on the effects of the core mass in the equilibrium configurations.

3.1 Stable configurations of massless vortices

In the end of section 2.2, we have discussed how to model a quasi two-dimensional condensate characterized by the presence of point-like vortices. In particular, by exploiting the time-dependent variational Lagrangian approach, we obtained the effective Lagrangian defining such a system in both massless and massive vortex cases, respectively in equations (2.30) and (2.35). However, it is the system **free energy** $\boldsymbol{F}$ to play a crucial role in *determining the stability of the equilibrium configuration of the vortices* formed in a condensate confined in a rotating trap [2, 25].

Let us first consider that the **trap is circular with a radius** $\boldsymbol{R}$ sufficiently large (meaning vortex core $a \ll R$) and rotates at an ***angular velocity*** $\boldsymbol{\Omega}$ around its center $O = (0,\ 0)$ (coinciding with the origin of the xy plane). According to the nature of quantum vortices (see section 2.2), for sufficiently small rotations it is reasonable to expect very few single charged vortices, or even none, which are parallel to rotation axis. Then as the trap rotates faster and faster, the number of these vortices increases, up to reach for sufficiently high velocity Ω values a system that instead behave classically, performing a *solid-body rotation* [2, 25]. In general for both possible vortex descriptions, **the stable**

equilibrium patterns are determined by globally minimizing the free-energy function with respect to the spatial vortex coordinates $\{\boldsymbol{r}_j = (x_j,\ y_j)\}_{j=1}^N$, having previously fixed the number of vortices N and the value of rotational speed Ω.

Therefore the free-energy function F, associated to a rotating system, is of the form $\boldsymbol{F = E - \Omega L_z}$, with E the total mechanical energy and L_z the third component of the angular momentum of the system. Both terms are derivable from the effective Lagrangian $L = L(\{\boldsymbol{r}_j,\ \dot{\boldsymbol{r}}_j\}_{j=1}^N)$ defining the system, thanks to the following equation:

$$E \leftrightarrow H(\{\boldsymbol{r}_j, \dot{\boldsymbol{r}}_j\}_{j=1}^N) = \sum_{j=1}^N \left(\frac{\partial L}{\partial \dot{\boldsymbol{r}}_j} \cdot \dot{\boldsymbol{r}}_j\right) - L, \quad L_z(\{\boldsymbol{r}_j, \dot{\boldsymbol{r}}_j\}_{j=1}^N) = \sum_{j=1}^N \left(\boldsymbol{r}_j \times \frac{\partial L}{\partial \dot{\boldsymbol{r}}_j}\right) \cdot \hat{z}, \tag{3.1}$$

being $\dot{\boldsymbol{r}}_j = (\dot{x}_j, \dot{y}_j)$ the velocity of the j^{th} vortex and $H(\{\boldsymbol{r}_j, \dot{\boldsymbol{r}}_j\}_{j=1}^N)$ the energy function associated to the system and corresponding to a sort of Hamiltonian function, where the momenta are expressed in terms of the velocities.
It is also convenient to change the reference frame moving from the laboratory frame into the rotating reference frame of the trap $\{\boldsymbol{r}_j,\ \dot{\boldsymbol{r}}_j\}_{j=1}^N \to \{\boldsymbol{r}'_j,\ \dot{\boldsymbol{r}}'_j\}_{j=1}^N$ and exploiting the polar coordinates $\boldsymbol{r}'_j = (x'_j,\ y'_j) = r'_j(\cos\theta'_j,\ \sin\theta'_j)$ with $(r'_j = |\boldsymbol{r}'_j|)$, the coordinates become:

$$\boldsymbol{r}_j = r'_j \left(\cos\theta'_j \cos(\Omega t) - \sin\theta'_j \sin(\Omega t)\ ,\ \cos\theta'_j \sin(\Omega t) + \sin\theta'_j \cos(\Omega t)\right). \tag{3.2}$$

In this way the effective Lagrangian L written as a function of this new working frame variables could be named $L' = L'(\{\boldsymbol{r}'_j, \dot{\boldsymbol{r}}'_j\}_{j=1}^N)$ and its associated energy function H' is

$$H' = H'(\{\boldsymbol{r}'_j, \dot{\boldsymbol{r}}'_j\}_{j=1}^N) = \sum_{j=1}^N \left(\frac{\partial L'}{\partial \dot{\boldsymbol{r}}'_j} \cdot \dot{\boldsymbol{r}}'_j\right) - L' = H(\{\dot{\boldsymbol{r}}'_j, \dot{\boldsymbol{r}}'_j\}_{j=1}^N) - \Omega L_z(\{\dot{\boldsymbol{r}}'_j, \dot{\boldsymbol{r}}'_j\}_{j=1}^N) \tag{3.3}$$

where $L_z(\{\dot{\boldsymbol{r}}'_j, \dot{\boldsymbol{r}}'_j\}_{j=1}^N))$ and $H(\{\dot{\boldsymbol{r}}'_j, \dot{\boldsymbol{r}}'_j\}_{j=1}^N)$ are respectively the angular momentum (3^{rd} component) and the energy function defined in (3.1) w.r.t the laboratory frame but with $\boldsymbol{r}'_j = (x'_j, y'_j)$ instead of $\boldsymbol{r}_j = (x_j, y_j)$. Note that, since we are in the rotating reference frame, in the derivation of the H' we must assume the velocities to be $(\dot{r}'_j,\ \dot{\theta}_j) = 0$. Such a derivation is coherent to the one present in Ref. [13] regarding the derivation of the Hamiltonian function for a single vortex w.r.t. to the rotating reference frame.
Except for an additive constant $N\ln(R/a)$ indicating the creation of N vortices with core radius a, the free energy F corresponds to the energy function H', defined in equation (3.3), and for the sake of generality it can be expressed in term of energy units:

$$F = E - \Omega L_z = \frac{mnk^2}{4\pi} f, \quad f = E\frac{4\pi}{mnk^2} - \omega\frac{2}{mnkR^2}L_z, \quad \omega = \frac{2\pi R^2}{k}\Omega, \tag{3.4}$$

where $m,\ n,\ k = \frac{h}{m}$ are respectively the atomic mass and the numerical planar density of the condensate and the quantum of circulation; instead $\boldsymbol{f}$ and $\boldsymbol{\omega}$ are the ***dimensionless free energy*** and ***dimensionless angular velocity***. It is important to specify that **in such a rescaling** we are considering $\boldsymbol{2\pi R^2/k}$ and $\boldsymbol{R}$ to be **respectively the units of**

time and length.

Let us start our study of the equilibrium patterns taking into account first the already well known case of empty vortex core in a such a way that we can secondly extend it to the filled vortex cores case.

3.1.1 Minimization of the free energy and boundary effects issues

In the above introductory discussion, we have anticipated how at the equilibrium the vortices formed in the confined condensate are characterized by unit charge (or equivalently unit circulation). Indeed, recall that according to the energy function H (2.27), describing a many-vortex configuration in an analogous trapped two-dimensional condensate, the energetically favourite (massless) many-vortex configurations present vortex charges $q_j = \pm 1\ \forall j$, or equivalently (according to (2.20)) $k_j = q_j h/m \rightarrow k_j = \pm h/m = \pm k\ \forall j$, with $k = h/m$ the quantum of circulation.
Assuming for the sake of simplicity $q_j = +1,\ k_j = k = h/m\ \forall j$, the effective Lagrangian L defined in equation "massless" (2.30) becomes:

$$\begin{aligned} L = &\sum_{j=1}^{N} \left[\frac{kmn}{2} (\dot{\boldsymbol{r}}_j \times \boldsymbol{r}_j \cdot \hat{z}) \frac{r_j^2 - R^2}{r_j^2} - \frac{k^2 nm}{4\pi} \ln\left(1 - \frac{r_j^2}{R^2}\right) \right] \\ &- \sum_{j>i}^{N} \frac{k^2 nm}{4\pi} \ln\left[\frac{R^2 - 2\boldsymbol{r}_i \cdot \boldsymbol{r}_j + r_i^2 r_j^2 / R^2}{r_i^2 - 2\boldsymbol{r}_i \cdot \boldsymbol{r}_j + r_j^2} \right]. \end{aligned} \tag{3.5}$$

Then, according to the previously explained derivation (consisting in the equations (3.1), (3.2), (3.3) (3.4)), we used this Lagrangian L in order to obtain the dimensionless free energy f expressed with respect to the rotating reference frame, considering $|\boldsymbol{r}'_j| = r'_j \rightarrow R r_j$. This means that we *rescaled the vortex variable r'_j in units of R*, the trap radius, and we dropped the prime symbol for the sake of brevity, i.e. $0 \leq r_j \leq 1$ (actually < 1 as we are going to see in the following).

Therefore the dimensionless free energy f, coherently to (3.4), in the case of N point-like vortices with empty cores (recall core size negligible compared to the size of the system $a \ll R$) assumes the following form:

$$\begin{aligned} f = &- \sum_{j>i=1}^{N} \ln[r_i^2 + r_j^2 - 2 r_i r_j \cos(\theta_i - \theta_j)] \\ &+ \frac{1}{2} \sum_{i,j=1}^{N} \ln[1 + r_i^2 r_j^2 - 2 r_i r_j \cos(\theta_i - \theta_j)] - \omega \sum_{i=1}^{N} (1 - r_i^2) + N \ln(R/a). \end{aligned} \tag{3.6}$$

Notice that, as we expected, the first two terms corresponds to the dimensionless and rescaled version of the energy function H we obtained in equation (2.27). In particular, the first term refers to the (repulsive) interactions between any couple of "real" vortices, the second one contains the (attractive) interactions of each "real" vortex with all the

"image" vortices (not only its own image, but also all the other vortex images). Instead, the ω term ensues from the **trap rotation which generates apparent forces pulling the vortices towards the trap center**, since their overall energetic term is $+\sum_i \omega\, r_i^2$.

Such a free energy f corresponds exactly to the free-energy function reported by Campbell and Ziff in their article *"Vortex patterns and energies in a rotating superfluid"* [25], where they have faced and discussed the same problem here considered.
Their most relevant observations are the following:

- at a fixed ω and for each possible value of N, the **vortices at equilibrium form configurations made up of concentric (exactly or almost) regular polygons**, called **rings**, around the center $O = (0,\ 0)$ of the trap;
- as the rotation rate $\boldsymbol{\omega}$ **increases the distance of each ring from the center** $\boldsymbol{O}$ **decreases** and furthermore each N vortex pattern is a **physically meaningful stable pattern from a certain critical value** $\boldsymbol{\omega^*}$,
- since the system is rotational invariant, **configurations differing by a global azimuthal rotation are equivalent**.

In light of these fundamental observations, we firstly focused on minimizing the free energy f in order to verify these results and in a second moment to consider them as a solid base when studying the effects of core mass on these arrays (see section 3.2).

Since the number of massless vortices N strictly depends only on the trap rotation rate ω, by varying ω in a discrete range of values, at each of these fixed values we firstly performed the minimization of the free energy f with respect to the vortex polar coordinates $\{r_j, \theta_j\}_{j=1}^{N}$ for all the possible values of N, and we secondly determined the absolute stable configuration and the associated value N at each ω value. Doing so, we **were able to identify for each kind of** N **vortex-array a rotation rate** $\boldsymbol{\omega}$ **interval between two critical values**, out of which the considered pattern is no longer stable and the system is stable only if it increases or decreases by one the number of vortices ($N \to N-1$ or $N \to N+1$).
Especially we considered $N = 0,\ 1, \ldots,\ N_{max}$ and the range of the rotation rates was taken as $[0,\ \omega_{max}]$, with very small steps and the top value ω_{max} depending on the N_{max} value: in principle it is **possible to study both the curves of the energetic minima and the equilibrium radial position of a vortex as a function of the rotation rate**.

More precisely all the following analysis considered the vortex core radius $a = 10^{-6}$ nm (nanometers) and the trap radius $R = 50 \times 10^{-6} \implies R \gg a$ (in fact we are neglecting the vortex core size and considering an uniform condensate density).

Analytic study for the "symmetric" configurations.
The previous predictions affirm that the vortex-array is a composition of rings presenting almost or exactly a regular polygonal structure: then, for a small number N ($N < 8$), it is reasonable that the vortices form a single regular N-polygon. Actually, according

to the spatial configurations reported by Campbell and Ziff [25], the equilibrium vortex pattern consists in a single ring for $N \leq 5$, with a N-fold rotational symmetry (the regular N-polygon), while for $N > 5$ but still sufficiently small, the ring admits a vortex in the trap center $O = (0,\ 0)$ with $(N-1)$-fold symmetry (Ref. [26]). Referring to these simple cases as ***"symmetric" configurations***, the associated free energy f results be just a function of a unique radial vortex variable, since $\forall j\ r_1 = r_j$ and $\theta_j = 2\pi(j-1)/N$, and with respect to which it **can be analytically minimized**. Note that the case $N = 0$ corresponds to $f = 0$, accordingly to the fact that there are no vortices, and that those configurations with a vortex in the center are indicated as $N = (N-1) + 1$. Here in the following we show same simple example (up to 3 vortices) of the form for the *symmetric free energy* f as function of the r_1 (namely the vortex ring radius):

$$\begin{aligned}
&N = 1,\ Sym \implies f = \ln(R/a) + \ln(1 - r_1^2) - \omega(1 - r_1^2),\\
&N = 2,\ Sym \implies f = 2\ln(R/a) - \ln(4r_1^2) + 2[\ln(1 - r_1^2) + \ln(1 + r_1^2)] - 2\omega(1 - r_1^2),\\
&N = 3,\ Sym \implies f = 3\ln(R/a) - 3\ln(3r_1^2) + 3[\ln(1 - r_1^2) + 2\ln(1 + r_1^2)] - 3\omega(1 - r_1^2).
\end{aligned} \tag{3.7}$$

Considering $N = 0,\ 1, \ldots, 7$ ($N_{max} = 7$), we analytically performed the global minimization of the symmetric free-energy function f with respect to its unique variable r_1 for an ω in the discrete range $[0,\ 15]$ ($\omega_{max} = 15$) (with an ω step of 0.1). Figure 3.1 shows the curve for the symmetric free-energy minima (left panel) and the curve for the values of variable r_1 minimizing the symmetric free energy f (right panel), both plotted according the rotation rate ω.

As expected, in the left panel of Figure (3.1), we can observe how a spatial rearrangement of 6 (or 7) vortices does not correspond to a regular hexagon (or heptagon), but to a pentagon (or hexagon) with a vortex in the center. In addiction, the right panel shows

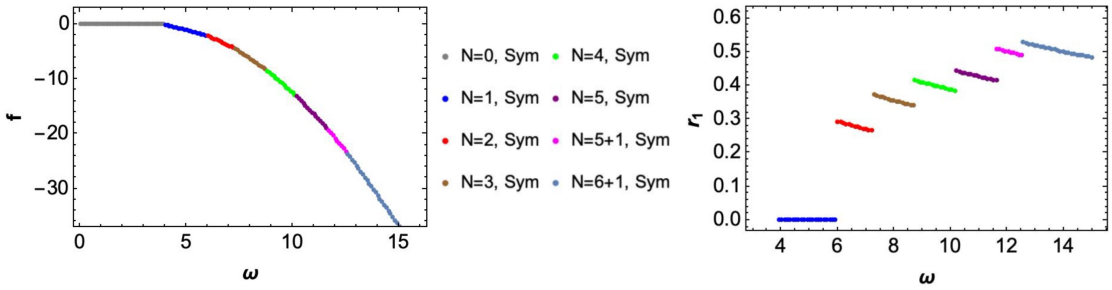

Figure 3.1: Left panel: profile of the symmetric free-energy absolute minima computed with respect to the variable r_1, identifying the radial position of all the vortices in the symmetric ring configuration. Right panel: profile of the r_1 values minimizing the symmetric free energy f. Both curves are plotted according the rotation rate ω, which discretely varies (steps of 0.1) between 0 and 15. Such analytical results show as the trap rotation is increased the system is stable only increasing its number of vortices, corresponding to a spatial configuration with a ring farther from the center.

that, when the system changes its equilibrium configuration by adding a vortex, the radial component of a vortex in the symmetric ring jumps to an higher value and then decreases up to the successive critical value where it jumps again, accordingly to our expectations. We also calculated analytically the ω values at which each N vortex pattern is no longer the stable spatial configuration and a transition $N \to N+1$ occurs: $\mathbf{0 \to 1}$ at $\omega = 3.9120$, $\mathbf{1 \to 2}$ at $\omega = 5.9955$, $\mathbf{2 \to 3}$ at $\omega = 7.2819$, $\mathbf{3 \to 4}$ $\omega = 8.7319$, $\mathbf{4 \to 5}$ at $\omega = 10.2021$, $\mathbf{5 \to 5+1}$ at $\omega = 11.6252$ and $\mathbf{5+1 \to 6+1}$ at $\omega = 12.5677$.
Notice that such values coincide with the configuration transitions shown in Figure 3.1.

As further check for such results we also studied the profile of the symmetric function f according to the radial position r_1, continuously varying in its domain $[0,\ 1]$ at a fixed rotation rate ω. Figure 3.2 compares of such free-energy profiles obtained for the $N = 0,\ 1, \ldots,\ 7$ at $\omega = 2.0$ (left panel) and $\omega = 15.0$ (right panel), showing in which configuration the free energy has the lowest local minimum coherently to the results of the global minimization done before.

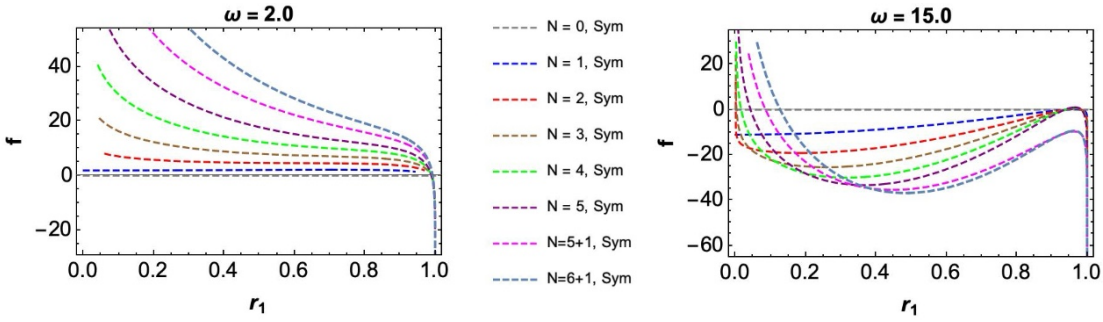

Figure 3.2: Profile of the symmetric free-energy function f considering $r_1 \in [0,1]$, for $N = 0,\ 1, \ldots,\ 7$ at rotation rate $\omega = 2.0$ (left) and $\omega = 15.0$ (right). The curve with the lowest local minimum gives corresponds to the absolute stable configuration N: at $\omega = 2.0$ there are no vortices, while at $\omega = 15.0$ the equilibrium configuration is a regular hexagon with a vortex in the center.

The *"symmetry" configuration* case, so far analyzed, is quite instructive and it has enabled us to analytically verify some of the previously announced results. In fact due to its complexity, the free-energy function f (3.6) could be *analytically minimized only for not large number vortices* N (perhaps $N < 9$).
This is why we need to approach the problem from a numerical point of view, considering that the free energy f depends on the $2N$ vortex variables, $\{r_j, \theta_j\}_{j=1}^{N}$. However this dependence can be reduced to $2N-1$, by fixing at zero one of the angles θ_j's, since at each N there are many equilibrium patterns that are equal to each other except for a global rotation around the trap centre $O = (0,0)$.

Approximation for negligible boundary effects.
Furthermore, according to the concept of "image" vortices introduced in section 2.2, recall

that **all the equilibrium configurations of N vortices**, deriving from such a free energy minimization problem, are **physically meaningful if and only if none of them is too close to the border, otherwise the vortex would collide at the wall with its respective image vortex and undergo to annihilation**.
But at the same time, the previous analytic analysis clearly shows in Figure 3.2 that the symmetric free energy f profile presents for $r_1 \to 1$ a *vertical asymptote towards negative values which grows as higher trap rotation velocities are explored.* This means that the system should present less energy values when vortices go towards the domain wall, which is nonphysical. Such an undesired effect, which also appears for the more generic and complicated free energy, complicates a lot the determination of the physically meaningful stable patterns of vortices at the equilibrium.

It is then clear that the presence of the images vortices in our descriptions leads to undesired issue, but at the same time (see Ref. [25]) their energetic contributions in the free-energy function f are very small and overall do not affect so much the resulting spatial configurations at equilibrium. Coherently to the approximation taken into account by Campbell and Ziff, we can assume **assume negligible boundary effects**, or equivalently no image vortices in the system, defining a new dimensionless free energy f_0 describing the system, related to f (3.6) in the following way:

$$\begin{aligned} f_0 =& f - \frac{1}{2}\sum_{i,j=1}^{N} \ln[1 + r_i^2 r_j^2 - 2 r_i r_j \cos(\theta_i - \theta_j)] \\ =& -\sum_{j>i=1}^{N} \ln[r_i^2 + r_j^2 - 2 r_i r_j \cos(\theta_i - \theta_j)] - \omega \sum_{i=1}^{N} (1 - r_i^2) + N \ln(R/a). \end{aligned} \tag{3.8}$$

Within this approximation, since this function f_0 only contains the contribution of the repulsive interactions between vortices and the term associated apparent centripetal force (apart from the constant $N \ln(R/a)$), the new free-energy profile should present at fixed ω and N values some local minima with respect to the vortex coordinates without the previous registered divergence towards the domain wall.

In order to ensure this and also to verify the validity of such an approximated function f_0, once again we firstly focus again on the "symmetric" configuration cases of regular polygonal vortex patterns for $N \leq 7$. Then, the previous equations for the symmetric free function f (3.7) for $N = 1,\ 2,\ 3$ here become:

$$\begin{aligned} &N = 1,\ Sym \implies f_0 = \ln(R/a) - \omega(1 - r_1^2), \\ &N = 2,\ Sym \implies f_0 = 2\ln(R/a) - \ln(4 r_1^2) - 2\omega(1 - r_1^2), \\ &N = 3,\ Sym \implies f_0 = 3\ln(R/a) - 3\ln(3 r_1^2) - 3\omega(1 - r_1^2). \end{aligned} \tag{3.9}$$

It is evident how all the logarithmic image-vortex interaction terms have been excluded. Repeating exactly the previously seen (for the function f) analytic procedure for the *symmetric* dimensionless free energy f_0, we obtain the graphs in Figure 3.3: not only the function f plotted with respect to $r_1 \in [0,\ 1]$ presents just a global minima without the

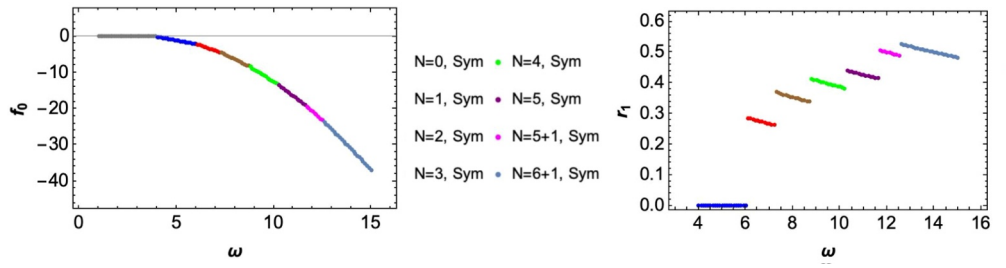

(a)

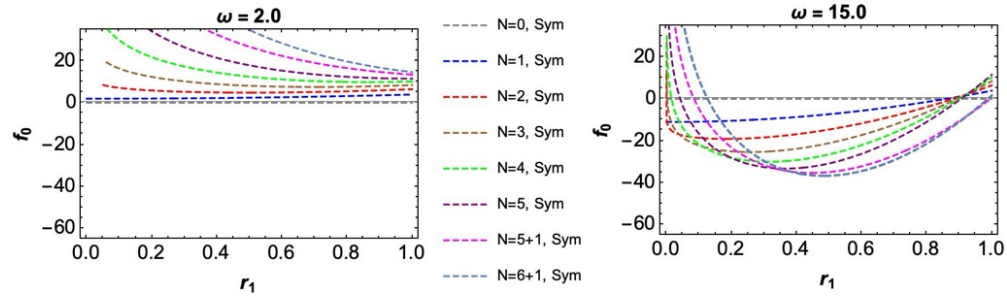

(b)

Figure 3.3: (a) Left: curve of minima of the symmetric free energy f_0, computed with respect to the radial vortex position r_1 in the symmetric ring. Right: Curve of the r_1 values minimizing the symmetric f_0 as function of ω. Both curves plotted according to rotation rate in the discrete interval $\omega \in [0,\ 15]$ (with 0.1 steps). **(b)** Profile of the symmetric free-energy function f_0 considering $r_1 \in [0,1]$, for $N = 0,\ 1, \ldots,\ 7$ at rotation rate $\omega = 2.0$ (left) and $\omega = 15.0$ (right). The curve with the lowest local minimum gives corresponds to the absolute stable configuration N: at $\omega = 2.0$ there are no vortices, while at $\omega = 15.0$ the equilibrium configuration is a regular hexagon with a vortex in the center. Note that, contrary to Figure 3.2, the free-energy function f_0 (for negligible boundary effects) does not have any vertical asymptote for $r_1 \to\ 1$.

asymptotic divergence for $r_1 \to 1$ (Figure 3.3b), the transitions of the equilibrium vortex configurations occur at ω values very close to the critical ones calculated for the (non approximated) symmetric function f (Figure 3.3a).

Numerical study about the absolute stable vortex patterns.
After this simple and analytic case has been analysed, we can proceed by **numerically solving the global minimization problem** in order to obtain the equilibrium vortex patterns at a certain angular velocity of the circular trap.
The free-energy function f_0 must be minimized, at a fixed ω value, according to the $2N$ vortex coordinates r_j's and θ_j's: actually as seen for the function f, we could fix one of the θ_j's, i.e. $\theta_1 = 0$, reducing the dependence to $2N - 1$ variables. In particular to ensure that the solution corresponds to a global minimum at certain ω value, we need to considering the following:

- for each possible value of N, the lowest local minimum of the f_0 is the smallest of the ones computed considering a finite set of different initial random configurations of *non-overlapping* vortices;
- being $N = 0,\ 1, \ldots,\ N_{max}$, from the $(N_{max} + 1)$ lowest minima obtained before at the ω value considered, we extract the absolute minimum of the free-energy, its associated spatial configuration and the corresponding value N;
- we repeat these two previous steps for all the values of the rotation rate that we consider.

By considering for $N_{max} = 21$ and for ω varying in a discrete range between 0 and $\omega_{max} = 30$ with steps of 0.3, we plotted the obtained global minima of the free energy f_0 according to the rotation angular velocity ω as in Figure 3.4a.

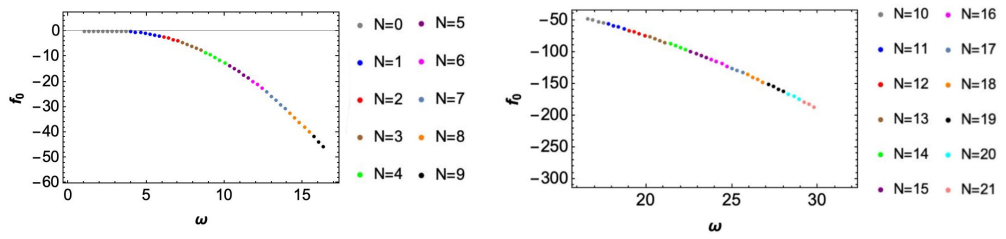

(a)

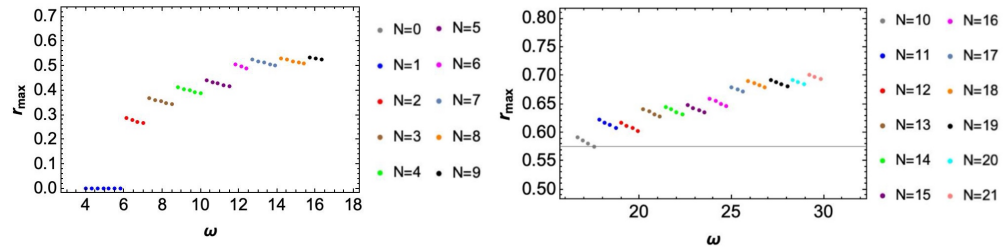

(b)

Figure 3.4: **(a)** Curves of the global minima of free energy f_0, computed numerically with respect to the radial vortex polar coordinates r_j's and θ_j's, and plotted according to the rotation rate $\omega \in (0,\ 30)$ (with 0.3 steps). **(b)** Curves of the radial position r_{max} of the farthest vortex from the center (living into the outermost ring in the corresponding equilibrium pattern) globally minimizing the f_0 with respect $\omega \in (0,\ 30)$ (with 0.3 steps). Note that in both subfigures we have considered on the left $N = 0,\ 1, \ldots,\ 9$ and $N = 10, \ldots,\ 21$ to highlight through the colors the corresponding equilibrium patter N, whose ring structure is reported in the table below.

Meanwhile, in the Figure 3.4b we plotted, with respect to the same ω range, the values of the radial position of the farthest vortex from the center $O = (0,\ 0)$ in the obtained equilibrium spatial configurations, essentially corresponding to the radial position of the outermost ring.
As expected, we find that for small angular velocity the resulting equilibrium vortex pattern is an array of few vortices: we also can note that the transitions between two subsequent configurations occurs around the critical values of ω found analytically.
We also find, for sufficiently large values of N, that not always the respective equilibrium pattern can rearrange the vortices in the same rings exactly at the same radial distances and the single vortex on the center O, due to the *intrinsic asymmetry* of the array: for this reason we assumed two vortices i and j to live on the same shell if their radial distances r_i, r_j satisfy $|r_i - r_j| \leq 2\%$ for $N < 50$, coherently to Ref. [25] (while $|r_i - r_j| \leq 5\%$ for $N > 50$, not treated in this work).

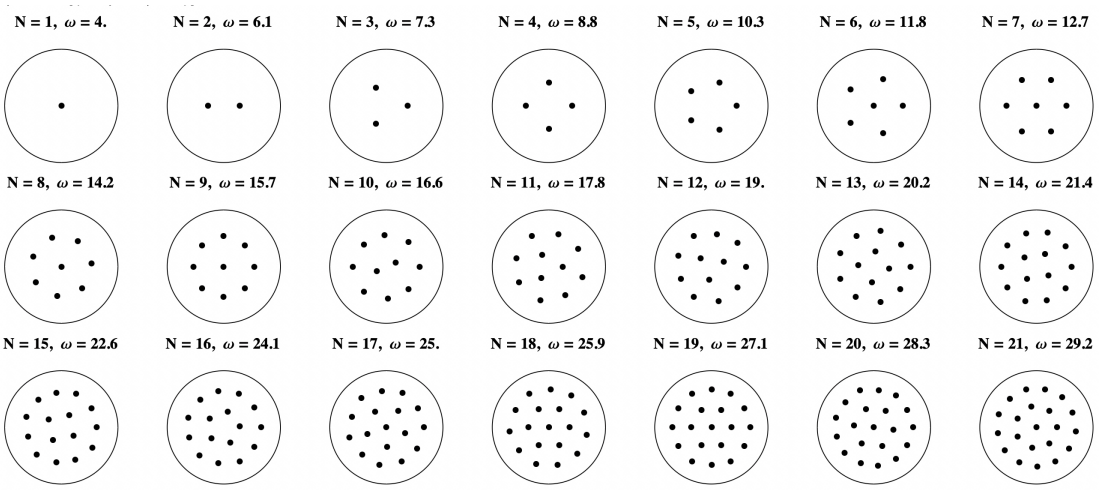

Figure 3.5: Equilibrium vortex patterns assumed by the system at rotation rate ω values close to each transition of the internal structure, for $N = 1, \ldots,\ 21$. Each pattern N is obtained by considering an ω value in the interval where it is the absolute stable spatial configuration according to Figure 3.4.

Furthermore, considering the same notation used by Campbell and Ziff in Ref. [25], for each equilibrium pattern, here indicated by the number of present vortices N, we can associated a sequence of numbers, called *ring numbers*, representing the vortices composing each (exactly or almost) regular polygon: for example the configuration 1, 5, 11 associated to $N = 17$ means that there is a vortex in the center, surrounded by pentagon and an outermost (regular) polygon formed by the remaining 11 vortices.

The equilibrium spatial configurations of a vortex-array found for $N = 1, \ldots,\ 21$, plotted in Figure 3.5, are grouped in the following table:

N	Rings	N	Rings	N	Rings	N	Rings	N	Rings	N	Rings
1	1	2	2	3	3	4	4	5	5	6	1, 5
7	1, 6	8	7, 1	9	1, 8	10	2, 4, 4	11	3, 8	12	3, 3, 6
13	4, 9	14	4, 10	15	4, 11	16	5, 11	17	1, 5, 11	18	1, 6, 11
19	1, 6, 6, 6	20	1, 6, 13	21	1, 7, 13						

These vortex-crystal configurations exactly coincide with the ones reported Campbell and Ziff in their article [25]. It is important to notice that in such an analysis are treated only cases with a moderate N for sake of simplicity. However if N is large enough the equilibrium patterns are in particular triangular vortex lattice (further information in Ref. [11, 25]).

3.2 Stable configurations of massive vortices

In the assumption that in the confined condensate the vortices could trap in their cores some impurity atoms, we expect that the vortex masses must affect somehow the equilibrium spatial configurations of massless vortices well discussed in section [3.1].
According to the modeling considered in section 2.2 for a system of N massive vortices in a trapped condensate of radius R, we consider that each vortex j hosts in its core $N_{b,j}$ atomic particles of mass m_b: then each total vortex mass is $M_{b,j} = N_{b,j} m_b$.
Since the aim of the study is studying the properties of the system according the value of this mass, for the sake of simplicity we consider that each vortex is trapping the same number of atoms ($\forall j \; N_{b,j} = N_b$) and that the atomic species of the impurity particles is the same of the superfluid one (choice suggested also by Ref. [12]). The latter assumption means that the atomic mass of the superfluid m is equal to the impurity atomic mass m_b, leading to a total mass of a generic vortex to be defined as:

$$M \doteq M_{b,j} = N_b m \quad \rightarrow \quad N_b = \frac{M}{m}. \tag{3.10}$$

Please note that the actual driving parameter in our description is N_b.

The effective Lagrangian L describing such a system is given by the formula (3.11):

$$\begin{aligned} L = & \sum_{j=1}^{N} \left[\frac{M}{2} (\dot{\boldsymbol{r}}_j)^2 + \frac{k_j m n}{2} (\dot{\boldsymbol{r}}_j \times \boldsymbol{r}_j \cdot \hat{z}) \frac{r_j^2 - R^2}{r_j^2} - \frac{k_j^2 n m}{4\pi} \ln \left(1 - \frac{r_j^2}{R^2} \right) \right] \\ & - \sum_{j>i=1}^{N} \frac{k_i k_j n m}{4\pi} \ln \left(\frac{R^2 - 2\boldsymbol{r}_i \cdot \boldsymbol{r}_j + r_i^2 r_j^2 / R^2}{r_i^2 - 2\boldsymbol{r}_i \cdot \boldsymbol{r}_j + r_j^2} \right), \end{aligned} \tag{3.11}$$

with n the planar numerical density of the condensate, $k_j = q_j \frac{h}{m}$ the vortex strength associated to q_j the vortex charge.

Note that since this "massive" effective Lagrangian differs from the "massless" one (2.30) only for the term $\sum_{j=1}^{N} \frac{M}{2}(\dot{\boldsymbol{r}}_j)^2$, the associated "massive" effective Hamiltonian, apart from the M term, corresponds to the (massless) effective Hamiltonian H defined in equation (2.27): it follows that all the massive vortices in an energetically favored configuration are single charged ones, and coherently to the massless case we consider $\forall j \; q_j = +1$ and $k \doteq \frac{h}{m}$.
By applying this "massive" L to the derivation of the free energy of the system (consisting in equations (3.1), (3.2), (3.3) (3.4)), we can find the dimensionless free energy f associated to such a massive description.
More precisely, as done in the massless case, we consider the following condition $|\boldsymbol{r}'_j| = r'_j \to Rr_j$, where we rescal the vortex variable r'_j in units of R, the trap radius, and we drop the prime symbol for the sake of brevity, i.e. $0 \leq rj < 1$ (we are excluding the nonphysical case of vortices colliding to the domain wall).

Then, the *"massive" dimensionless free energy* f assumes the following form:

$$\begin{aligned} f = &- \sum_{j>i=1}^{N} \ln[r_i^2 + r_j^2 - 2r_i r_j \cos(\theta_i - \theta_j)] + \frac{1}{2} \sum_{i,j=1}^{N} \ln[1 + r_i^2 r_j^2 - 2r_i r_j \cos(\theta_i - \theta_j)] \\ &- \omega \sum_{i=1}^{N} (1 - r_i^2) - \frac{M\omega^2}{2m\pi n R^2} \sum_{i=1}^{N} r_i^2 + N \ln(R/a) \end{aligned} \tag{3.12}$$

Looking to the free-energy function (3.6) for the massless description, we can say that the massive free energy f corresponds to the massless but with the additional term proportional (for each vortex i) to $-M\omega^2 r_i^2$. This energetic contribution signalises the **effect of a centrifugal force acting on the impurity atoms in each vortex**, which is radially directed towards the circular boundary.
According to this observation, the case of no trapped impurity particles $N_b = 0$ is expected to correspond to the massless case and the resulting equilibrium vortex patterns must coincide for with the ones previously obtained in subsection 3.1 (or equivalently to the ones reported in Ref. [25]).

Approximation of negligible boundary effects
Since the free energy f (3.12) is just a "massive" generalization of the massless free-energy function (3.6), the previously seen vertical asymptote of f as a vortex approach the boundary is still present. Then, let us **consider the approximation of *negligible boundary effects* (no image vortices)** also for this generalized case, obtaining that the *approximated massive dimensionless free energy* f_0 is:

$$\begin{aligned} f_0 = &- \sum_{j>i=1}^{N} \ln[r_i^2 + r_j^2 - 2r_i r_j \cos(\theta_i - \theta_j)] \\ &- \omega \sum_{i=1}^{N} (1 - r_i^2) - \frac{M\omega^2}{2m\pi n R^2} \sum_{i=1}^{N} r_i^2 + N \ln(R/a). \end{aligned} \tag{3.13}$$

Please note that the f_0 function is still dimensionless since the ratio in the new massive term contains: $M/m = N_b$ (just the number of particles per vortex) from (3.10), $\pi R^2 n = N_a$ the number of particles in the superfluid condensate.

Analytic study for the "symmetric" configurations In order to properly analyze this massive version of global minimization problem, already discussed for the massless case, we will firstly focus on the analytic case of "symmetric configurations" for $N \leq 7$, few vortices in the system, but at different N_b values.
Such cases are described by a symmetric free-energy function f_0, depending only on a unique radial vortex variable, i.e r_1, indicating the radial position of all the vortices rearranged in a regular polygonal ring (see subsection 3.1). Here the symmetric massive free energy f_0 for the symmetric example seen before corresponds just to a massive generalization of the equations (3.9):

$$\begin{aligned} N = 1,\ Sym &\implies f = \ln(R/a) - \omega(1 - r_1^2) - \frac{M\omega^2 r_1^2}{2\pi R^2 mn}, \\ N = 2,\ Sym &\implies f = 2\ln(R/a) - \ln(4r_1^2) - 2\omega(1 - r_1^2) - 2\,\frac{M\omega^2 r_1^2}{2\pi R^2 mn}, \\ N = 3,\ Sym &\implies f = 3\ln(R/a) - 3\ln(3r_1^2) - 3\omega(1 - r_1^2) - 3\,\frac{M\omega^2 r_1^2}{2\pi R^2 mn}. \end{aligned} \tag{3.14}$$

At first, the symmetric f_0 can be plotted as a function of its only variable r_1 varying in its domain [0,1), considering the number of possible vortices N (in particular for $N = 0,\ 1, \ldots,\ 7$), at a fixed values of both the ω rotation rate and the number of trapped atoms N_b ($N_b = 0,\ 1000,\ 2500$).

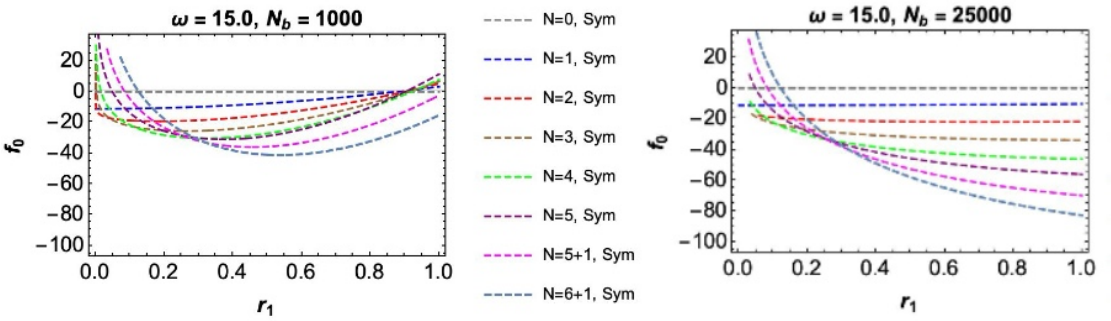

Figure 3.6: Profile of the symmetric free-energy function f_0 according its unique position variable r_1, varying in its domain $r_1 \in [0,1)$, for $N = 0,\ 1, \ldots,\ 7$ at rotation rate $\omega = 15.0$ and for a number of massive trapped particle per vortex $N_b = 1000,\ 25000$. The curve with the lowest local minimum gives corresponds to the absolute stable configuration N: $N_b = 1000$ the equilibrium configuration is a regular hexagon with a vortex in the center, similarly to the massless case, while at $N = 25000$ there is no stable symmetric configuration at this rotation rate.

Taking $\omega = 15.0$, such a profile coincide with the analogous massless one in Figure 3.3b when $N_b = 0$, while in the other two cases we it corresponds to the ones shown in Figure 3.6: we note how, as the number of massive trapped particles per vortex N_b increases, the free-energy function does not present anymore any local minima, meaning that all the symmetric configurations here analysed are no longer stable at rotation frequency $\omega = 15.0$.

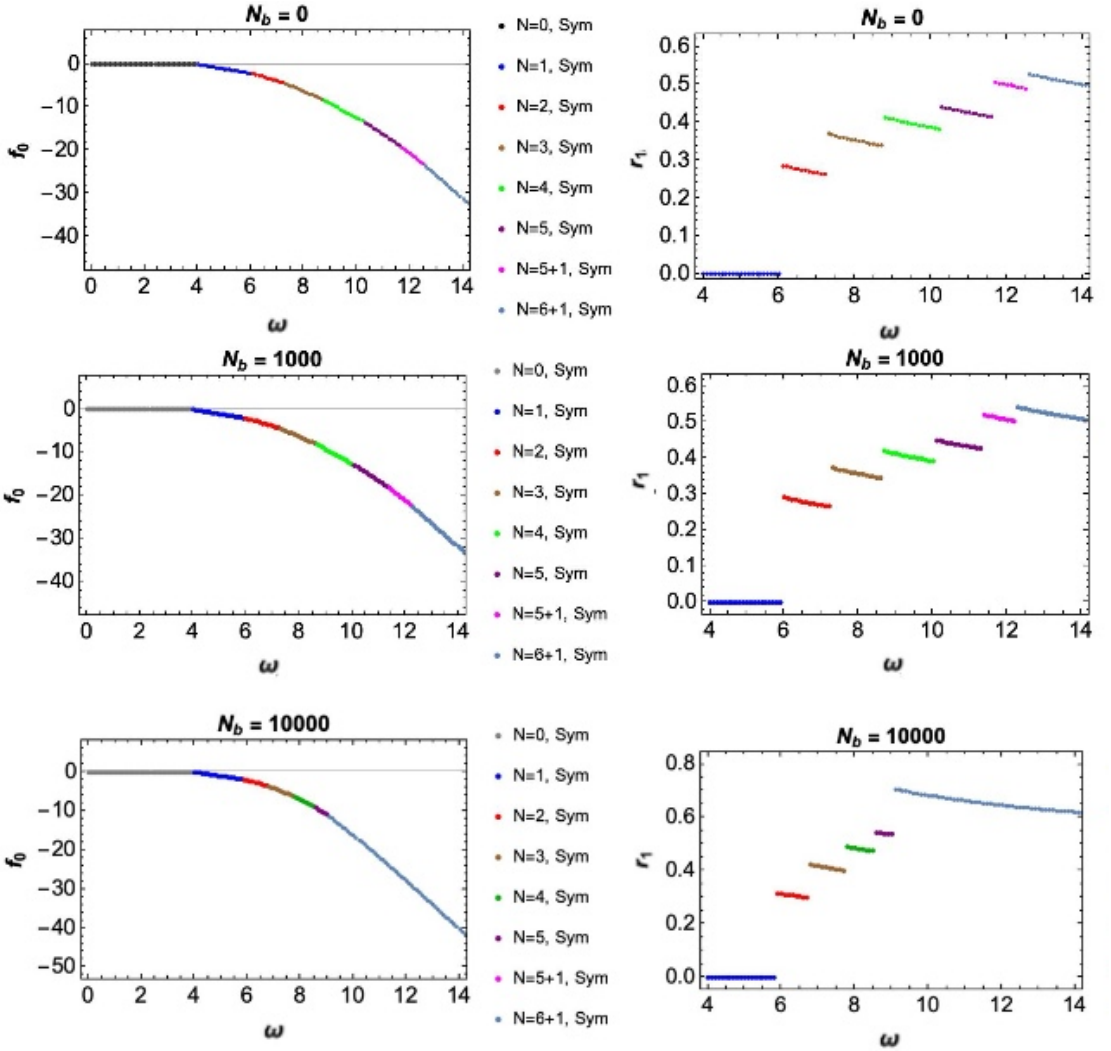

Figure 3.7: The panels on the left column represents the minima of symmetric free energy f_0, computed with respect to the unique vortex polar coordinate r_1, plotted according to the rotation rate $\omega \in [0,\ 15]$ (with 0.3 steps), for $N \leq 7$ and for $N_b = 0,\ 1000,\ 10000$. Meanwhile the panels on the right column are the curves associated to the r_1 minimizing the symmetric function f_0. Note as the N_b is increased at sufficiently large rotations configurations with many vortices become stable for lower ranges.

Secondly we can plot the obtained global minima of the symmetric free-energy function f_0, computed w.r.t. its only r_1 variable, and the r_1 values that minimize f_0, both according to ω in the discrete range $[0,\ 15]$ (with 0.1 steps) for $N \leq 7$ and $N_b = 0,\ 1000,\ 10000$ (Figure 3.7).

From all these analytical results it is important to remark the following observations:

- we note not only a **shift of the critical ω ranges towards smaller values** but also an **enlargement of the ring of vortices**, which become significant as the core mass increases (effect visible in Figure 3.7);
- in the free-energy function profile for the analytic symmetric configurations, Figure 3.6, there seems to be a **shift of the local minimum towards larger values of the position r_1 of the (symmetric) vortices**, until a *"critical value"* of the trapped particle per vortex N_b such that, at both higher ω rate and N number of vortices, the *function has no longer any minima* as clearly visible for case $\omega = 15.0,\ N_b = 25000$.

Then, all these observations suggest the existence, for each N value of possible vortices, of ***some critical value of the vortex mass M* (or of N_b), after which it should be impossible to find a stable massive vortex-array at the equilibrium**.

In order to verify this hypothesis, a useful study consists in focusing on the symmetric case of two vortices ($N = 2$) and analytically analyzing the dimensionless angular velocity ω of the trap as a function of the radial position r of the two symmetric vortices. So by varying the number of trapped particles N_b per vortex and considering the dimensional rotational velocity Ω plotted according to dimensional distance x from the center (0,0) we obtained Figure 3.8. Such a graph highlights that as the vortex mass increases, that is for large N_b, the trap admits only lower Ω values for reduced distance between the two vortices, that is $2x$: in particular for $N_b > 45400$ there are no longer Ω physical values,

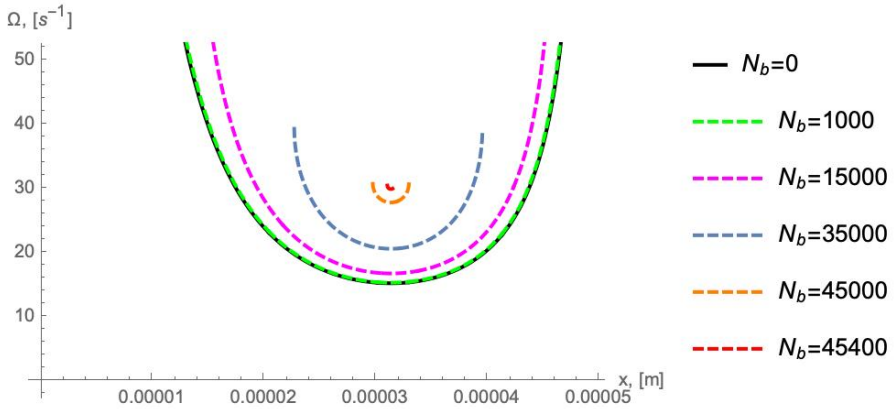

Figure 3.8: Analytic plots of the rotational velocity Ω profiles as a function of the distance x from the center $O = (0,0)$ of one of the two symmetric vortices, $(N = 2)$ computed at different number N_b of trapped particles per vortex.

meaning that the forces acting on the two vortices are not longer balanced and then the symmetric $N = 2$ configuration is no longer stable.

Numerical analysis for the equilibrium patterns of massive vortices.
Since the analytic approach enables us to investigate only up to few vortices on the system, also in this massive version it is obviously convenient to numerically solve the global minimization problem.
The function to minimize is the free energy f_0 defined by the equation (3.13), which contains an *additional parameter* $M = mN_b$, representing the total mass of the N_b particles trapped in each of the N formed vortices.
This is why, **the numerical global minimization procedure we considered for this massive description is identical to the one applied for the massless one** and discussed in details in section 3.1, **but we repeated it at different fixed values of M (or equivalently N_b)**.

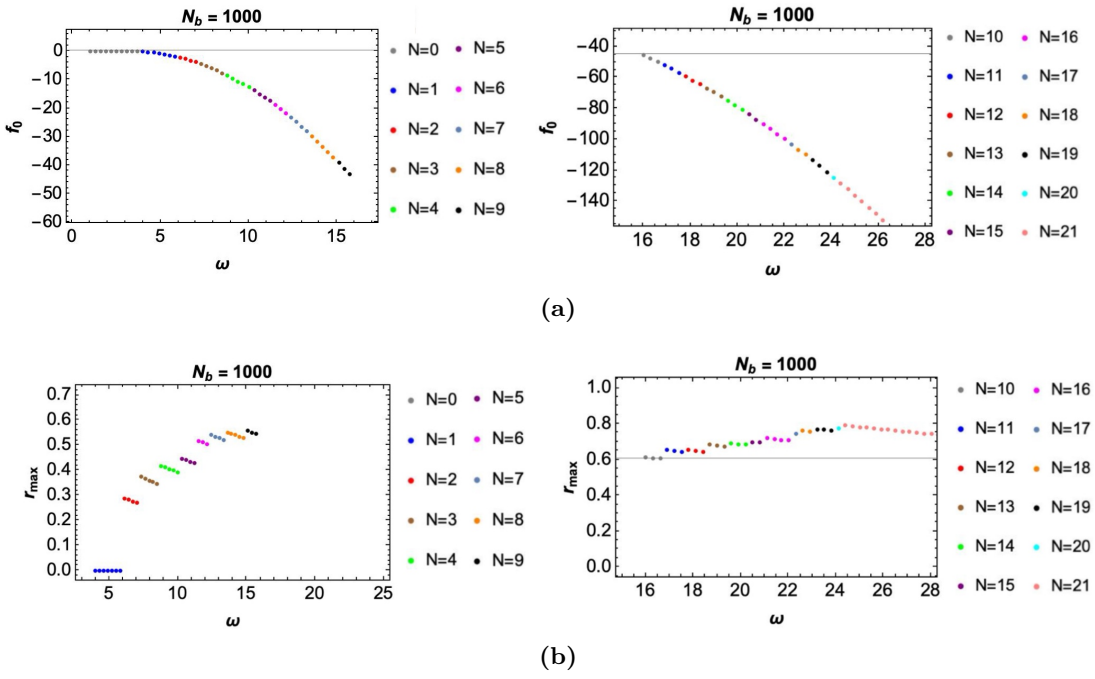

(a)

(b)

Figure 3.9: **(a)** Curves of the global minima of free energy f_0, computed numerically with respect to the radial vortex polar coordinates r_j's and θ_j's, and plotted according to the rotation rate $\omega \in (0,\ 30)$ (with 0.3 steps). **(b)** Curves of the radial position r_{max} of the farthest vortex from the center (living into the outermost ring in the corresponding equilibrium pattern) globally minimizing the f_0 with respect $\omega \in (0,\ 30)$ (with 0.3 steps). Note that $N_b = 1000$ and that in both subfigures we have considered on the left $N = 0,\ 1, \ldots,\ 9$ and $N = 10, \ldots,\ 21$ to highlight through the colors the corresponding equilibrium patter N, whose ring structure is reported in the table of Figure 3.11.

Taking $\boldsymbol{N_{max} = 21}$ as the maximum possible value of the number N of the formed vortices, we computed the global minima of the massive free energy f_0 at $\boldsymbol{N_b = 0,\ 1000}$ and plotted these values and the radial component r_{max} of the outermost vortex minimizing the function, both according to the rotation rate ω.
Coherently to our predictions, such curves associated to $N_b = 0$ are nothing but the graphs in Figure 3.4 obtained within the massless description; while the ones obtained for the case $N_b = 1000$ are shown in Figure 3.9.

Then, the corresponding spatial equilibrium configuration for the $N_b = 0$ coincide with the ones in Figure 3.5, instead for $N_b = 1000$ are those reported in Figure 3.10.

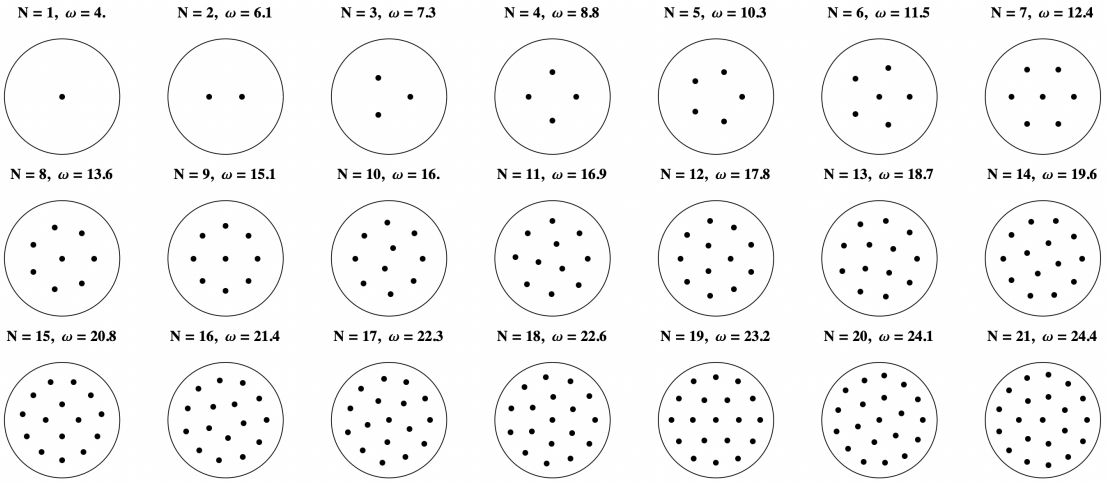

Figure 3.10: Equilibrium vortex patterns assumed by the system at rotation rate ω values close to each transition of the internal structure, for $N = 1, \ldots,\ 21$ and each vortex hosting $N_b = 1000$. Each pattern N is obtained by considering an ω value in the interval where it is the absolute stable spatial configuration according to Figure 3.4.

A fundamental evidence coming from these results is that the structure of the **an absolute stable pattern**, presenting N massive vortices at a certain rotational velocity of the trap, **shares with the corresponding well known massless vortex patter $\boldsymbol{N}$ the same *concentric rings composition***, (the 2% approximation is still valid). This can be also seen on the table in Figure 3.11 reporting the ring numbers obtained for $N = 1,\ \ldots,\ 21$ both for $N_b = 0$ and $N_b = 1000$.

Furthermore, we can also confirm the presence of a **shift of the critical $\boldsymbol{\omega}$ ranges towards values smaller than the massless ones**, structurally corresponding to higher $\boldsymbol{N}$ massless stable pattern with radially drifted vortices towards the wall.

Such results are clearer if we directly compare at a certain fixed rotation rate the vortex patterns evaluated for the two considered cases and also the ones ensuing from the further case of $N_b = 2000$. Doing this as shown in Figure 3.12 at both we $\omega = 15.1,\ 24.1$, **we**

	N_b=0	N_b=1000		N_b=0	N_b=1000		N_b=0	N_b=1000
N=1	1	1	**N=8**	1,7	1,7	**N=15**	4,11	4,11
N=2	2	2	**N=9**	1,8	1,8	**N=16**	5,11	5,11
N=3	3	3	**N=10**	2,4,4	2,4,4	**N=17**	1,5,11	1,5,11
N=4	4	4	**N=11**	3,8	3,8	**N=18**	1,6,11	1,6,11
N=5	5	5	**N=12**	3,3,6	3,3,6	**N=19**	1,6,6,6	1,6,6,6
N=6	1,5	1,5	**N=13**	4,9	4,9	**N=20**	1,6,13	1,6,13
N=7	1,6	1,6	**N=14**	4,10	4,10	**N=21**	1,7,13	1,7,13

Figure 3.11: Table of the resulting ring numbers for absolute stable configurations $N = 1, \ldots, 21$ for $N_b = 0$ (massless case) and for $N_b = 1000$ (massive case) particles filling each vortex core. Each sequence represents the number of vortices composing each (exactly or almost) regular polygon: for example the configuration 1, 5, 11 associated to $N = 17$ means that there is a vortex in the center, surrounded by pentagon and an outermost (regular) polygon formed by the remaining 11 vortices.

observe that at sufficiently large fixed ω values as the number N_b of particles in each vortex core increases, the system actually increases its number N of possible vortices at equilibrium:
- $\omega = 15.1 \implies N_b = 0 \to 1,\ 7;\ N_b = 1000 \to 1,\ 8;\ N_b = 2000 \to 2,\ 8;$
- $\omega = 24.1 \implies N_b = 0 \to 5,\ 11;\ N_b = 1000 \to 1,\ 6,\ 13.$

The fact that in the comparison taken into account at $\omega = 15$ a vortex-array for $N_b = 2000$ does not appear is strictly related to the nature of the considered massive description. Indeed let us recall that such registered deviations from the massless results lay on the centrifugal energetic term depending on $-\sum_{j=1}^{N} M\omega^2 r_i^2$ (3.13): then when dealing with high values of vortex mass M at sufficiently large rotation rate ω, the higher the corresponding number N of vortices is, the stronger the centrifugal radial drift is, perhaps *leading to energetically favored configurations with outermost vortices too close to the boundary*. Such possible results are nothing but ***numerical artifacts*** corresponding to nonphysical solutions, where the vortices tend to annihilate with corresponding images just at the other side of the boundary.

A reasonable way to bypass this numerical issue could be either to reduce the maximum number N_{max} of possible formed vortices according to both the rotational velocity ω at which the circular trap rotates and to the number of trapped particles per vortex (N_b), or more in general to chose a trade of for these value such that the product in $\sum_{j=1}^{N} M\omega^2 r_i^2$ is sufficiently small.

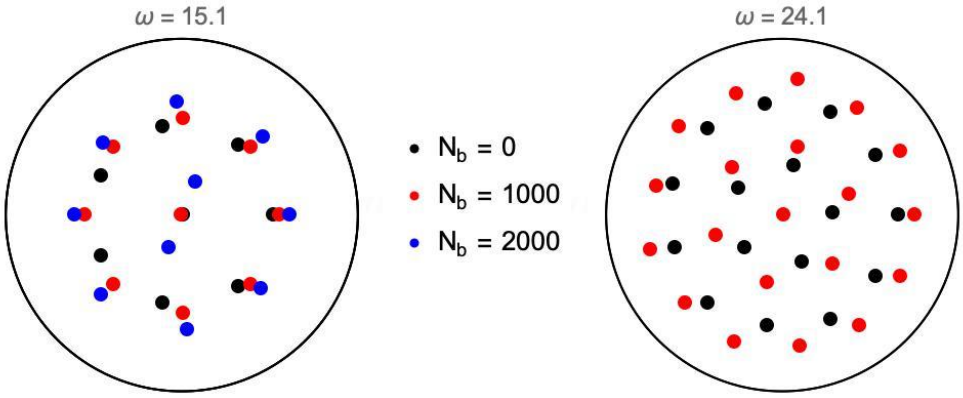

Figure 3.12: Caparison, at fixed trap rotation rate ω, between the equilibrium spatial configurations of massive vortices for different number of identical massive particles N_b filling each vortex. *Left panel*: at $\omega = 15.1$ it is visible how from a massless case $N_b = 0$ with $N = 8$ vortices $(1,\ 7 =$ an heptagon with one vortex in the center), we move to a configuration $N = 9$ $(1,\ 8 =$ an octagon with one vortex in the center) for $N_b = 1000$ and to $N = 10$ $(2,\ 4,\ 4 =$ two symmetric inner vortices surrounded by two external squares) for $N_b = 2000$. *Right panel*: at $\omega = 24.1$ for massless case ($N_b = 0$) a $N = 16$ configuration $(5,\ 11 =$ pentagon surrendered by a hendecagon), while for $N_b = 1000$ $(1,\ 6,\ 13 =$ a vortex surrounded by an hexagon and an external tridecagon). Note that here no configuration for $N_b = 2000$ because of numerical artifacts.

Here in the following we have taken into account $N_{max} = 10$ since it enables to analyze a wider set of vortex mass values, without encountering numerical issues: in particular have considered $N_b = 0$, 1000, 1500, 2000, 3000, 3500, 4000.

The curves regarding the minima of the dimensionless free energy f_0 and of radial distance r_{max} of the outermost vortex, shown in Figure 3.14, plotted according to ω, finally ensure the validity of all the expected effects of particles filling vortex cores discussed in this section.
As further verification, in the end we also compared each massless ($N_b = 0$) equilibrium configuration N obtained from the numerical global minimization (results in Figure 3.13) with the ones having the same value of N, but obtained at a different $N_b \neq 0$, in order to graphically show that, apart from a global rotation and the centrifugal force action, each massive pattern N (for all the massive cases analyzed) still presents the same ring composition of the corresponding massless one.

	N_b=0	N_b=1000	N_b=1500	N_b=2000	N_b=3000	N_b=3500	N_b=4000
N=1	1	1	1	1	1	1	1
N=2	2	2	2	2	2	2	2
N=3	3	3	3	3	3	3	3
N=4	4	4	4	4	4	4	4
N=5	5	5	5	5	5	5	5
N=6	1,5	1,5	1,5	1,5	1,5	1,5	1,5
N=7	1,6	1,6	1,6	1,6	1,6	1,6	1,6
N=8	1,7	1,7	1,7	1,7	1,7	1,7	1,7
N=9	1,8	1,8	1,8	1,8	1,8	1,8	1,8
N=10	2,4,4	2,4,4	2,4,4	2,4,4	2,4,4	2,4,4	2,4,4

Figure 3.13: Table of the ring numbers associated to the absolute stable configurations $N = 1, \ldots, 10$ for different values of the number N_b of massive particles filling each vortex core. Each sequence represents the number of vortices composing each (exactly or almost) regular polygon: for example the configuration 1, 8 associated to $N = 9$ refers to an octagon with a vortex in the center. This table shows as in the assumption of negligible boundary effects the geometry of the massless vortex patterns at equilibrium is formally maintained in the case of massive vortices.

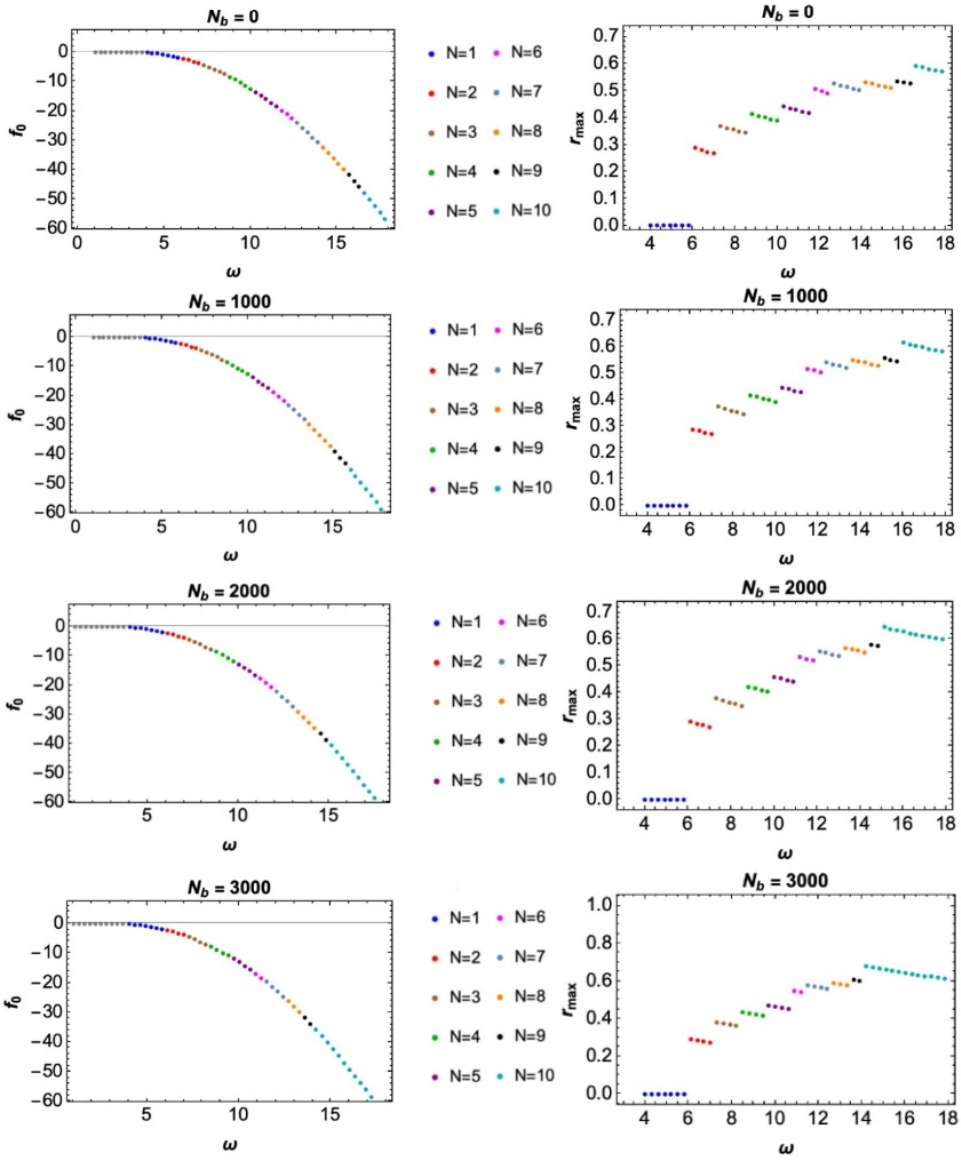

Figure 3.14: Left panels) Curves of the global minima of free energy f_0 (3.13), computed numerically with respect to the radial vortex polar coordinates r_j's and θ_j's, and plotted according to the rotation rate $\omega \in (0,\ 30)$ (with 0.3 steps) for different massive cases (number of massive particles N_b per vortex). **Right panels)** Curves of the radial position r_{max} of the farthest vortex from the center (living into the outermost ring in the corresponding equilibrium pattern) globally minimizing the f_0, plotted according to ω.

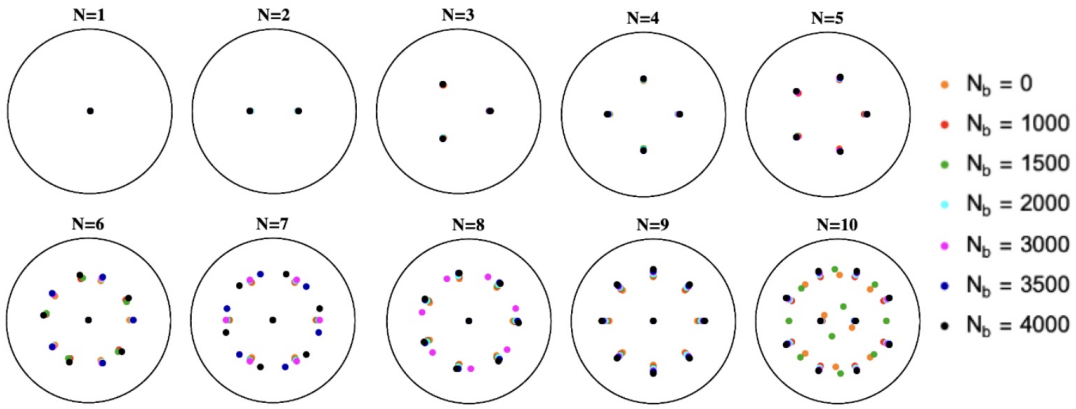

Figure 3.15: Comparison between all the equilibrium patterns containing the same number of massive vortices N, but at different values of the trapped massive particles N_b in each core. Note that except for a global rotation and an enlargement of the rings due to the centrifugal force acting on the particles, formally the geometry of the equilibrium vortex patters in the massive case results the same (more precisely in this approximation of negligible boundary effects).

Chapter 4

Excitations of the Equilibrium Vortex Patterns

In this chapter we will discuss the dynamics of point-like quantum vortices in a superfluid, particularly focusing on the case of a trapped condensate in a circular domain. The first part is dedicated to the derivation of the dynamical equations defining the motion of vortices, especially exploiting the Lagrange formalism, both in the "massless" and "massive" descriptions, where in particular we will present the main difference among the two cases. While the second part focuses on the effect ensuing from the vortex mass on the non-trivial excitations of vortices around their equilibrium positions, discussed in Chapter 3, known as the *Tkachenko modes*.

4.1 Superfluid vortex dynamics

So far we have seen how to deal with quantum vortices in a generic superfluid, especially focusing on their point-like modeling in both cases of infinite large and confined quasi two-dimensional systems, also treating the scenario of filled vortex cores (see the section 2.2), but the study about their dynamics has not yet been deepened.
At first let us recall that the whole system could be described, within then Hydrodynamic picture, by means of a complex and single valued wavefunction ψ depending on the (real valued) density n and phase S fields as the Madelung transform $\psi = \sqrt{n}e^{iS}$ (section 2.4). From the section 2.2, we also know that, considering an unbounded and planar system (no external trapping potential) with vanishingly small spatial variations of the density n ($n \approx const$ and negligible vortex core size), the fluid is nonviscous, irrotational and incompressible and associated to a velocity field $\boldsymbol{v}$ of the two completely equivalent following forms, according to equations (2.2) and (2.13):

$$\boldsymbol{v}(\boldsymbol{r}) = \frac{\hbar}{m}\nabla S(\boldsymbol{r}), \quad \boldsymbol{v}(\boldsymbol{r}) = \frac{\hbar}{m}\hat{e}_z \times \nabla A(\boldsymbol{r}) = -\frac{\hbar}{m}\nabla \times [\hat{e}_z A(\boldsymbol{r})]\,, \tag{4.1}$$

where $\boldsymbol{r} = (x,\ y)$, m the superfluid particle atomic mass, the phase filed S plays the role of a *velocity potential* and the potential flow function A corresponds to the *stream function*.

In order to be equivalent, this two expressions leads to the *Cauchy-Reimann conditions* for the two functions S and A

$$\nabla S = -\nabla \times [\hat{e}_z A] \quad \Longrightarrow \quad \frac{\partial S}{\partial x} = -\frac{\partial A}{\partial y}, \quad \frac{\partial S}{\partial y} = \frac{\partial A}{\partial x}. \tag{4.2}$$

Please note that here the velocity field depends explicitly on the spatial positions $\boldsymbol{r}$, $\boldsymbol{r}_j$'s, according to the equations (2.13) and (2.17): it depends on time only implicitly since the positions are time dependent $\boldsymbol{r} = \boldsymbol{r}(t)$. This is why we consider the phase field as $S(\boldsymbol{r})$.

It is possible to describe the flow of the fluid taking into account the ***complex potential F*** (as done in Ref. [13]) in the complex plane according to $z = x + iy$ defined as:

$$F(z) = A(\boldsymbol{r}) + iS(\boldsymbol{r}), \qquad F'(z) = \frac{\partial A}{\partial x} + i\frac{\partial S}{\partial x} = \frac{\partial S}{\partial y} - i\frac{\partial A}{\partial y}, \tag{4.3}$$

with $F'(z)$ the complex derivative of F, corresponding by combing it with the formulas in (4.2) to $F'(z) = (m/\hbar)\ (v_y + iv_x)$. From this, the complex velocity of a generic vortex at $z_0 = x_0 + iy_0$ could be obtained from

$$i\dot{z}_0^* = \dot{y}_0 + i\dot{x}_0 = \frac{\hbar}{m} \lim_{z \to z_0} \left[F'(z) - \frac{1}{z - z_0} \right], \tag{4.4}$$

being z^* the complex conjugate of z_0. Therefore this equation can be used to find the equations of the motion of each vortex in the systems and giving in particular *first order differential* dynamical equations, coherently to the fact that here the vortices are massless objects.

Dynamics of massless vortices in an infinitely large system.
In the case of N vortices in an infinitely large condensate, notice that such a method to derive the dynamics of the massless vortices takes into account equations (2.18) and (2.19) for the phase filed S and the potential flow function (stream function) A, which are

$$S(\boldsymbol{r}) = \sum_{i=1}^{N} q_i \arctan\left(\frac{y - y_i}{x - x_i}\right), \quad A(\boldsymbol{r}) = \sum_{i=1}^{N} \frac{q_i}{2} \ln\left(\frac{(x - x_i)^2 + (y - y_i)^2}{a_0^2}\right), \tag{4.5}$$

with q_i's the (integer) vortex charges and a_0 the vortex core radius. Then applying these definitions to the equation (4.4) ones find that each vortex at point $\boldsymbol{r}_j$ has a velocity $\dot{\boldsymbol{r}}_j$ of the form

$$\dot{\boldsymbol{r}}_j = \sum_{i \neq j} q_i \frac{\hbar}{m}\ \hat{e}_z \times \frac{\boldsymbol{r}_j - \boldsymbol{r}_i}{|\boldsymbol{r}_j - \boldsymbol{r}_i|^2}. \tag{4.6}$$

Such dynamical equations are known as the ***Helmholtz-Kirchhoff equations*** and are nothing but first order differential equations depending just on the vortex position $\boldsymbol{r}_j$'s and vortex velocities $\dot{\boldsymbol{r}}_j$'s.

Whenever the system has only two point-like vortices at a distance $d \gg a_0$ of charges $q_1,\ q_2$, the resulting configuration of the couple would corresponds either to a ***vortex-antivortex***

pair or to a ***corotating pair***.
A vortex-antivortex pair consists in a vortex with positive charge around which the flow is counterclockwise and another with negative charge, said *antivortex*, associated to a clockwise flow. In particular in Figure 4.1 we can note that on the mid-point of the two vortices the two flow fields are directed along the same directions, and thus the resulting superposition effect leads to a couple of vortices travelling along the same direction.

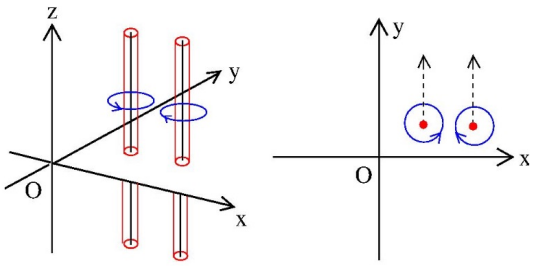

Figure 4.1: Scheme on the xy plane of two straight vortex lines of opposite circulation. The right panel shows as the vortex (on the left) and the antivortex (on the right) flow fields are directed along the same directions on the mid-point of the two vortices: the resulting superposition effect leads to a couple of vortices travelling along the same direction. Figure taken from Ref. [2].

While a corotating pair corresponds to two vortices or two antivortices, for which the resulting net effect is a co-rotation of the vortices around their mid-point. In the case of two single charged vortices at large distance they appears as a unique vortex of double charge (or in general $q_1 + q_2$).

Dynamics of massless vortices in a condensate confined in a circular trap. Let us now move to the case of a quasi two-dimensional condensate confined in a circular bucket of radius R by means of a bucket-like trapping potential V, see equation (2.23). In such a case we already know that the boundary effect on each vortex is described by means of the image vortex, a virtual vortex of opposite charge and placed outside the trap at position $\boldsymbol{r}_0'$ given by equation (2.24). Considering a configuration of N massless vortex, now the stream function A and the phase field S, according to (2.25) and (2.26), become:

$$A(\vec{r}) = \sum_{j=1}^{N_v} q_j \ \ln\left|\frac{\vec{r}-\vec{r}_j}{\vec{r}-\vec{r}\,'_j}\right|, \quad S(\boldsymbol{r}) = \sum_{i=1}^{N} q_i \left[\arctan\left(\frac{y-y_i}{x-x_i}\right) - \arctan\left(\frac{y-y_i'}{x-x_i'}\right)\right], \quad (4.7)$$

leading then to a complex potential F, defined in (4.3), as

$$F(z) = \sum_{i=1}^{N} q_i \ln\left(\frac{z-z_i}{z-z_i'}\right), \quad \text{with} \quad z_i' = x_i' + iy_j'. \quad (4.8)$$

Therefore by considering such a function F into the equation (4.4) we find that the velocity of each vortex j at a position $r_j = (x_j,\ y_j)$ satisfies the following equation of motion

$$0 = \hat{e}_z \times \dot{\boldsymbol{r}}_j + \frac{q_j\hbar}{m}\frac{\boldsymbol{r_j}}{R^2 - r_j^2} + \sum_{i\neq j}\frac{q_i\hbar}{m}\left[\frac{\boldsymbol{r}_j - \boldsymbol{r}_i}{|\boldsymbol{r}_j - \boldsymbol{r}_i|^2} + \frac{R^2\boldsymbol{r}_i - r_i^2\boldsymbol{r_j}}{R^4 - 2R^2\boldsymbol{r}_i\cdot\boldsymbol{r}_j + r_i^2 r_j^2}\right]. \tag{4.9}$$

This equation is correctly a first order differential equation, where the terms depending on the radius of the trap R are respectively related to the interactions of the vortex with its own image and with all the rest of image vortices. Indeed if $R \to \infty$, this equation would correspond to the motion equation (4.6) for a vortex in an infinitely large planar condensate.

Dynamics of massive vortices by means of the Lagrangian Equations.
Such a way of achieving the equations of motion does not fit well when we want to consider the possibility of vortex cores hosting massive particles. As proposed in Ref. [13], in order to study the dynamics of vortices in this "massive" generalization we can exploit the Lagrangian formalism seen in section 2.2 with the goal of solving the *Euler-Lagrange* equations.

Let us start by focusing on the simple case of a unique massless singled charged vortex ($q_0 = 1$) in a trapped system at a position $\boldsymbol{r}_0 = (x_0,\ y_0)$, for which according to a wavefunction $\psi = \sqrt{n}\exp(iS)$ within the time-dependent variational ansatz (2.29), the effective Lagrangian L (2.30) reduces to

$$L = \hbar n\pi(\dot{\boldsymbol{r}}_0 \times \boldsymbol{r}_0 \cdot \hat{z})\frac{r_0^2 - R^2}{r_0^2} - \frac{\hbar^2 n\pi}{m}\ln\left[1 - \frac{r_0^2}{R^2}\right]. \tag{4.10}$$

The resulting Euler-Lagrange equation associated to this system's L is

$$0 = \hat{e}_z \times \dot{\boldsymbol{r}}_0 + \frac{\hbar}{m}\frac{\boldsymbol{r_0}}{R^2 - r_0^2}, \tag{4.11}$$

which is manifestly equivalent to the first order differential motion equation derivable from the more generic motion equations (4.9). In particular it describes a uniform circular motion [13] of the vortex around the center $(0,\ 0)$ of the trap and whose radius corresponds to r_0 and whose precession rate Ω_0 (that is its angular velocity) is given by

$$\Omega_0 = \frac{\hbar}{m(R^2 - r_0^2)}. \tag{4.12}$$

Meanwhile considering the more generalized description for massive vortices discussed at the end of section 2.2, we know that the particles hosted in the vortex cores can be treated as a different condensate allowing the whole system to be described as a two-component BEC. Indeed according to equations (2.32), (2.33), (2.34) and (2.35) the confined planar condensate, with a single charged massive vortex at $\boldsymbol{r}_0$ hosting N_b atomic particles of mass m_b stuck in its core (core mass $M_b = N_b m_b$), is described by an effective Lagrangian L of the following form

$$L = \frac{1}{2}M_b\dot{\boldsymbol{r}}_0^2 + \hbar n_a\pi(\dot{\boldsymbol{r}}_0 \times \boldsymbol{r}_0 \cdot \hat{e}_z)\frac{r_0^2 - R^2}{r_0^2} - \frac{\hbar^2 n_a\pi}{m_a}\ln\left[1 - \frac{r_0^2}{R^2}\right], \tag{4.13}$$

where we have used the subscript a for the physical quantities related to the massless component of the condensate, and the subscript b for the massive particles. Recall that here due to the immisciability of the two components, we are considering the vortex variable $\boldsymbol{r}_0$ in the a-component wavefunction ψ_a to denote also the position of b-component inertial particles (see section 2.2 or Ref. [13, 15, 24]).

Notice that such an effective Lagrangian L is nothing but a *massive generalization* of the massless one in (4.10), containing an additional term depending on the $M_b\dot{\boldsymbol{r}}_0^2$, which is responsible for the appearance of an ***inertial term*** (*a second order time derivative*) on the dynamical equations. Indeed the *Euler-Lagrange* equation describing the motion of a massive vortex in circular confined superfluid system is

$$M_b\ddot{\boldsymbol{r}}_0 = 2\pi n_a\hbar\left[\hat{e}_z\times\dot{\boldsymbol{r}}_0 + \frac{\hbar}{m_a}\frac{\boldsymbol{r_0}}{R^2-r_0^2}\right], \tag{4.14}$$

which as expected is a ***second order differential equation*** depending not only on the vortex coordinates and velocities but also on the vortex accelerations $\ddot{\boldsymbol{r}}_j$'s, meaning that the total number of dynamical variables associated to system compared to the massless case is doubled. Note also that it correctly reduces to the first order Helmholtz-Kirchhoff motion equation (4.11) as $M_b\to 0$.

Among all the possible different kind of solutions of the (massive) dynamical equation (4.14), there is one which corresponds to a massive vortex in uniform circular motion [13] given by

$$\boldsymbol{r}_0 = r_0(\cos(\Omega_0 t),\ \sin(\Omega_0 t)), \tag{4.15}$$

being Ω_0 the precession frequency (or equivalently the angular velocity) depending on both the radius of the circular orbit r_0 and on the core mass $M_b = N_b m_b$. By rescaling the considered physical quantities as $\tilde{r}_0 \doteq r_0/R$, $\tilde{\Omega}_0 \doteq \Omega_0\hbar/(m_a R^2)$ and $\mu \doteq M_b/M_a = (N_b m_b)/(n_a\pi R^2 m_a)$, the two possible solutions corresponds to angular frequencies $\tilde{\Omega}_0^{(+)}$ and $\tilde{\Omega}_0^{(-)}$

$$\begin{aligned}\tilde{\Omega}_0^{(+)} &= \frac{\sqrt{1-2\mu/(1-\tilde{r}_0^2)}}{\mu},\\ \tilde{\Omega}_0^{(-)} &= \frac{2/(1-\tilde{r}_0^2)}{\sqrt{1-2\mu/(1-\tilde{r}_0^2)}}.\end{aligned} \tag{4.16}$$

Observe how, in the limit of very small vortex mass $\mu\to 0$, we obtain an unphysical solution corresponding to the divergent frequency $\tilde{\Omega}_0^{(+)}\sim 2/\mu\to\infty$ and the physical meaningful frequency $\tilde{\Omega}_0^{(-)}\to(1-\tilde{r}_0^2)^{-1}$ equivalent to the dimensionless version of the massless solution obtained in (4.12). In addition, since the mass should be sufficiently small, we can say that such a uniform circular orbit defining the trajectory of the single massive vortex exits only if the parameter μ satisfies the following condition:

$$\mu < \mu_\Omega \doteq \frac{(1-\tilde{r}_0^2)}{2}. \tag{4.17}$$

Thus we can conclude (such a discussion based on Ref. [13]) that, among the possible physical meaningful trajectories defining the dynamics of a single massive vortex of unit charge, *uniform circular orbits are admitted if the core mass satisfying the above regime*, but on the other hand **there exists also orbits**, which consist in **circular orbit with superimposed small-amplitude oscillations along transverse radial directions**, also known as ***cyclotron normal modes***. Such trajectories can be clearly seen in Figure 4.2, where we can observe, at fixed value of $\mu = 4 \times 10^{-2}$, both a circular uniform orbit (the green curve) and circular orbit presenting the typical cyclotron-like corrections (red curve), obtained (from the first one) for tiny perturbations of the initial conditions, while at $\mu = 0.5$ we observe a vortex colliding with the domain wall, since (4.17) is violated.

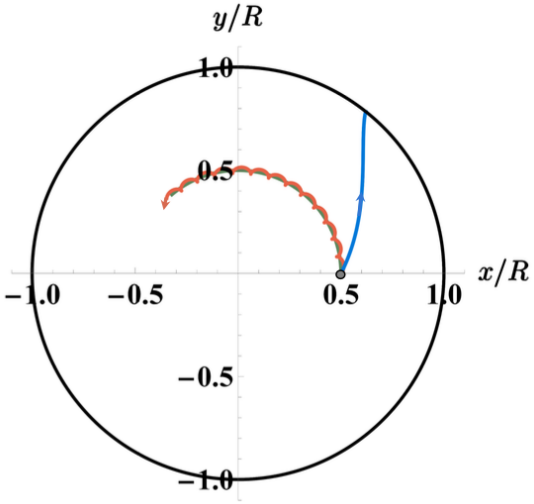

Figure 4.2: Plot of three possible trajectory of a massive vortex in a circular domain of radius R. Green curve obtained considering $\boldsymbol{r}_0(0)/R = (0.5,\ 0)$ and $\dot{\boldsymbol{r}}_0(0)/R = \left(0,\ r_0\Omega_0^{(-)}\right)$, while red curve by considering small perturbations of the previous initial conditions (both curves at $\mu = 4 \times 10^{-2}$). Blue curve, obtained for $\mu = 0.5$, shows a massive vortex colliding at the domain wall with its respective image outside the system. Figure taken from [13].

.

At this point we could generalize our discussion to the many-vortex configurations, considering for the sake of simplicity the case of $N = 2$ massive vortices of generic charge $q_1,\ q_2$ (for the moment) and respectively with core masses $M_{b,j} = m_b N_{b,j}$ for $j = 1,\ 2$. Being such a system identified by an effective Lagrange L ensuing from equation (2.35) and corresponding to

$$\begin{aligned} L = &\sum_{j=1}^{N}\left[\frac{M_{b,j}}{2}\dot{\boldsymbol{r}}_j^2 + \frac{k_j m_a n_a}{2}(\dot{\boldsymbol{r}}_j \times \boldsymbol{r}_j \cdot \hat{e}_z)\frac{r_j^2 - R^2}{r_j^2} - \frac{k_j^2 n_a m_a}{4\pi}\ln\left(1 - \frac{r_j^2}{R^2}\right)\right] \\ &- \sum_{j>i}^{N=2}\frac{k_i k_j n_a m_a}{4\pi}\ln\left(\frac{R^2 - 2\boldsymbol{r}_i \cdot \boldsymbol{r}_j + r_i^2 r_j^2/R^2}{r_i^2 - 2\boldsymbol{r}_i \cdot \boldsymbol{r}_j + r_j^2}\right). \end{aligned} \tag{4.18}$$

where $N = 2$, $k_j = q_j h/m_a$ and the last term represents the two-vortex interaction. Therefore the Euler-Lagrange equations (for $i, j = 1,\ 2$ and $i \neq j$) are written as

$$M_{b,j}\ddot{\boldsymbol{r}}_j = k_j m_a n_a\ \hat{e}_z \times \dot{\boldsymbol{r}}_j + \frac{m_a n_a k_j}{2\pi}\left[\frac{k_i(\boldsymbol{r}_j - \boldsymbol{r}_i)}{|\boldsymbol{r}_j - \boldsymbol{r}_i|^2} + \frac{k_j \boldsymbol{r_j}}{R^2 - r_j^2} + \frac{k_i(R^2\boldsymbol{r}_i - r_i^2\boldsymbol{r_j})}{R^4 - 2R^2\boldsymbol{r}_i \cdot \boldsymbol{r}_j + r_i^2 r_j^2}\right]. \tag{4.19}$$

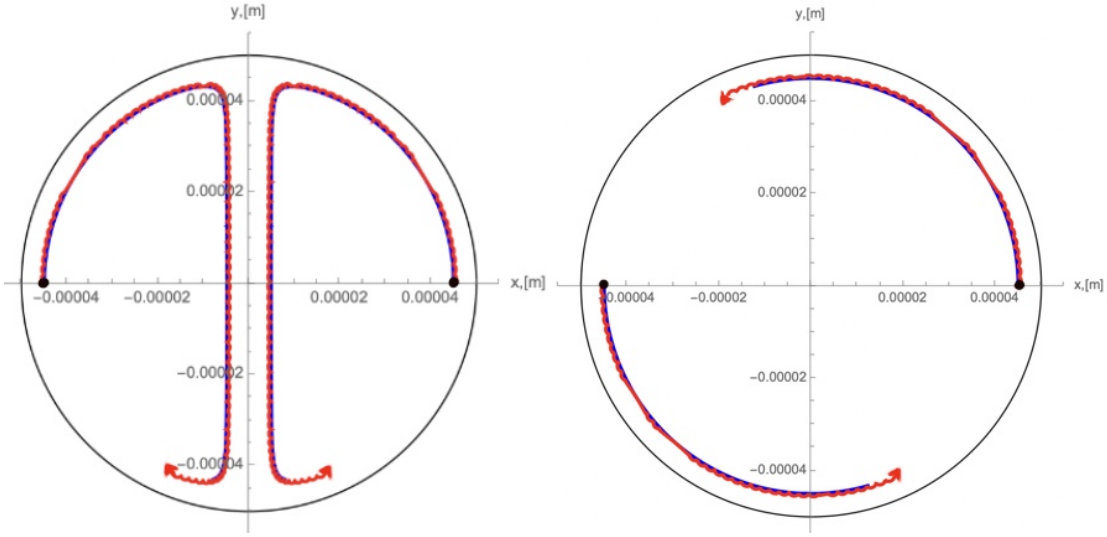

Figure 4.3: Plot on the xy plane of the trajectories associated to the motion of a symmetric vortex-antivortex pair, $q_1 = +1,\ q_2 = -1$, (left panel) and of a symmetric corotating pair (right panel), $q_1 = +1,\ q_2 = +1$. Blue curves represent the massless cases and the red ones the massive case of cores trapping $N_b = 500$ atoms of the same species of the superfluid particles. Results obtained by solving the dynamical equations (4.19) for $R = 50 \times 10^{-6}$ m (meters), sodium (^{23}Na) atomic condensate and initial conditions $x_1(0) = -x_2(0) = 45 \times 10^{-6}$ m , $y_1(0) = y_2(0) = 0$ m, and for the massive case also for $\dot{x}_i(0) = \dot{y}_i(0) = 0\ m/s$ (meters per seconds) for $i = 1$,2. Note the cyclotron excitation modes characterizing the massive case.

An instructive example, especially in view of the study of the excitations of a vortex crystal, is the analysis of two symmetric vortices (with respect to the origin $O = (0,\ 0)$) both in the cases of opposite unit circulations ($q_1 = +1,\ q_2 = -1$) and same unit circulations ($q_1 = q_2 = +1$). From the Helmholtz-Kirchhoff dynamical equations (4.9) we expect that in the case of a massless symmetric vortex-antivortex couple moving in a circularly confined system (R the radius trap), the two real vortices would move together when they are sufficiently close to each other and at the same time sufficiently far from the boundary (this corresponds to the effect seen in Figure 4.1): in fact as they approach the border, the vortex-image attractions become significant and the two vortices would separate and circulate in circular orbits near the domain wall until they would be again sufficiently close.

Such a motion in the simple massive case of vortices trapping the same number N_b of particles with same atomic species of the condensate ($m_{b,j} = m,\ j = 1{,}2$) still remains but in addition we have superimposed some small-amplitude oscillations along transverse radial directions. Meanwhile in the case of a symmetric corotating pair we observe a circular precession motion around the trap center arising both from the repulsion between the two vortices ad the vortex-image attractions near the border and in the massive case (the previous one) we find the cyclotron-like oscillations. These two examples are shown in Figure 4.3.

Electromagnetic equivalence.
It is important to highlight the fact that such dynamical equations, extendable to higher values of N just considering the sum for $i \neq j$, formally coincide with the motion equations for massive charged living in two-dimensional domains in the presence of magnetic fields. The latter equivalence, i.e called *Electromagnetic equivalence*, can be shown through the following mapping, based on $k'_j = -k_j$ and $\boldsymbol{r}'_j = R^2\boldsymbol{r}_j/r_j^2$ the image vortex coordinate from (2.24), for $i, j = 1,\ 2$ and $i \neq j$:

$$M_{b,j}\ddot{\boldsymbol{r}}_j = k_j\dot{\boldsymbol{r}}_j \times (-m_a n_a \hat{e}_z) + \frac{m_a n_a}{2\pi}\left[k_j k'_j \frac{\boldsymbol{r}_j - \boldsymbol{r}'_j}{|\boldsymbol{r}_j - \boldsymbol{r}_j|^2} + k_i k_j \frac{\boldsymbol{r}_j - \boldsymbol{r}_i}{|\boldsymbol{r}_j - \boldsymbol{r}_i|^2} + k_j k'_i \frac{\boldsymbol{r}_j - \boldsymbol{r}'_i}{|\boldsymbol{r}_j - \boldsymbol{r}'_i|^2}\right]. \tag{4.20}$$

The above equation is completely equivalent to $M_{b,j}\ddot{\boldsymbol{r}}_j = \boldsymbol{F}_j$ the second Newton's law for defining the resulting total force acting on a charged particle of non zero small mass $M_{b,j}$ in an electromagnetic field: the force $\boldsymbol{F}_j$ acting on vortex j is a the sum of *Lorentz-like* force (the first term on the r.h.s.), perpendicular to $\dot{\boldsymbol{r}}_j$ the vortex velocity and producing a zero work, and a total *Coulomb-like* force coming from the superposition of all the "electric fields" generated by all the other "charges" (both real and virtual ones)in system. However, note that despite the electric charge like vortex description, the latter force similar to a Coulomb one scales with respect to the inter-vortex distance as $1/(\boldsymbol{r}_j - \boldsymbol{r}_i)$, which is typical of two-dimensional electrostatic problems, instead of scaling as $1/(\boldsymbol{r}_j - \boldsymbol{r}_i)^2$ which is typical for two electric charges in three dimensions.
Furthermore, since $k_j\dot{\boldsymbol{r}}_j \times (-m_a n_a \hat{e}_z)$ behaves similarly to a Lorentz, it follows that the *effective magnetic field* $\boldsymbol{B}$, related to an *effective vector potential* $\boldsymbol{A}$, is defined as

$$\boldsymbol{B} \doteq -m_a n_a \hat{e}_z = \nabla \times \boldsymbol{A}, \qquad \boldsymbol{A} \doteq \frac{m_a n_a}{2}(y,\ -x), \tag{4.21}$$

according to the planar matter density $n_a m_a$ of the superfluid; while the *effective electric field* ensues from the inter-vortex interactions and from the geometric boundaries.

4.2 Excitations of a vortex lattice around its equilibrium positions

After having briefly described the dynamics of quantum vortices especially for the massive case (as in section 4.1), it is possible to study the motion of N excited vortices around

their equilibrium positions (w.r.t. to rotating bucket's frame), given by the corresponding N stable vortex pattern configuration (see chapter 3). In particular, the main focus of the following discussion would be centered on visualize the principal effects on such vortex oscillations ensuing from the presence of a *small non-zero* core mass.

First of all, recall that up to now our whole point-like modeling for quantum straight vortex lines in a superfluid has been based on the assumption of dealing with an incompressible, irrotational and nonviscous superfluid, in particular a quasi two-dimensional weakly interacting atomic BEC. In addition, it has also been assumed infinitesimal vortex core size ($= 2a_0$ the core diameter), compared to the typical length scale of the system size, and negligible fluid density filed spatial variations, namely uniform condensate.

Let us consider once again the case in which the system is confined in the usual circular trapping domain of radius R and rotating at the angular velocity Ω. For such a physical scenario, in section 3.1 we have shown the way we obtained the well-known equilibrium vortex patterns: more precisely for sake of simplicity in this work we have presented only the study up to a moderate number of vortices N and then up to a moderate rotation rate ω. In high rotating Bose-Einstein condensates the equilibrium vortex patterns are triangular lattices (or crystals) with a large number of vortices, for more information Ref. [11, 25].

In such an ideal scenario for an irrotational and irrotational condensate it is well know that transverse vortex-displacement waves propagating on the equilibrium lattice can be observed: these are known as ***Tkachenko modes*** (see Ref. [27, 28]). Such normal excitation modes are microscopically characterized by an *elliptical precession motion against the trap rotation of each vortex about its equilibrium position*, which on a macroscopic level result in *harmonic distortions shearing the vortex lattice* and causing a rotation that alternately slows down and speeds up.
For further information give a look to Ref. [27, 28, 29].

Therefore we could investigate the excitation of these motion by solving the proper Euler-Lagrange equations for tiny random perturbations of the initial vortex equilibrium positions given by the corresponding crystal configuration. To do so, we followed the sequent procedure.

Tkachenko modes and core mass.
As a starting point, let us approached the above considered confined system in the generalized massive description for quantum vortices of small vortex mass, within the double assumption (3.10) of atomic species of the massive particles trapped in the cores equal to the superfluid condensate and all vortices of same core mass. In this way the massive effective Lagrangian L (2.35), describing such a system, reduces to the form (3.11) which

is

$$L = \sum_{j=1}^{N} \left[\frac{M}{2}(\dot{\boldsymbol{r}}_j)^2 + \frac{k_j mn}{2}(\dot{\boldsymbol{r}}_j \times \boldsymbol{r}_j \cdot \hat{z}) \frac{r_j^2 - R^2}{r_j^2} - \frac{k_j^2 nm}{4\pi} \ln\left(1 - \frac{r_j^2}{R^2}\right) \right] - \sum_{j>i=1}^{N} \frac{k_i k_j nm}{4\pi} \ln\left(\frac{R^2 - 2\boldsymbol{r}_i \cdot \boldsymbol{r}_j + r_i^2 r_j^2 / R^2}{r_i^2 - 2\boldsymbol{r}_i \cdot \boldsymbol{r}_j + r_j^2} \right), \tag{4.22}$$

where m, n are respectively the atomic mass and the numerical planar density of the superfluid, $M = N_b m$ the total mass of the N_b impurity particle per vortex core and $k_i = q_i h/m \to k = h/m$ since vortex charge $q_i = +1 \ \forall j$ (see section 3.2).

Furthermore due to the fact that in chapter 3 we have have obtained the equilibrium many vortex configurations requiring the approximation for *negligible boundary effects* ensuing from the geometric trapping of the system, i.e. no image vortices, we should solve dynamical equations of the type

$$M\ddot{\boldsymbol{r}}_j = -k\dot{\boldsymbol{r}}_j \times (-mn\hat{z}) + \frac{mnk^2}{2\pi} \sum_{i \neq j} \frac{\boldsymbol{r}_j - \boldsymbol{r}_i}{|\boldsymbol{r}_j - \boldsymbol{r}_i|^2} \quad \text{for} \ \ j = 1, \ \ldots, \ N \tag{4.23}$$

corresponding to dynamical equations (4.20) ($N > 2$ version) for no image vortices and vortex positions of magnitude $0 \leq r_j < R$ (not $\leq R$ to avoid nonphysical configurations).

Especially, to be coherent with dimensionless formalism used in section 3.2, we can move once again to the reference frame of the trap rotating at (dimensionful) angular velocity Ω $x'Oy'$ where, being $\boldsymbol{r}'_j = (x'_j, \ y'_j) = r_j(\cos\theta'_j, \ \sin\theta'_j)$ the vortex position in the new frame expressed in terms of polar coordinates r'_j's and θ'_j's, the old vortex coordinate vortex coordinate $\boldsymbol{r}_j$ becomes

$$\boldsymbol{r}_j = r'_j \left(\cos\theta'_j \cos(\Omega t) - \sin\theta'_j \sin(\Omega t) \ , \ \cos\theta'_j \sin(\Omega t) + \sin\theta'_j \cos(\Omega t) \right). \tag{4.24}$$

Then, by first writing the system's Lagrangian L (4.22) w.r.t this new reference frame and taking its dimensionless version by multiplying for $4\pi/(mnk^2)$ according to equation (3.4) (L is dimensionally an energy), and finally by subtracting the dimensionless image vortices contribution (exactly as done in (3.13) for the free-energy function), we obtained a dimensionless approximated effective Lagrangian $\tilde{L}$. Note that in such a derivation, before the subtraction we change the notation considering the vortex coordinates as $\{r'_j, \ \theta'_j\} \to \{Rr_j, \theta_j\}$, where now $0 \leq r_j < 1$ and $0 \leq \theta_j \leq 2\pi$ are the *dimensionless position variables* of the j^{th} vortex and both its *dimensionless radial* and *angular velocities* $\dot{r}_j, \ \dot{\theta}_j$ are derived as $\{\dot{r}'_j, \ \dot{\theta}'_j\} \to \{k/(2\pi R) \ \dot{r}_j, \ k/(2\pi R^2) \ \dot{\theta}_j\}$. Thus, the Lagrangian $\tilde{L}$ is a function depending on the position variables r_j's, θ_j's and velocities variables $\dot{r}_j$'s, $\dot{\theta}_j$'s of the N present massive vortices, with as further parameters the total core vortex mass M (or equivalently on N_b the number of trapped massive particles per vortex), the atomic mass and planar numerical density $m, \ n$ of the superfluid and on the dimensionless rotation frequency $\omega \doteq (2\pi R^2)/k \ \Omega$.

It follows that such an equation would lead to a total of $2N$ Euler-Lagrange equations, whose dimensionful version written in terms the laboratory reference frame Cartesian coordinates $\boldsymbol{r}_j = (x_j,\ y_j)$ coincides to the (compact notation) N dynamical ones in formula (4.23).
For our analysis we have considered a trap of radius $R = 50 \times 10^{-6}$ meters (in particular 50 times larger than core radius a_0), and 2×10^5 particles of ultracold sodium ^{23}Na (m is the corresponding atomic mass) of a planar density $n = (2 \times 10^5)/(\pi R^2)$.

Especially in order to verify at first the validity of our procedure we analyzed the massless case $N_b = 0$ of $N = 21$ vortices, characterized by an equilibrium lattice configuration as in Figure 3.5 (1, 7, 13 in ring numbers notation according to section 3.1). Taking as rotation rate $\omega = 29.2$ (counterclockwise rotation) and as initial condition a configuration obtained by perturbing all the vortex angular equilibrium positions θ_j's randomly in a small range up to 5 degrees, we found that the excited vortices move clockwise according the trajectories shown in Figure 4.4.

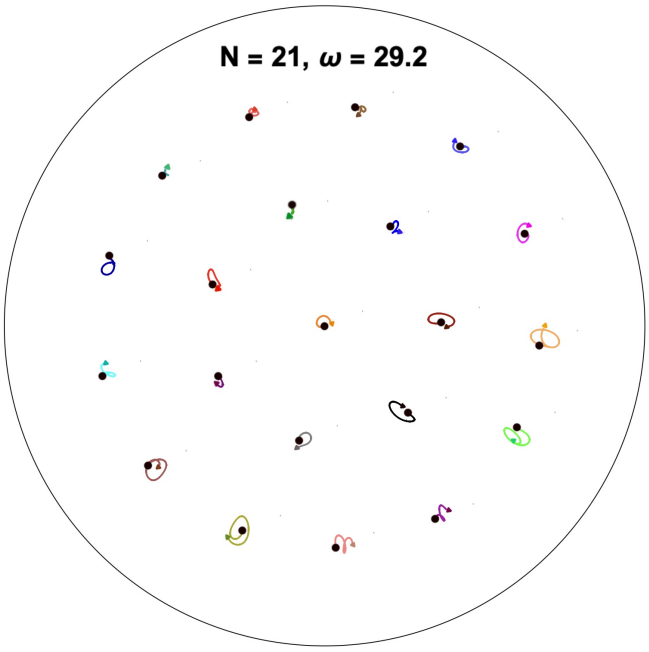

Figure 4.4: Plot of the trajectories of $N = 21$ massless vortices around their equilibrium crystal configuration (see Figure 3.5), each representing a combination of many Tkachenko modes. In fact, the excited vortices move clockwise against the trap rotation direction (which is counterclockwise since positive rotation rate ω). The considered initial configuration was obtained by perturbing the vortex angular equilibrium positions randomly in a small range up to 5 degrees.

Such vortex excitations do not present elliptical orbits as expected from what we have

previously declared about a Tkachenko mode. In fact the obtained results actually correspond to a superposition of more than one different Tkachenko modes for each vortex, ensuing from having activated the oscillations by means of tiny random perturbations of the equilibrium configuration.

After having verified that through this procedure we are activating the Tkachenko modes for massless vortex, let us go further focusing on the study of the core mass effects. First of all, looking back to the description of the dynamics of a massive vortex (see 4.1), one could expect to find the excitations similar to the one seen before, but at the same time affected by the typical cyclotron-like orbit corrections depending on the value of the small mass. Therefore, for such an analysis we focus on the case of fewer vortices, i.e. $N = 10$, for which we already have studied the equilibrium configuration (see 3.2) in the cases $N_b = 0$, 1000, 1500, 2000, 3000, 3500, 4000 (number of massive particles per each vortex core). In particular, the associated dynamical equations for each of these N_b values are solved, by taking a trap rotation rate ω value so that the $N = 10$ equilibrium vortex lattice (2, 4, 4 in ring notation) corresponds to the energetically favored configuration. Then, as done in Figure 4.5, we chose just one vortex in the system and plot its trajectories associated to the different massive cases.

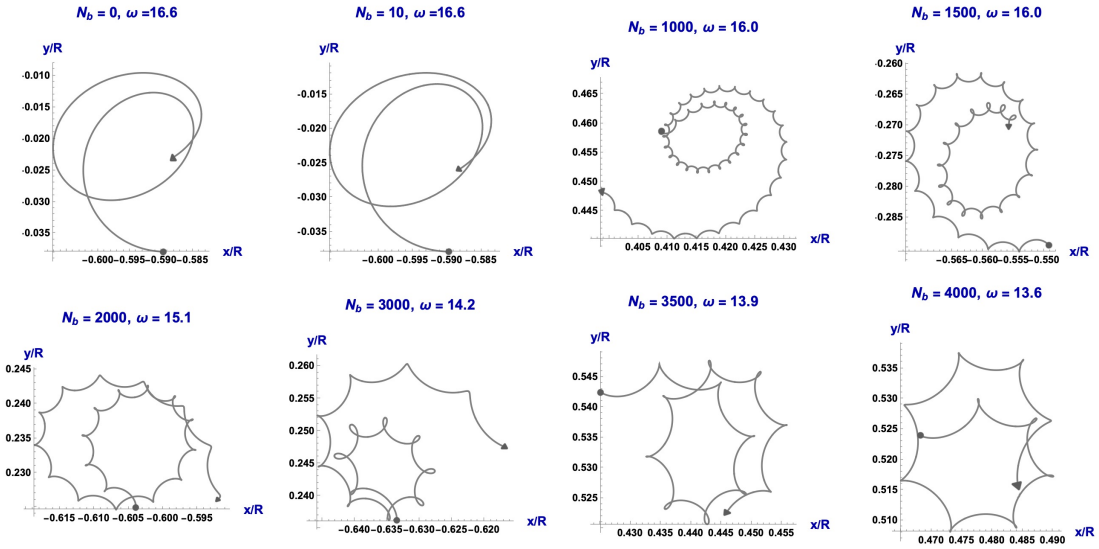

Figure 4.5: Plots of the trajectory of a single excited vortex oscillating around its equilibrium position in a vortex lattice for $N = 10$. Each curve has been obtained for different values of the number N_b of massive particles per vortex, considering a suitable rotation rate ω such that the crystal with $N = 10$ corresponds to the equilibrium pattern. Note that each trajectory is travelled clockwise (opposite direction of the trap rotation), and corresponds to a linear combination of many Tkachenko modes and according to N_b of the cyclotron modes, which becomes significant as the core mass is increased.

Looking to this picture, as expected we visualize some overall oscillation orbits clockwise travelled, which are given by the superposition of two different contributions: the first is the linear combination of many Tkachenko modes for a single vortex, corresponding to a motion of the vortex; while the second one coincide with the cyclotron-like excitation modes, the small-amplitude transverse oscillations along the radial direction ensuing from the small vortex mass.
Notice that when the number of trapped particles per each vortex is very small, i.e. $N_b = 10$, the vortex should behave as massless one, coherently to the generalized massive description (discussed in the previous subsection 4.1). Indeed, in Figure 4.5, the case $N_b = 10$ identically reproduces the massless case $N_b = 0$. Instead as the vortex mass is increased, the cyclotron-like orbit corrections present a lowered frequency, then becoming more evident.
In light of such observations we suggest that in general there should exist a sufficiently large value of core mass at which one may observe the hybridization of the two different families of normal modes.

Chapter 5

Summary and conclusions

Ever since it has been realized that the vortex cores may host massive particles, the scientific community has been vividly interested in analyzing the properties of vortices in such a new "massive" configuration. The main reason for such an interest lays on the fact that quantized vortices represents a distinctive feature of *Superfluidity*, and thus the study about massive vortices becomes crucial to further investigate superfluid systems, such as *mixtures of Bose-Einstein condensates* also including the *fermionic condensates* and the so called *quantum fluids of light*.
Therefore, in the past few years it has been proposed an effective Point-Vortex model for massive vortices, which is a generalization of the well-known model describing the vortices in a quasi two-dimensional superfluid as point-like massless particles: in particular this model consider the massive particles strictly localized in the vortex cores.

In this thesis project we have investigated, within such a theoretical model, the main effects of the core masses on the static and dynamic properties of the vortex crystals formed in a rotating two-dimensional superfluid. More precisely we focused on the case of a nonviscous, irrotational, imcompressible and homogeneous two-dimensional condensate confined in a circular rotating trap. Furthermore we have assumed the length scales of the system (here corresponding to the trap radius size) much larger than the spatial variations of the condensate density due to both the vortex cores and the boundaries effects.
We firstly focused on correctly reproduce, at least up to a moderate number of massless vortices, the well-known equilibrium patterns (in the rotating reference frame) of single charged vortices consisting in concentric (almost or exactly) regular polygons, by globally minimizing the system free energy with respect to the vortex positions. Unfortunately the presence of the boundaries, represented by the image vortices, leads to nonphysical solutions corresponding to vortices colliding at the domain wall and annihilating with their own images. This is why we have also assumed negligible boundary effects. Solving such a minimization problem, within this approximation, in some discrete ranges of the trap rotational velocity, we have been able to achieve, for each resulting equilibrium pattern of N vortices, not only the expected configuration but also a range of rotational velocities in which it corresponds to the globally stable vortex-array among all the possible ones.
Once we have completed the study for the massless case, we repeated the same global

minimization procedure for the case of massive vortices. For the sake of simplicity, in such analysis we have considered all the vortices hosting the same number of identical particles (meaning same core mass) of the same atomic species of condensate. We have obtained a free-energy function in the approximation of negligible boundary effects which is essentially a generalization of the massless one containing just an additional term related to the centrifugal apparent forces acting on the core masses. Such a term is responsible for the following effects that we have observed in the equilibrium massive vortex patterns:

- in the limit of zero massive particles in each vortex core, the resulting equilibrium vortex-arrays coincide with the mass less one;
- as the core mass increases there is a significant shift towards lower values in the rotation-rate ranges defining the stability of equilibrium configurations with numerous vortices, meaning that at a fixed rotational velocity the massive array has more vortices if compared to corresponding massless one;
- the geometry of each massive equilibrium pattern is formally the same to the one of the massless configurations, expect for an enlargement of all the rings towards the wall;
- there should exists some critical value of the core mass such that for sufficiently large rotational velocities there are no longer stable spatial configurations, meaning that the free energy does not present any local minima.

In light of such observations we also remark that this semi-analytical procedure strictly depends on the maximum number of possible vortices in the system and on the considered range of the rotational velocities.
As far as the dynamic properties of a crystal of vortices, we have studied the effect of the core mass on the well-known Tkachenko modes representing the non-trivial excitations of a massless vortex-array around its equilibrium (crystal) configuration. They consist in a precession motion of each vortex around its equilibrium position along elliptical trajectories travelled in opposite direction to the trap rotation one: on a macroscopic level they causes harmonic distortions shearing the vortex lattice and causing a rotation that alternately slows down and speeds up.
The considered Point-Vortex for massive vortices shows that, by means of the Euler-Lagrange equations, the dynamical equations are no longer the (first order differential) Helmholtz-Kirchhoff equations which describe the motion of massless vortices. In fact the presence of the core mass is responsible for an additional second order time derivative which leads to some particular dynamical solutions: motion characterized by small-amplitude transverse radial oscillations, superimposed to the well-known trajectories of massless vortices. Such oscillations are cyclotron-like excitation modes and they should affect the trajectories of the non-trivially excited vortices in a vortex crystal.
We have been able to see the superposition of such two different families of normal modes, by solving the dynamical equations in the approximation of negligible boundary effects considering as initial configurations small random perturbations of the equilibrium vortex patterns. Doing so we actually have found a linear combination of Tkachenko modes per each vortex and the expected superimposed cyclotron-like orbits, which was more evident

as the core mass was increased. We suggest that in general there should exist a sufficiently large value of core mass at which one may observe the hybridization of the two different families of normal modes.

The presented study can be further developed by investigating the actual boundary effects on the globally stable equilibrium patterns of massive vortices: one may study if the presence of the images would significantly influence the vortex rearrangement on the system. Another interesting application could be to consider a Bose-Hubbard model for these systems presenting massive vortices, where the trapped massive particles can tunnel among the different vortices.

Bibliography

[1] MJ Buckingham and WM Fairbank. «Chapter III The Nature of the λ-Transition in Liquid Helium». In: *Progress in low temperature physics*. Vol. 3. Elsevier, 1961, pp. 80–112 (cit. on p. vi).

[2] Carlo F Barenghi and Nick G Parker. *A primer on quantum fluids*. Springer, 2016 (cit. on pp. vi, 3, 4, 8–13, 15, 17–22, 27, 51).

[3] L. Landau. «Theory of the Superfluidity of Helium II». In: *Phys. Rev.* 60 (4 Aug. 1941), pp. 356–358. DOI: 10.1103/PhysRev.60.356. URL: https://link.aps.org/doi/10.1103/PhysRev.60.356 (cit. on p. vi).

[4] James F Annett. *Superconductivity, superfluids and condensates*. Vol. 5. Oxford University Press, 2004 (cit. on p. vii).

[5] Mike H Anderson, Jason R Ensher, Michael R Matthews, Carl E Wieman, and Eric A Cornell. «Observation of Bose-Einstein condensation in a dilute atomic vapor». In: *science* 269.5221 (1995), pp. 198–201 (cit. on p. vii).

[6] K. B. Davis, M. -O. Mewes, M. R. Andrews, N. J. van Druten, D. S. Durfee, D. M. Kurn, and W. Ketterle. «Bose-Einstein Condensation in a Gas of Sodium Atoms». In: *Phys. Rev. Lett.* 75 (22 Nov. 1995), pp. 3969–3973. DOI: 10.1103/PhysRevLett.75.3969. URL: https://link.aps.org/doi/10.1103/PhysRevLett.75.3969 (cit. on p. vii).

[7] M. R. Matthews, B. P. Anderson, P. C. Haljan, D. S. Hall, C. E. Wieman, and E. A. Cornell. «Vortices in a Bose-Einstein Condensate». In: *Phys. Rev. Lett.* 83 (13 Sept. 1999), pp. 2498–2501. DOI: 10.1103/PhysRevLett.83.2498. URL: https://link.aps.org/doi/10.1103/PhysRevLett.83.2498 (cit. on p. vii).

[8] Brian DeMarco and Deborah S Jin. «Onset of Fermi degeneracy in a trapped atomic gas». In: *science* 285.5434 (1999), pp. 1703–1706 (cit. on p. vii).

[9] R.P. Feynman. «Chapter II Application of Quantum Mechanics to Liquid Helium». In: ed. by C.J. Gorter. Vol. 1. Progress in Low Temperature Physics. Elsevier, 1955, pp. 17–53. DOI: https://doi.org/10.1016/S0079-6417(08)60077-3. URL: https://www.sciencedirect.com/science/article/pii/S0079641708600773 (cit. on p. vii).

[10] Russell J Donnelly. *Quantized vortices in helium II*. Cambridge University Press, 1991 (cit. on pp. vii, 8, 18, 19).

[11] Jamil R Abo-Shaeer, Chandra Raman, Johnny M Vogels, and Wolfgang Ketterle. «Observation of vortex lattices in Bose-Einstein condensates». In: *Science* 292.5516 (2001), pp. 476–479 (cit. on pp. vii, 37, 57).

[12] Brian P Anderson, PC Haljan, Carl E Wieman, and Eric A Cornell. «Vortex precession in Bose-Einstein condensates: Observations with filled and empty cores». In: *Physical Review Letters* 85.14 (2000), p. 2857 (cit. on pp. vii, 25, 37).

[13] Andrea Richaud, Vittorio Penna, and Alexander L Fetter. «Massive quantum vortices in superfluids». In: *Journal of Physics: Conference Series*. Vol. 2494. 1. IOP Publishing. 2023, p. 012016 (cit. on pp. vii, 22–25, 28, 50, 52–54).

[14] Andrea Richaud, Vittorio Penna, Ricardo Mayol, and Montserrat Guilleumas. «Vortices with massive cores in a binary mixture of Bose-Einstein condensates». In: *Physical Review A* 101.1 (2020), p. 013630 (cit. on pp. vii, 23, 25).

[15] Andrea Richaud, Vittorio Penna, and Alexander L. Fetter. «Dynamics of massive point vortices in a binary mixture of Bose-Einstein condensates». In: *Phys. Rev. A* 103 (2 Feb. 2021), p. 023311. DOI: 10.1103/PhysRevA.103.023311. URL: https://link.aps.org/doi/10.1103/PhysRevA.103.023311 (cit. on pp. vii, 23, 25, 26, 53).

[16] Kerson Huang. «Statistical Mechanics». In: *Statistical Mechanics* (1987) (cit. on pp. 1, 3, 4).

[17] Erode Subramanian Raja Gopal. «Statistical mechanics and properties of matter: theory and applications». In: *(No Title)* (1974) (cit. on pp. 1, 4).

[18] W. Greiner. *Quantum Mechanics (Special Chapters)*. Springer-Verlag, Berlin, Heidelberg, 1998 (cit. on pp. 1, 4, 5).

[19] Franz Mandl. *Statistical physics*. Vol. 14. John Wiley & Sons, 1991 (cit. on p. 4).

[20] Walter Greiner and Joachim Reinhardt. *Field quantization*. Springer Science & Business Media, 2013 (cit. on p. 4).

[21] LP Pitaevskii and S Stringari. *Bose-Einstein Condensation, Clarendon*. 2003 (cit. on pp. 4–8, 17).

[22] VI Yukalov. «Cold bosons in optical lattices». In: *Laser Physics* 19 (2009), pp. 1–110 (cit. on pp. 6, 7).

[23] Philip G Saffman. *Vortex dynamics*. Cambridge university press, 1995 (cit. on pp. 18, 19, 22).

[24] Andrea Richaud, Pietro Massignan, Vittorio Penna, and Alexander L Fetter. «Dynamics of a massive superfluid vortex in r k confining potentials». In: *Physical Review A* 106.6 (2022), p. 063307 (cit. on pp. 25, 53).

[25] L. J. Campbell and Robert M. Ziff. «Vortex patterns and energies in a rotating superfluid». In: *Phys. Rev. B* 20 (5 Sept. 1979), pp. 1886–1902. DOI: 10.1103/PhysRevB.20.1886. URL: https://link.aps.org/doi/10.1103/PhysRevB.20.1886 (cit. on pp. 27, 30, 31, 33, 36–38, 57).

[26] Jong-Kwan Kim and Alexander L Fetter. «Dynamics of a single ring of vortices in two-dimensional trapped Bose-Einstein condensates». In: *Physical Review A* 70.4 (2004), p. 043624 (cit. on p. 31).

[27] VK Tkachenko. «Stability of vortex lattices». In: *Sov. Phys. JETP* 23.6 (1966), pp. 1049–1056 (cit. on p. 57).

[28] LO Baksmaty, SJ Woo, S Choi, and NP Bigelow. «Tkachenko waves in rapidly rotating Bose-Einstein condensates». In: *Physical review letters* 92.16 (2004), p. 160405 (cit. on p. 57).

[29] Ian Coddington, Peter Engels, Volker Schweikhard, and Eric A Cornell. «Observation of Tkachenko oscillations in rapidly rotating Bose-Einstein condensates». In: *Physical review letters* 91.10 (2003), p. 100402 (cit. on p. 57).